LASER DATA TRANSFER
FLIGHT EXPERIMENT DEFINITION

Prepared by J. R. Merritt

McDonnell Douglas Corporation
P.O. Box 516
St. Louis, Missouri 63166

December 1975

Final Report

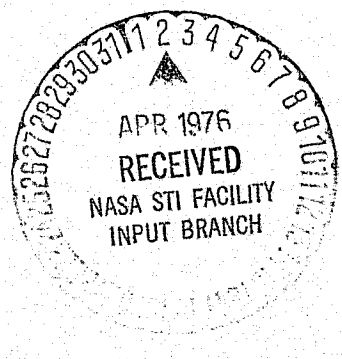

Prepared for

GODDARD SPACE FLIGHT CENTER
Greenbelt, Maryland 20771

TABLE OF CONTENTS

		Page
1.	STUDY SCOPE	1
2.	SUMMARY	2
3.	SPACE TERMINALS	5
	3.1 RELAY SATELLITE PAYLOAD	5
	3.1.1 Nd:YAG Laser Communications Subsystem	5
	3.1.2 CO_2 Laser Communications Subsystem	8
	3.2 RELAY SATELLITE SUPPORT SUBSYSTEMS	10
	3.2.1 Electrical Power Subsystem	10
	3.2.2 Thermal Control Subsystem	11
	3.2.3 Attitude Reference and Control	11
	3.2.4 Telemetry, Tracking and Command	12
	3.2.5 Propulsion Subsystem	12
	3.3 RELAY SATELLITE	12
	3.4 SHUTTLE INTERFACES	15
	3.5 SHUTTLE PAYLOAD	21
	3.6 RELAY SATELLITE ORBIT	23
	3.6.1 Baseline Relay Satellite Orbit	24
	3.6.1.1 Baseline Orbit Selection	26
	3.6.1.2 CO_2 Detector Radiation Cooler Performance	33
	3.6.1.3 Relay Satellite to Shuttle Link Kinematics	37
	3.6.2 Alternate Experiment Orbits	50
	3.6.2.1 12.5 Hour, i = 63.4 Degree Orbit	50
	3.6.2.2 Semi-synchronous, Equatorial Orbit	50
4.	GROUND TERMINALS	54
	4.1 GROUND STATION DEFINITION	54
	4.2 OPTICAL SCHEMATICS	57
	4.3 GROUND STATION INSTRUMENTATION	60

TABLE OF CONTENTS (CONTINUED)

		Page
5.	EXPERIMENT MEASUREMENTS PLAN	63
	5.1 EXPERIMENT PLAN SUMMARY	63
	5.2 PARAMETER MEASUREMENTS	63
	5.2.1 Satellite Parameters	65
	5.2.2 Ground Station Parameters	66
	5.3 LINK QUALITY MEASUREMENTS	68
	5.3.1 Uplink Bit Error Rate	68
	5.3.2 Uplink Tracking Error	72
	5.3.3 Uplink Pointing Error	72
	5.3.4 Uplink Beam Pattern Measurement	75
	5.3.5 Downlink Bit Error Rate	78
	5.3.6 Downlink Burst Rate	80
	5.3.7 Downlink Tracking Error	81
	5.3.8 Downlink Beam Pattern and Pointing Error	81
	5.3.9 Acquisition Time	81
	5.4 EXPERIMENT SCHEDULES	85
	5.4.1 Experiment Schedule Orbit Considerations	85
	5.4.2 Ground Station Design	86
	5.4.3 Initial Functional Checkout	87
	5.4.4 Long Term Schedule	89
	5.4.5 Typical Experiment Sequence	89

This report contains

Title page

and pages

ii through v
1 through 91

LIST OF FIGURES

Number	Title	Page
3-001	Relay Satellite Nd:YAG Transmitter Subsystem Block Diagram . .	6
3-002	CO_2 Laser Communications Transceiver	9
3-003	Laser Communications Spaceflight Experiment Spacecraft	13
3-004	Baseline Configuration - Preliminary Weights	14
3-005	Spacecraft Weight Summary	15
3-006	Shuttle Spacelab Flights	16
3-007	1981 Shuttle Cargo Manifest	17
3-008	Spacelab Gimbal Range	18
3-009	95% Envelope of RCS Exhaust Products	19
3-010	Pallet Electrical Power Supply	20
3-011	Shuttle Link Margins	21
3-012	Experiment Orbit Selection Criteria	24
3-013	Baseline Experiment Orbit Parameters	25
3-014	Goddard Daily View Time and Range for Repeating Orbits	27
3-015	Relay Satellite Range from Goddard for Baseline Experiment Orbit	28
3-016	Goddard Viewing Time Versus Relative Longitude of Apogee for Baseline 11.96 HR Orbit	29
3-017	Ground Track for Baseline Orbit	30
3-018	Relay Satellite Elevation at Goddard	31
3-019	Geometry for Determination of Incidence Angle of Sun's Rays on Satellite	34
3-020	Sun Elevation Profiles for Ω = 0 and 180 Degrees	36
3-021	Worst Case Sun Line - CO_2 Radiator FOV Geometry	37
3-022	Time Period that Moon-in-the-FOV Conditions Exist for Several 30 Day Periods	38
3-023	Angle Between Line of Sight to the Moon and Center of CO_2 Radiation Cooler FOV	39
3-024	Relay Satellite/Shuttle Terminals Pointing Angle Geometry . .	41
3-025	Relay Satellite Gimbal Axis/Body Axis Geometry	42
3-026	Relay Satellite Pointing Angles and Pointing Angle Rates - Relay Sat. to Shuttle Link	44

LIST OF FIGURES (CONTINUED)

Number	Title	Page
3-027	Shuttle Pointing Angles and Pointing Angle Rates - Relay Satellite to Shuttle Link	45
3-028	Range and Range Rate Histories for Relay Satellite/Space Shuttle Link	46
3-029	Relay Satellite Pointing Angles and Pointing Angle Rates - Relay Sat./Shuttle Link	47
3-030	Shuttle Pointing Angles and Pointing Angle Rates - Relay Satellite/Shuttle Link	48
3-031	Range & Range Rate Histories for Relay Satellite to Shuttle Link	49
3-032	Goddard Viewing Time Versus Relative Longitude of Apogee for 12 1/2 HR Orbit	51
3-033	Goddard Viewing Opportunities for 24 Day Period with a 40 Degree Elevation Constraint	52
3-034	Goddard Viewing Time for a Semi-Synchronous, Equatorial Orbit.	53
4-001	Ground Station Terminal Functional Block Diagram	55
4-002	Mobile Ground Station Terminal Optical Schematic	58
4-003	Stationary Ground Station Terminal Optical Schematic	58
4-004	Laser Terminal Optical Schematic	59
4-005	Ground Station Instrumentation Block Diagram	61
4-006	Bit Error Measurement Instrumentation	62
5-001	Uplink Bit Error Rate Analysis	71
5-002	Uplink Tracking Error Analysis	73
5-003	Uplink Pointing Error Analysis	75
5-004	Uplink Beam Pattern Measurement	76
5-005	Downlink Bit Error Rate Analysis	79
5-006	Downlink Burst Rate Analysis	80
5-007	Downlink Tracking Error Analysis	82
5-008	Downlink Beam Pattern and Pointing Error Measurement	83
5-009	Acquisition Time Measurement	84

LIST OF TABLES

Number	Title	Page
5.2-1	Measured Parameters Characteristics	64

1. STUDY SCOPE

This study was performed for the National Aeronautics and Space Administration, Goddard Space Flight Center, under contract NAS5-20585.

The purpose of the study was to synthesize and evaluate a set of laser communication flight experiments which can provide the engineering data and confidence level necessary for the subsequent deployment of operational data relay systems. The experiments will be performed between a joint DoD and NASA experimental relay satellite, ground terminals and the Space Shuttle. The results of the study include a definition of the space terminals, NASA ground terminals, test methods and test schedules required to perform the experiments.

2. EXPERIMENT DESIGN SUMMARY

The satellite definition data presented establishes the feasibility of utilizing an Atlas F booster for the launch of a combined DoD and NASA payload. The item of greatest concern in any further satellite design activity is the capability of the CO_2 detector radiation cooler. The candidate relay satellite defined herein provides the capability to keep the sun and earth out of the cooler field-of-view. However, if the moon in the field-of-view or the sun close to the field-of-view impacts the CO_2 performance, a new satellite concept may be required.

The feasibility of performing experiments between the Space Shuttle and the candidate relay satellite is established based on two assumptions. The first assumption is that NASA continues with the development of a 400 Mbps 1.06 μm laser communications link. The second assumption is that the total payload complement of the specific Shuttle flight is compatible with the view angles and attitude control modes required by the experiment.

The optics design data and block diagrams of the ground station demonstrate that both the NASA 48" and 30" ground stations are adaptable to the Nd:YAG experiment. No problems are foreseen for this adaptation other than the design problems normally encountered in the implementation of advanced technology equipment.

Several alternate orbits were evaluated. Orbits which are minor modifications of the baseline 63.4° inclination orbit offer variations in viewing time, viewing angles and time of daily operations. Orbits with low inclinations cannot be achieved with the Atlas F booster.

The goal of this experiment is to demonstrate that gigabit optical communication between a low orbit and synchronous satellite is possible. This is primarily an engineering, as opposed to a scientific, experiment. We are taking a communication system which has already been demonstrated in the laboratory and putting part of it aboard a satellite. Thus the new information to be obtained from the experiment concerns the effects of being aboard a satellite and the effects of the atmospheric link.

The atmospheric effect is really an undesirable side effect which we wish to eliminate to the degree possible since it does not occur in a low orbit-to-synchronous satellite link. The main interaction of the satellite with the communication system is through the introduction of pointing and tracking errors and some minor environment effects such as optical surface degradation and the introduction of optical alignment errors. The effect of actual, as opposed to simulated, background will also be observable for the first time.

This experiment will directly measure acquisition time and bit error probability. These are the primary measures of system performance. The experiment will also monitor a large number of subsystem and environmental parameters which will be used during system operation for making real time experiment modifications and during post flight data analysis to understand the reasons for the observed system performance.

The basic data analysis approach consists of the following steps. First, determine if the received signal and noise characteristics are as predicted by theory. Second, determine if the system performance (probability of bit error, acquisition time, tracking error, etc.) is consistent with what the theory would predict given the experimental characterization of the received signal and noise. Third, if either analysis shows inconsistency, revise the theoretical analysis to better match the observed experimental results. This may require the addition of previously unconsidered effects or a more precise treatment of previously considered effects. An alternate approach is to ignore analytical models derived using physical laws and, rather, treat the variables of interest on a purely statistical basis using regression analysis to derive statistical correlations between the variables. This approach is primarily invoked to describe poorly understood physical processes.

Differences between experimental results and analytical predictions occur because of the following two basic areas of uncertainty. One area is the determination of functional relationships between performance and various atmospheric and system parameters. The other area of uncertainty is the experimental determination of the value of parameters themselves. The functional relationships have been analytically predicted so that at least trial solutions are already available. The parameters will be experimentally measured in real time and their values recorded. The data analyses will thus proceed by first taking the experimentally measured parameters and the analytic expressions for loss in performance and predicting the total loss. Equivalent loss, rather than probability of error, is often used for mathematical convenience. The predictions will then be compared with the experimentally measured total loss. If the predicted and measured loss are very close (say less than 2 dB), the models and parameter measurements will be considered to be valid and no more sophisticated data analyses will be required. On the other hand, if measured and predicted total loss do not agree to within an accuracy consistent with the expected experimentally measured parameter error, then it will be necessary to modify the analytical loss expressions.

Section 3 describes the space terminals which could be used in the laser data transfer experiment. A candidate relay satellite is defined, interfaces with the Space Shuttle are defined, suggestions for development of a Space Shuttle terminal are documented, the NASA CO_2 payload for the relay satellite is defined, and the Air Force Nd:YAG payload for the relay satellite is defined. During the latter weeks of this study the Air Force payload has changed, however these changes are not reflected in this report since the functions and performance have not been impacted.

Section 4 includes ground station design data oriented toward assisting GSFC in modifying the existing fixed 48 inch telescope ground station and mobile 30 inch telescope ground station.

Section 5 defines the parameters which need to be measured both in the spacecraft payload and in the ground station to perform the experiment. The methods of utilizing these parameters to measure the link quality is then described with block diagrams which identify input parameters, hardware and software elements, and the resulting measures of quality. Section 5 concludes with experiment schedules definition.

3. SPACE TERMINALS

This section of the report describes the space terminals along with their payloads and orbits to be utilized in the Laser Data Transfer Flight Experiment. The terminals include the Relay Satellite and the Space Shuttle. Experiment links will be established between each terminal and a ground station, and between the terminals themselves. We define the functional operation of the terminals and their payloads, describe subsystem interfaces, and show how the orbits selected affect experiment operations.

3.1 RELAY SATELLITE PAYLOAD. The Relay Satellite will carry two laser communications subsystems for in-flight evaluation. The NASA CO_2 subsystem radiates on a wavelength of 10.6 μm in the far infrared. The Relay Satellite will carry a transceiver terminal capable of simultaneous transmission and reception of 300 Mbps data on laser lines slightly displaced in frequency and orthogonal in polarization for separation of transmitted and received signals. The USAF Nd:YAG subsystem radiates on a wavelength of 0.53 μm in the visible spectrum (green) after having been frequency doubled from its 1.06 μm fundamental laser wavelength. The relay satellite transmits 1 Gbps at the 0.53 μm wavelength while receiving a 1.06 μm wavelength beacon which contains 10 Kbps data.

3.1.1 Nd:YAG Laser Communications Subsystem. Figure 3-001 is a block diagram of the Nd:YAG communications subsystem showing the interfaces among the components of the communications transmitter, acquisition, tracking, and command receivers, and pointing servo system.

Laser. The transmitter laser is a 500 Mpps mode-locked frequency-doubled Nd:YAG laser. It contains an acousto-optic mode-locker/frequency doubler (AOML/FD) which, in a single barium sodium niobate crystal, performs both the mode-locking and frequency doubling functions. Two lasers will be incorporated into the experiment package. One laser will be pumped by a potassium-rubidium lamp to produce 150 milliwatts of mode-locked power at 0.53 μm. The second will be pumped by the sun to produce upwards of 500 milliwatts. This laser must interface with a sun collecting optical system including a primary collector whose aperture diameter is between 18 and 24 inches.

FIGURE 3-001 RELAY SATELLITE ND: YAG
TRANSMITTER SUBSYSTEM BLOCK DIAGRAM

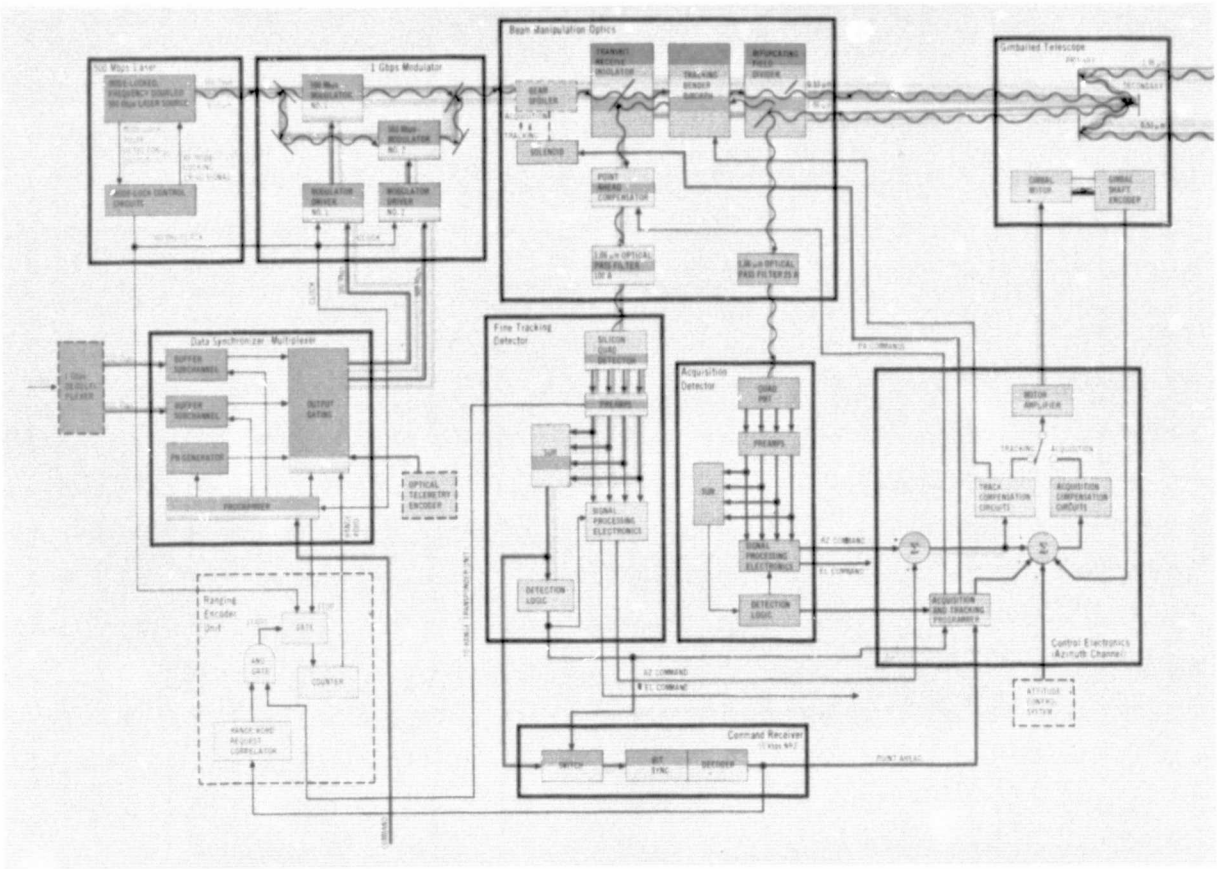

Modulator. The modulation format used in this subsystem is Pulse Quaternary Modulation (PQM). The modulator contains two polarization modulators to control both the polarization and time position of each laser pulse in accordance with the data to be transmitted. The linearly polarized pulse from the laser first enters modulator #1 where its polarization may remain unchanged or be shifted from horizontal to vertical polarization. The output pulse then enters a polarization sensitive time delay unit whose delay time is 1 nanosecond greater for a vertically polarized pulse than for a horizontally polarized pulse, thereby imposing the pulse position information on the pulse. The second modulator then again rotates the plane of polarization 90^{o} or not in accordance with its data input, thereby permitting four possible pulse states: horizontal undelayed, vertical delayed, vertical undelayed, horizontal delayed. Since two bits of

information are present on each pulse, the 500 Mpps laser pulse train can communicate data up to 1 Gbps. A quarter wave plate at the modulator output converts the linearly polarized light to circularly polarized light to avoid the necessity of special attitude constraints on the transmitter and receiver terminals with respect to roll about the line of sight.

Optics. The beam manipulation optics keep the beam pointed along the proper line of sight in accordance with tracking error signals developed in the beacon receiver. The Cassegrain telescope develops a final transmit beam which has five microradians dispersion at the $1/e^2$ (-8.7 dB) boundary. The telescope aperture is 7.5 inches in diameter.

Beacon Receivers. In its capacity as a receiver, the subsystem performs the functions of detection of acquisition and tracking signals and decoding of Pulse Interval Modulation (PIM) data on a 3000 pps 1.06 μm pulse train. During initial acquisition, the high data rate receiver at the opposite terminal scans its beacon beam over an uncertainty region such that the Relay Satellite receives ten 200 nanosecond 1.06-μm pulses per second. Since this light enters off axis, and is focused at the bifurcating mirror, it is reflected by that mirror, through a spectral filter, and onto the coarse acquisition detector assembly. The quadrant dividing lens separates the beam into four beams for illumination of the four PMTs. The illumination of each tube depends on the position of the spot on the lens. The signals from the tubes are processed to provide bang-bang control information. This control information steers the gimbals toward boresight until at 300 microradians from boresight the spot focused on the bifurcating mirror falls through the hole in the mirror, reflects off the fine acquisition mirror (a solenoid-operated flip mirror) and is focused on an image dividing reflecting pyramid. The four beams from the pyramid illuminate four PMTs in the Fine Acquisition Detector (FAD) assembly. The spot size is such that the PMT output can be processed to produce a proportional control signal to the gimbal and bender system with a linear range of plus or minus 35 microradians. In this mode, the pointing error is reduced such that the outgoing transmit beam, which has been spoiled to 100 microradians is illuminating the high data rate receiver in the opposite terminal. The acquisition and tracking sensors at the receive terminal detect the signal, stop the scanning of the 1.06 μm beam, and point it back along the line of sight. The received pulse rate at the FAD increases from 10 pps to 3000 pps. When the

FAD angle processor indicates a tracking error of 25 microradians or less, the fine acquisition mirror is pulled out of the beam to allow the Fine Tracking Detector (FTD) to be illuminated. The FTD is a silicon quadrant detector. The spot on the FTD is nearly diffraction-limited, such that the linear range of the processed tracking error has a five microradian radius. In this mode the tracking error of the system is less than one microradian rms for typical disturbances. This error signal drives both the gimbals and high frequency beam steering mirrors in order to hold the beam on boresight.

The quadrant sum signal is used to recover the PIM data imposed on the beacon beam.

3.1.2 CO_2 Laser Communications Subsystem. Figure 3-002 is a functional block diagram of the CO_2 laser communications transceiver.

Receiver Portion. The received 10.6 μm light is reflected off a steerable flat mirror into the telescope which forms the antenna of the receiver. The folded Gregorian optics include a fine pointing image motion compensator (IMC) similar to the beam steering mirrors in the Nd:YAG subsystem. The quarter-wave plate converts the polarization of the incoming wave from circular to linear so that the wiregrid polarization diplexer will pass the energy to the detector. Local oscillator insertion is accomplished by means of a 45° mirror with a central hole. The received beam is small and collimated and passes through the hole while the other is large and converging and is reflected 90° with some central obscuration. The convergence angle of the reflected beam is such that at the detector the beams match each other and the detector size. The detector is a mercury cadmium telluride (HgCdTe) photodiode which is maintained at approximately 100 degrees Kelvin by means of a radiation cooler to which the detector is mounted. The cooler requires a 120-degree view of dark space in order to maintain acceptably low temperatures. Therefore, neither the earth nor the sun may enter this field during flight. This constraint is easily satisfied on the operational geosynchronous orbit; however during the flight experiment, maneuvers are required to maintain the proper orientation.

The mixer output is at RF (about 400 MHz) and is synchronously demodulated by means of a phase-locked loop to produce the original data. The modulation format is double-sideband supressed carrier with some residual carrier. An outer frequency control loop tunes the local oscillator laser frequency to compensate for the doppler shift arising from the relative motion of

FIGURE 3-002 CO_2 LASER COMMUNICATIONS TRANSCEIVER
(This is a Copy of Figure 5.8 from NASA LDRL Proposal Vol. 1)

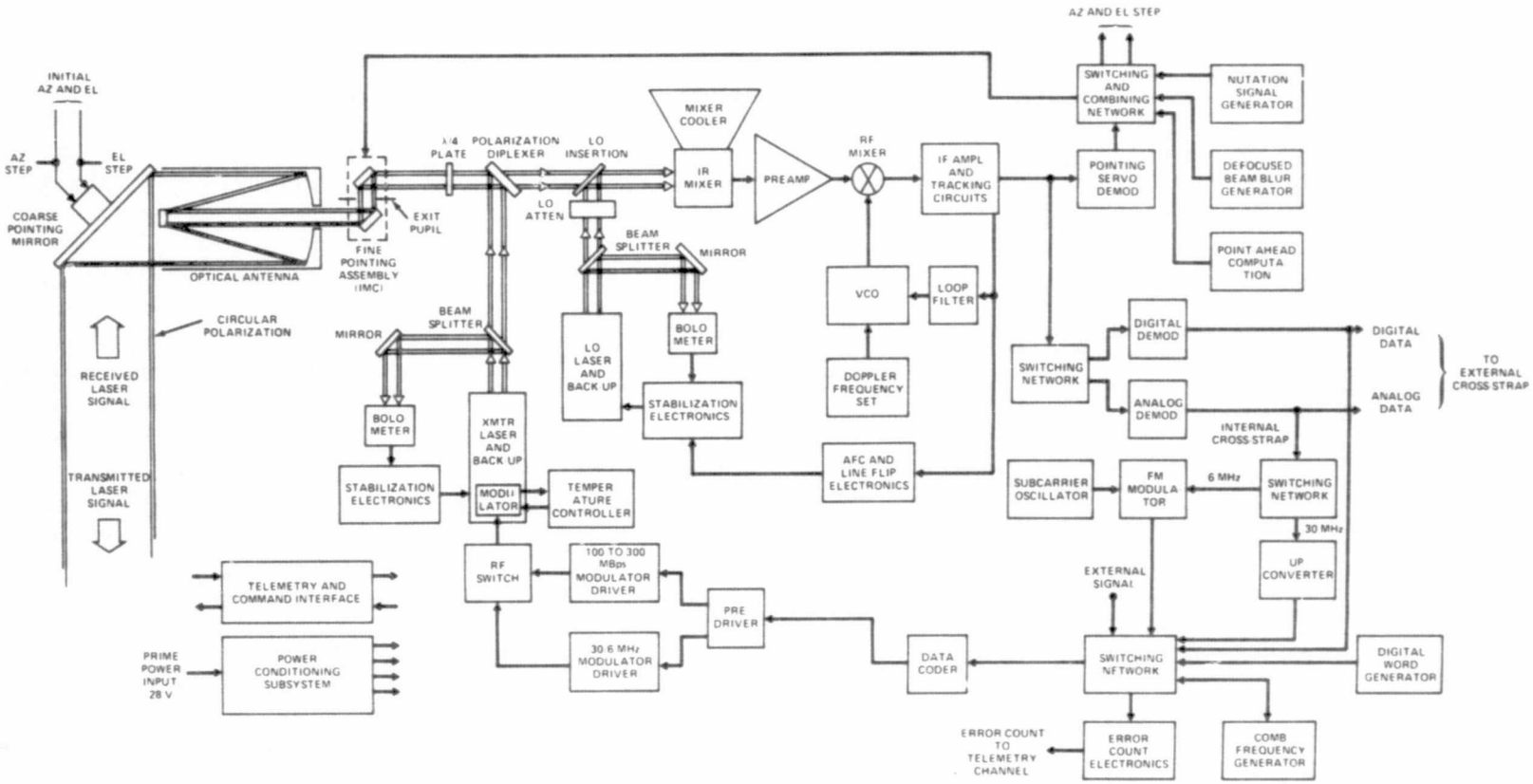

the transmit and receive terminals, thereby limiting the required range of the VCO in the phase-locked loop.

Acquisition and Tracking. Acquisition is accomplished by raster scanning the IMC until the signal strikes the detector. At this time the IMC orthogonal mirrors are driven sinusoidally in quadrature to produce a conically scanned beam on the detector. Any boresight misalignment causes low frequency sinusoidal amplitude modulation on the detector output. This modulation is detected and mixed with the scan drive signals to produce azimuth and elevation error signals in the conventional manner.

Transmitter. The transmitter laser is a waveguide CO_2 laser with a cadmium telluride intracavity coupling modulator. The modulator operates to couple energy out of the cavity in accordance with its drive signal such that a double-sideband suppressed carrier signal is generated. The operation of the laser/modulator is such that low frequency modulation is distorted. Consequently the coding modules are present to shift the data spectral lines away from dc. The polarization diplexer reflects the laser output beam into the transmitting optics.

3.2 RELAY SATELLITE SUPPORT SUBSYSTEMS. The payload support subsystems aboard the experiment satellite are comprised of the following:

a. Electrical
b. Thermal Control
c. Attitude Reference and Control
d. Propulsion
e. Telemetry, Tracking and Command
f. Structure

Following is a brief description of the support subsystems of the baseline spacecraft configuration.

3.2.1 Electrical Power Subsystem (EPS). The subsystem includes the power supply, storage and distribution sections. The subsystem sizing takes into account two modes of experiment operation, which are necessary because the YAG communications subsystem can be lamp pumped or sun pumped. The lamp pumping requires more power than the sun pumping.

"Condition I" mode includes the CO_2 laser communications subsystem operating in conjunction with the YAG laser communications subsystem operating in the sun pumped mode. "Condition II" mode is the YAG communications subsystem operating alone in the lamp pumped mode. Condition I results in the peak power condition used in sizing the storage and distribution section. Condition II results in the average power condition used in sizing the supply section, in this case, the solar panels. Spacecraft support subsystems requiring power are the Telemetry, Tracking and Command Subsystem and the Attitude Reference and Control Subsystem. The solar panels are sized for six hours of experiment operation in Condition I at the maximum sun angle.

The solar panels, in a fixed position after deployment, supply the spacecraft power requirements of 651 watts direct with the batteries supplementing the power requirements for peak loads and during the period that the solar panels are in the shadow of the earth. During the ecliptic periods the satellite is not in viewing range of the ground stations and therefore only spacecraft housekeeping functions are performed.

The power conditioning requirements are established assuming that motors can use the normal bus quality power without conditioning (100% efficiency), laser and modulators require some conditioning with a loss of 20% and logic circuits require the greatest conditioning with a loss of 50% in the conditioning process.

3.2.2 Thermal Control Subsystem (TCS). The CO_2 detector radiation cooler is not considered part of the TCS since it is an integral part of the CO_2 transceiver optomechanical unit. The spacecraft is comprised of an optical module and an equipment module with radiators located on each module to cool the components that it houses, thus minimizing heat transfer across the interface and simplifying design and installation. The YAG laser rod is cooled by a separate cold radiator branch. The remaining components such as YAG laser cavity and electronics are cold plate mounted or radiation cooled. The CO_2 subsystem cooling requirements are assumed to be satisfied by 20°C cold plates.

3.2.3 Attitude Reference and Control. This subsystem includes the reference sensors (1 earth and 3 sun), computer and gyros. The earth sensor is a single unit with four heads capable of viewing the Earth's horizon from the altitude of 20,300 NM where the earth view subtends an angle of 16° down to an altitude of 500 NM where the Earth view subtends an angle of 121°. The three sun sensors are

placed on the vehicle so that the sun will be in view continuously during the worst case travel of 180°. The earth and sun sensors are mounted on the optical module for precise orientation. A gyro package is used during insertion and acquisition phases of the mission and during mission phases when the Earth, satellite, and sun are nearly in a line.

3.2.4 Telemetry, Tracking and Command (TT&C). This SGLS-compatible subsystem includes all the equipment necessary to perform the housekeeping and experiment data collection, storage and reporting functions. The subsystem includes an S-Band transceiver for command uplink and housekeeping data downlink, an S-Band TM transmitter for experiment data down link, two tape recorders for data storage and the instrumentation wire bundles for data collection.

3.2.5 Propulsion Subsystem. This subsystem is a monopropellant blowdown type which includes thrusters, plumbing, propellant tankage, propellant and pressurant. A single storage tank contains the hydrazine and pressurant. The first use of the subsystem is a ΔV maneuver which raises the perigee and adjusts the orbit. The remaining propulsion subsystem mission is to provide attitude control for the mission duration.

3.3 RELAY SATELLITE. Company funded studies have resulted in the definition of a candidate relay satellite. Figure 3-003 illustrates this satellite which consists of an optical module, an equipment module, and a fixed erectable solar array, in addition to the payload. A preliminary weight summary for the satellite is shown in Figure 3-004. In order to assure that those weight estimates are realistic, a part of our study included the collection of data on a number of NASA automated satellites for comparison with our preliminary weight summary. The results of this portion of the study are presented in Figure 3-005 in which two versions of our candidate satellite design are compared with the other satellites. The salient point to be noted in Figure 3-005 is that the payload-to-total-satellite weight ratio of our candidate satellite is realistic.

FIGURE 3-003 LASER COMMUNICATIONS SPACEFLIGHT EXPERIMENT SPACECRAFT
Baseline Configuration

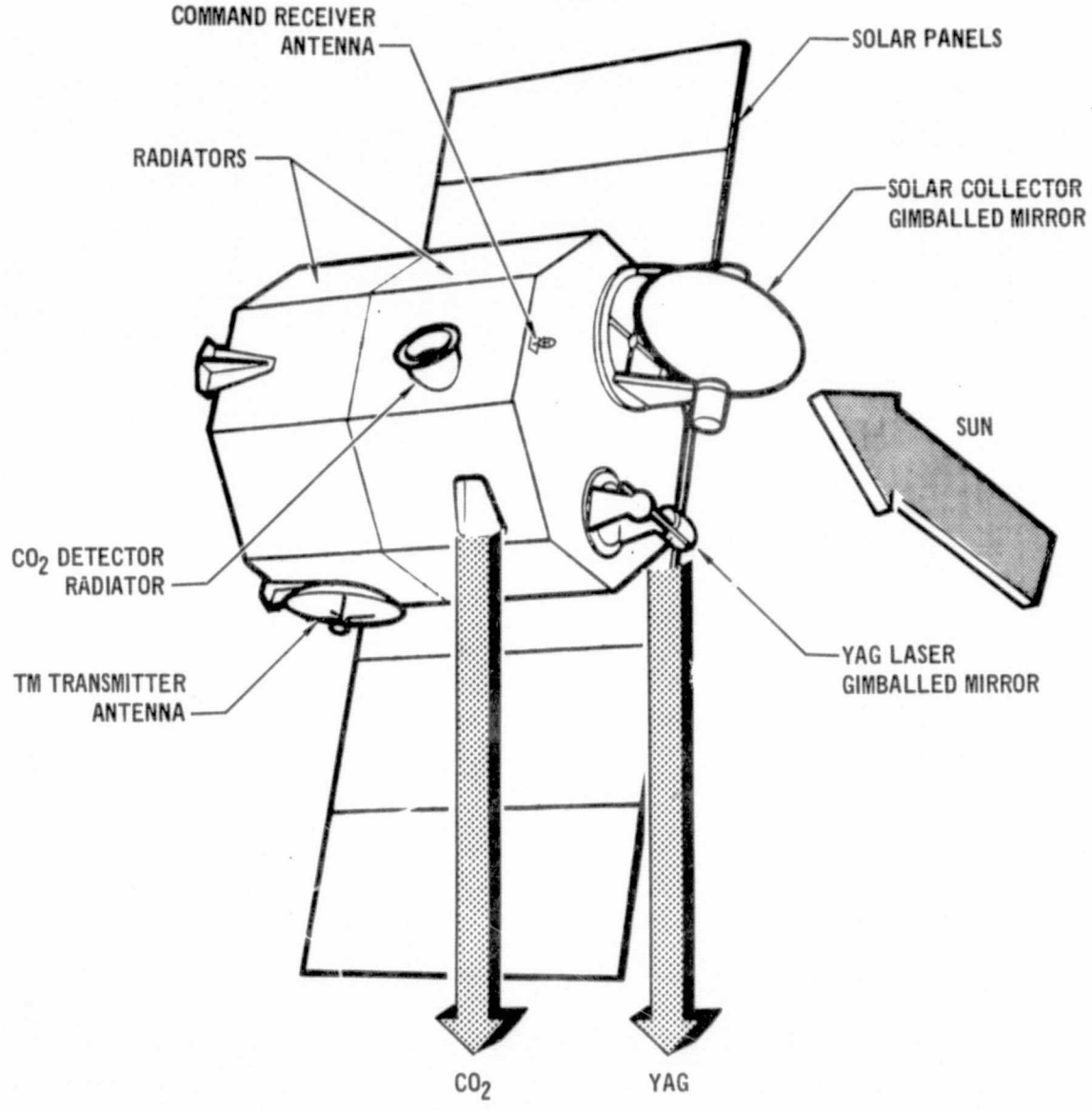

FIGURE 3-004 BASELINE CONFIGURATION – PRELIMINARY WEIGHTS

JANUARY 1975

2 YEAR MISSION
6 HR. ON TIME (DUTY CYCLE 6/24)

YAG "A" PACKAGE (7.5 IN)		PROPULSION	
OPTOMECHANICAL	79	USABLE PROPELLANT	37
SUPPORT ELECTRONICS	60	TRAPPED PROP	2
SUN COLLECTOR-OPTOMECH	72	PRESSURIZATION GAS	1
MOUNTING PROVISION	10	TANK	5
WIRING	6	TANK MOUNT	2
	227	THRUSTERS, LINES, VALVES & REG.	21
		MOUNTING PROVISION	4
		WIRING	2
			74
CO_2 TRANSCEIVER (6.0 IN)		T.T. & C. AND EXPR EQUIP.	
OPTOMECHANICAL	66	EQUIPMENT	60
SUPPORT ELECTRONICS	58	MOUNTING PROVISION	5
MOUNTING PROVISION	7	WIRING	20
WIRING	5		85
	136		
ATTITUDE CONTROL SYSTEM		STRUCTURE	
SENSORS	14	BASIC SHELL	46
COMPUTER	23	SECONDARY STRUCTURE	88
GYROS	10		134
MOUNTING PROVISION	3		
WIRING	5		
	55		
THERMAL CONTROL		ELECTRICAL	
COLD RADIATOR	5	SOLAR CELLS	68
HOT RADIATOR	66	BATTERIES	22
	71	CONTROLS	5
		MOUNTING PROVISION	5
		WIRING	1
			101
		TOTAL	882

FIGURE 3-005 SPACECRAFT WEIGHT SUMMARY
(% of Total)

SUBSYSTEM \ CATEGORY	PAYLOAD	ACS	TCS	PROP.	TT&C	STRUCT.	ELECT.
BASELINE FLT. EXP. 1-15-75	41	6	8	8	10	15	12
ALUM PRIMARY STRUCT FLT. EXP.	37	6	7	8	9	25	8
OAO (FIRST FLIGHT)	40	15	1	3	1	22	18
ERTS-A	33	13 1/2	4	8	5 1/2	13	23
ATS-F	34	8	6	6	4	23	19
HEAO-A (2-16-70)	67	3	1	1	1	20	7
HEAO-A (5-2-74)	45	←			55		→

Note that the satellite data reflects the status of the satellite definition in January 1975. During the latter weeks of this study the Nd:YAG payload has been increasing in capability and weight. Therefore, the total satellite has been increasing in weight above the estimates shown in this report. The functions and performance levels of the laser transmitter and beacon receiver have not changed, nor have the booster orbit parameters or viewing time changed. No changes have occurred which would impact the ground or Shuttle terminals nor the methods of performing experiments as defined in this report.

3.4 SHUTTLE INTERFACES. The 1980 and 1981 Space Shuttle flights which include the Spacelab and/or Pallet are summarized in Figures 3-006 and 3-007. The information shown includes the flight number, orbit altitude, orbit inclination, load factor, configuration (pallet only, Lab only or combination of Lab and pallet), and the payload type name and identification number. All the missions listed are for seven days duration. Analysis of the load factor shows that only one flight utilizes the payload capability of the Shuttle. The volume utilization is unknown. It is quite possible that the pallet "floor space" is completely filled without reaching the weight limitation. As the payloads are defined, the space compatibility with the laser communications subsystem can be determined.

FIGURE 3-006 SHUTTLE SPACELAB FLIGHTS (Pallet & Lab)

1980 SHUTTLE CARGO MANIFEST*								
FLT NO. **	LAUNCH SITE	ORBIT ALTITUDE		INCL DEG	LOAD FACTOR	SPACE LAB CONFIG.	PL	NAME
		NM	(KM)					
4	K	210	(389)	28.5	.470	P	AST-11A	SOLAR PHYSICS
5	K	120	(222)	28.5	.501	P	PHY GA&B	HIGH ENERGY PHYSICS
6	K	150	(278)	28.5	.600	L	LS-2A7	LIFE SCIENCES
7	K	150	(278)	28.5	.600	L	LS-247	LIFE SCIENCES
8	K	200	(371)	55.0	.584	L&P	ST-2A	SPACE TECHNOLOGY
9	K	200	(371)	55.0	.584	L&P	ST-2B	SPACE TECHNOLOGY
10	K	180	(334)	55.0	.583	L&P	OA-1A	OFFICE OF APPLIC.
11	K	180	(334)	55.0	.561	L&P	OA-1B	OFFICE OF APPLIC.
12	K	180	(334)	28.5	.499	L&P	SP-1A	SPACE PROCESSING
13	K	180	(334)	28.5	.504	L&P	NN/D 16A	EARTH OBSERVATIONS
14	K	200	(371)	28.5	.525	L&P	NN/D 16C	GPLI

* ALL MISSIONS ARE FOR 7 DAYS
** FLIGHT NUMBERS DO NOT REPRESENT A PRIORITY OR A SEQUENCE OF FLIGHTS
NN/D = NON-NASA/NON DOD
GPL = GENERAL PURPOSE SPACELAB

The laser communication subsystem gimbal range from a pallet is shown in Figure 3-008. A worst case condition is shown using a two module spacelab and one aft-mounted pallet. The gimbal range about the Y axis is 57° forward and 50° aft, and about the X axis is 180°. The full hemisphere gimbal range is available for 107° out of each side of the cargo bay between the spacelab module and the OMS pod. The following ground rule assumptions were made in establishing the gimbal range limits:

a. The receiver is mounted above the Z440 level during operation so that the full 180° gimbal range is available.

b. The receiver is mounted in the center of the pallet without other pallet payloads inhibiting the gimbal range.

A source of laser communication interference may be the RCS rocket exhaust plumes. Figure 3-009 shows the 95% exhaust envelope of the up and side firing RCS rocket engines. The rocket propellants are Nitrogen Tetroxide and Monomethylhydrazine.

FIGURE 3-007 1981 SHUTTLE CARGO MANIFEST*

FLT NO. **	LAUNCH SITE	ORBIT ALTITUDE NM	INCL DEG	LOAD FACTOR	SPACELAB CONFIG.	PL	NAME
1	K	160	28.5	.482	P	SP-1B	SPACE PROCESSING
2	K	160	28.5	.482	P	SP-1B	SPACE PROCESSING
3	K	160	28.5	.983	P	SP-1C	SPACE PROCESSING
7	K	160	55.0	.712	P	SP-1C	SPACE PROCESSING
16	K	162	28.5	.548	P	AST-10A	STELLAR ASTRONOMY
17	K	210	28.5	.470	P	AST-11A	SOLAR PHYSICS
18	K	120	55.0	.458	P	PHY-6C	HIGH ENERGY PHYSICS
19	K	120	28.5	.379	P	PHY-6D7	HIGH ENERGY PHYSICS
20	K	200	28.5	.555	L&P	PHY-7A	ATMOS. SPACE PHY.
21	K	150	28.5	.600	L	LS-2A7	LIFE SCIENCES
22	K	150	28.5	.600	L	LS-2A7	LIFE SCIENCES
23,24 25 & 26	K	200	55.0	.584	L&P	ST-2A, 2B, 2C & 2D	SPACE TECHNOLOGY
27 & 28	K	180	55.0	.583/ .561	L&P	OA-1A & 1B	OFFICE OF APPLICATION
29	K	180	28.5	.499	L&P	SP-1A	SPACE PROCESSING
30	K	180	28.5	.504	L&P	NN/D-16A	EARTH OBSERVATION
31	K	162	28.5	.488	P	NN/D-16B	ASTRONOMY
32	K	200	28.5	.525	L&P	NN/D-16C	GPL

*ALL MISSIONS ARE FOR 7 DAYS
**FLIGHT NUMBERS DO NOT REPRESENT A PRIORITY OR A SEQUENCE OF FLIGHTS
NN/D = NON-NASA/NON DOD
GPL = GENERAL PURPOSE SPACELAB

FIGURE 3-008 SPACELAB GIMBAL RANGE

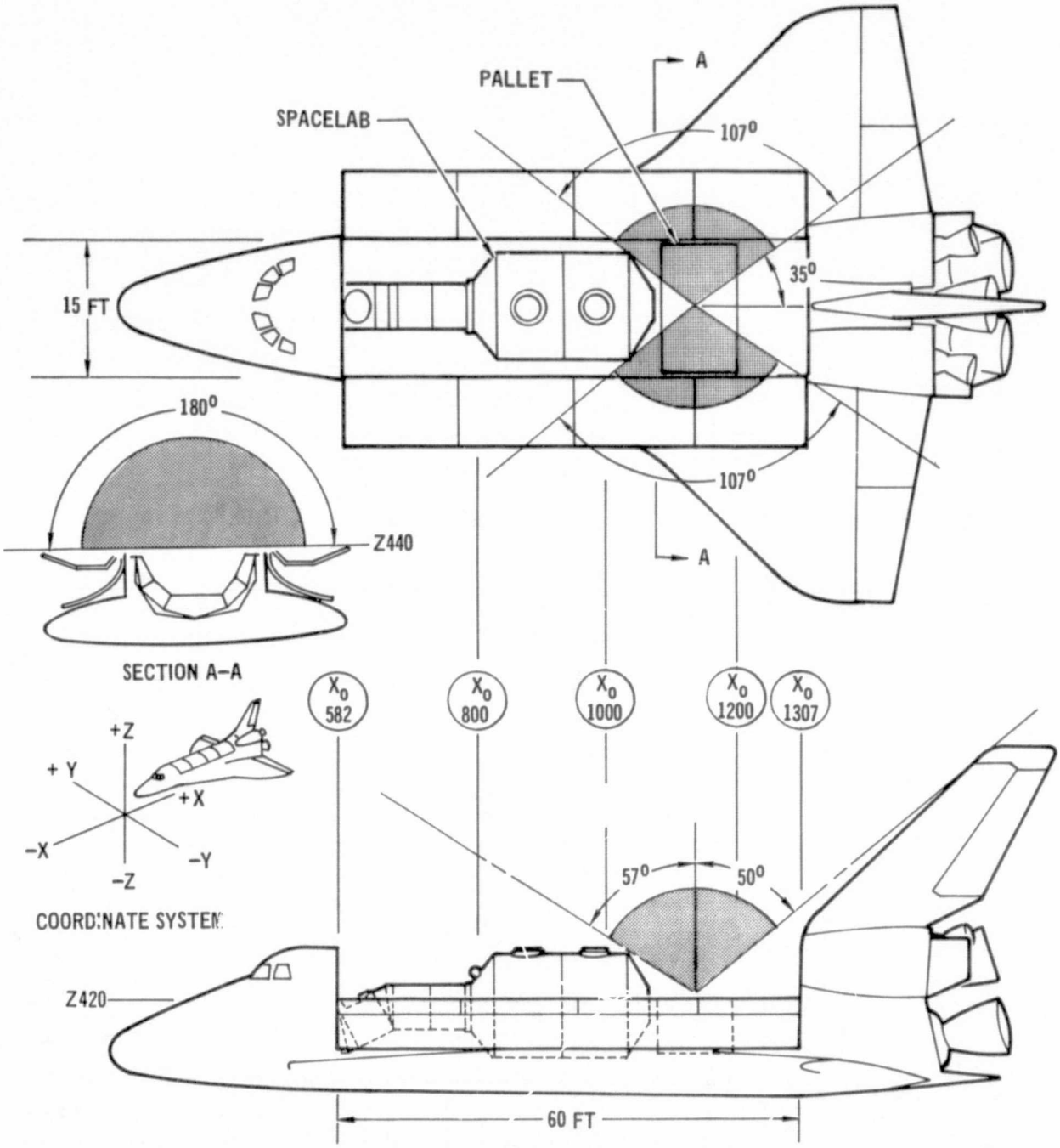

REF:
SPACE SHUTTLE PAYLOAD ACCOMMODATIONS – JSC 07700 VOL XIV REV. B 21 DEC 1973
SPACELAB PAYLOAD ACCOMMODATIONS HANDBOOK – REV. A APRIL 1974
ORBITER CONFIGURATION CONTROL DWG. – VL 70–0001400

FIGURE 3-009 95% ENVELOPE OF RCS EXHAUST PRODUCTS

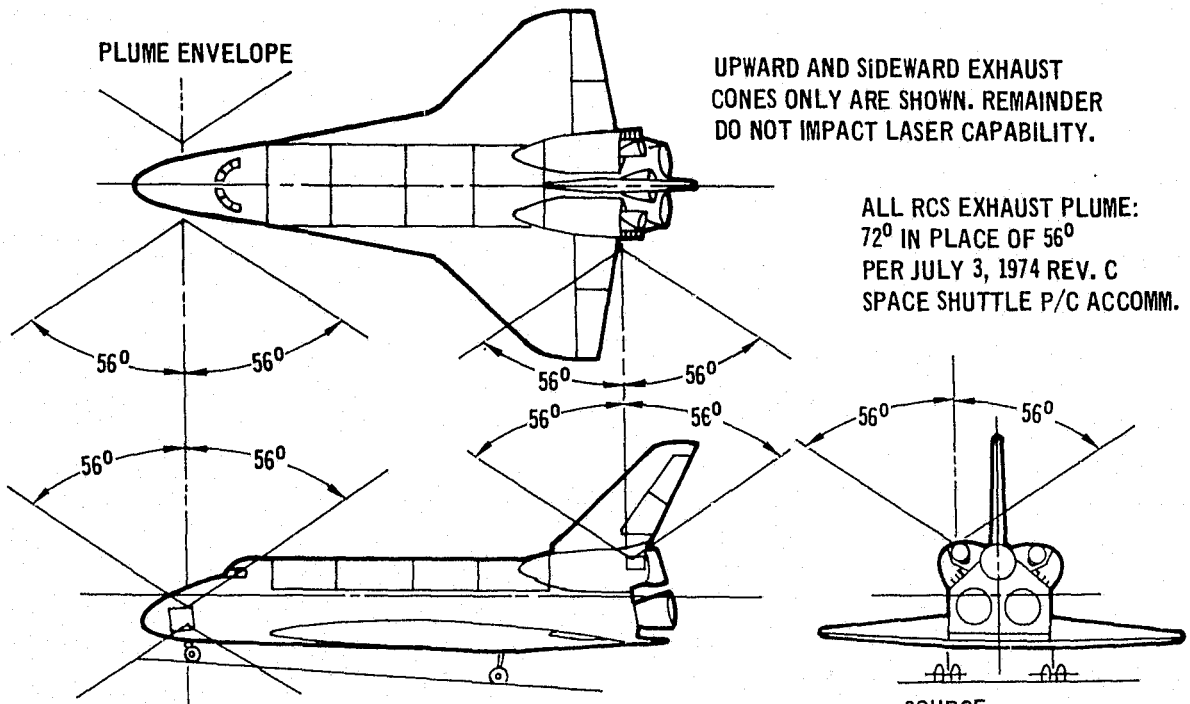

SOURCE:
SPACE SHUTTLE PAYLOAD ACCOMMODATIONS
JSC07700 VOL. XIV REV. B
21 DECEMBER 1973

The pallet electrical power supply is summarized in Figure 3-010. The information is incomplete at this time.

The information sources for the Spacelab data are the following documents:

a. Space Shuttle Payload Accommodations, JSC07700, Vol. XIV, Rev. B, 21 December 1973

b. Spacelab Payload Accommodations Handbook, Rev. A, April 1974

c. Orbiter Configuration Control Drawing, 16 August 1973, VL 70-0001400

d. October 1973 Space Shuttle Traffic Model (Jan. 1974), NASA TMX 64751, Rev. 2

In order to better define the laser communications subsystem installation concepts in Space Shuttle, candidate flights should be selected and the complete payload bay installation should be evaluated. Some of the pallet payloads are deployable telescopes and antennas which can present a major impact on the field-of-view of the laser communications receiver.

FIGURE 3-010 PALLET ELECTRICAL POWER SUPPLY

	DC		AC		
	UNREGULATED	REGULATED	400 HZ	50 HZ	60 HZ
VOLTAGE	23 TO 32 VDC	28 VDC ±2%	115/100 VAC ±5%	220 VAC ±5%	115 VAC ±5%
OUTPUTS	–	–	3 PHASE	1 PHASE	1 PHASE
FREQUENCY	–	–	400 HZ ±1%	50 HZ ±1%	60 HZ ±1%
POWER (AVG)		500 W	2.25 KVA	2 KVA	1 KVA
POWER (PEAK)		TBD	TBD	TBD	TBD
EFFICIENCY	–	90%	85%	75%	75%

SOURCE: SPACELAB PAYLOAD ACCOMMODATION HANDBOOK – REV.A APRIL 1974

3.5 SHUTTLE PAYLOAD. The Shuttle laser terminal is required to have a 1.06 μm output which will interface with the Air Force Package A in the experiment relay satellite. In addition, this terminal is required to interface with a ground station to communicate a high data rate (assumed to be 400 Mbps) from Shuttle to ground. The high data rate 0.53 μm transmitter in the experiment relay satellite is to be used as a beacon for uplink Shuttle to relay satellite pointing and a compatible ground beacon is needed for downlink Shuttle to ground pointing.

During the uplink mode of operation the Shuttle terminal must be pulsed at 3000 pulses per second with the pulse width equal to approximately 200 nsec. This mode of operation is compatible with the relay satellite Air Force Package A. For the downlink mode of operation we have assumed a link design identical to the high data rate links in the High Data Rate Optical Transceiver Terminal Final Report, Contract NAS 5-23154, May 1973. Therefore, this link requires a 400 Mbps PQM mode-locked laser output. Pulses are output in a PQM format with a nominal pulse width of 300 psec. Figure 3-011 shows the link analyses for these links.

FIGURE 3-011 SHUTTLE LINK MARGINS

PARAMETER	SHUTTLE-RELAY ACQ (VALUE) – dB		SHUTTLE-GROUND COMM (VALUE) – dB	
TRANSMITTED POWER (WATTS)	(0.234)	– 6	(0.012)	– 19
TRANSMITTED JOULES/PULSE		– 38		–105
TRANSMITTER LOSSES		– 1		– 1
POINTING LOSSES		– 4		Nil
ANTENNA GAIN (μ RAD)	(300)	86	(100)	95
SPACE LOSS		–296		–252
ATMOSPHERIC LOSS		0		– 10
RECEIVE ANTENNA GAIN (INCHES)	(7.5)	115	(48)	128
RECEIVER LOSSES		– 3		– 5
RECEIVED JOULES/PULSE		–141		–150
RECEIVED PHOTONS/PULSE		46		37
QUANTUM EFFICIENCY (%)	(1)	– 20	(1)	– 20
RECEIVED PE/PULSE		26		17
REQUIRED PE/PULSE		20		11
MARGIN		6		6

The link margins are shown for the worst case links (i.e., those requiring highest transmit power) and are based on typical telescope sizes, beamwidths and quantum efficiency.

The possibility of using a single laser for both links was examined. A mode-locked laser using external modulation to achieve bursts of mode-locked pulses for the uplink PIM pulses incurs a 35-dB loss due to the low duty factor of the resulting signal. We discarded this approach since a mode-locked laser with hundreds of watts of output would be required.

A laser which is capable of both mode-locked operation and Q-switched operation could be developed. The development of this dual-mode laser would require a compromise of nonoptimum design characteristics. Parameters such as rod length and end-mirror reflectivity would be compromised for each mode of operation. It is likely that considerable development expense would be required in order to achieve the 234 mW required for the uplink with these compromises.

A third method is to develop a mode-locked cavity-dumped laser. This laser would be optimized for mode-locked operation and would include an additional intra-cavity element to dump the mode-lock pulses either continuously for downlink communications or in bursts for uplink communications. A laser of this type suitable for the uplink has considerable excess margins for the downlink. This margin could go to reduce the Shuttle power drain with a laser designed only for the downlink, affording a minor benefit to Shuttle with its ample power availability. In any case, a new laser is required for this approach.

A method which requires no additional laser development program would utilize separate uplink and downlink lasers. For the uplink, the laser would be identical to the beacon laser being developed by the Air Force Program 405B. For the downlink, the laser would be identical to the high data rate laser being developed by NASA. This terminal would use components developed in the current ongoing programs as follows:

Component	Similar To*
Acquisition and Tracking Detector and Electronics	Package B
Command Receiver	New
High Data Rate Laser	HDROTT
High Data Rate Modulator	HDROTT
8 Inch Telescope	New
Beam Manipulation Optics	Package B

*Package B is the high data rate receive terminal defined in Space Data Relay Subsystem, Laser Communications, Preliminary Subsystem Design, SAMSO TR 71-251, November 1971. HDROTT refers to High Data Rate Optical Transceiver Terminal, Contract NAS 5023154 Final Report, May 1973.

The ground station would be implemented with either a CW or mode-locked 0.53 μm laser since either is compatible with the deflectable photomultiplier tracking detector. This approach is recommended for its minimal program impact.

The Shuttle payload instrumentation will consist of buffering and scaling amplifiers to interface with on-board display equipment as well as telemetry equipment for transmission to the ground. The monitored points will be available at a patch panel for cross-connection into a multi-channel strip chart recorder, high-speed counter/timer, and an oscillosope. Cabling precludes monitoring very high-speed signals on pallet-mounted equipment without EVA. EVA is undertaken only if diagnostics indicate a high probability that repair will be successful.

3.6 RELAY SATELLITE ORBIT. A description of the baseline orbit for the Laser Data Transfer Flight Experiment is presented in this section. Comparative advantages and disadvantages of alternative orbits also are discussed.

Experiment orbit selection criteria are defined in Figure 3-012. A primary requirement for the experiment orbit is that it shall permit evaluation of system performance over communication links similar to those envisioned for an operational communications system in order to enhance the credibility of laser communication system flight demonstration results. Two operational missions that have been identified are (1) a data relay link between a low altitude satellite and a synchronous satellite and (2) a data relay link between two

FIGURE 3-012 EXPERIMENT ORBIT SELECTION CRITERIA

- SYNCHRONOUS RELAY SATELLITE-TO-GROUND STATION RANGE DURING COMMUNICATION PERIOD
- ATLAS F LAUNCH VEHICLE
- WESTERN TEST RANGE LAUNCH SITE
- DAILY VIEW TIME FROM GODDARD SPACE FLIGHT CENTER
- CONTINUOUS DEEP SPACE VIEW ANGLE FOR CO_2 DETECTOR RADIATION COOLER

synchronous satellites. It is desirable that range and range rate dynamics of the experiment orbit be similar to those for the low altitude to synchronous altitude link. The extremely long ranges attainable in the synchronous altitude to synchronous altitude link cannot be duplicated by any practical experiment orbit. Other primary requirements constraining experiment orbit selection are that it provide a daily viewing opportunity at GSFC for NASA and Cloudcroft for the Air Force and that the relay satellite be launched out of the Western Test Range on an Atlas F launch vehicle.

3.6.1 Baseline Relay Satellite Orbit. A twelve hour, 63.4 degree inclination, synchronous apogee altitude orbit which provides more than ten hours daily viewing time to both ground sites is recommended for the Laser Data Transfer Flight Experiment. Key baseline relay satellite orbit parameters are presented in Figure 3-013. The orbit is highly eccentric with a 926 km perigee altitude and a 39,438 km apogee altitude. The baseline orbit is in compliance with the synchronous range requirement, and it is compatible with an Atlas F launch out of WTR for the 700 pound to 1000 pound projected on-orbit satellite weight. Apogee location is maintained over a fixed ground site, 63.4 degrees North latitude and 91.5 degrees West longitude, for the mission duration and, thus daily viewing opportunities are realized.

FIGURE 3-013 BASELINE EXPERIMENT ORBIT PARAMETERS

APOGEE ALTITUDE	39,438 Km
PERIGEE ALTITUDE	926 Km
ORBIT PERIOD	11.96 HR
NOMINAL EARTH-REFERENCED APOGEE LOCATION	63.4° N LAT 91.5° W LONG

ORBITAL ELEMENTS	
SEMI-MAJOR AXIS (a)	26,562 Km
ECCENTRICITY (e)	0.725
ARGUMENT OF ASCENDING NODE (Ω)	TBD
INCLINATION (i)	63.4 DEG
ARGUMENT OF PERIGEE (u_p)	-90.0 DEG
TIME OF PERIGEE PASSAGE (τ_p)	TBD

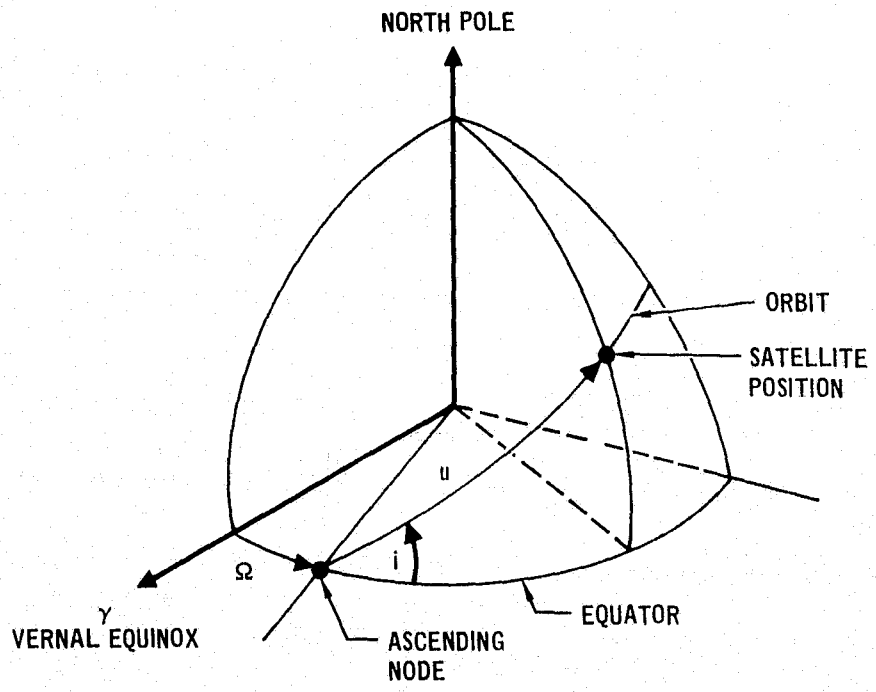

The -90 degree argument of perigee places apogee at the northernmost geographic latitude (i.e., 63.4 degrees) at time τ_p corresponding to time of occurrence of first operational apogee. Earth-referenced longitude of apogee at time τ_p then is defined by the argument of ascending node (Ω) which is measured eastward from vernal equinox. Both τ_p and Ω currently are undefined since they depend upon a launch time to be specified.

The basis for the baseline experiment orbit recommendation, impact of the recommended orbit on deep space view availability for the CO_2 detector radiation cooler, and communication link kinematics are presented in the following paragraphs.

3.6.1.1 Baseline Orbit Selection. The three primary orbit requirements that influence orbit selection are (1) synchronous range during a portion of each communication experiment period, (2) daily viewing opportunities at ground sites, and (3) Atlas F launch out of WTR.

An equatorial, synchronous orbit can provide continuous viewing capability if the relay satellite were stationed within approximately 40 degrees longitude of a ground site. This orbit would also duplicate the relay satellite orbit of an operational program. However, the Atlas F launch vehicle cannot place a 700 pound to 1000 pound satellite in an equatorial synchronous orbit.

Orbits with repeating ground tracks on a daily basis also can provide daily viewing opportunities. The daily view time at Goddard for several elliptical repeating ground track orbits is shown in Figure 3-014, where view time is defined as the interval during which the relay satellite elevation at Goddard is greater than 30 degrees. The available daily view time is approximately 10.8 hours, 6.5 hours, and 4.2 hours for the N=2, N=3, and N=4 orbits, respectively. However, Figure 3-014 also shows that only one of the repeating orbits, the N=2 orbit, provides low altitude to synchronous relay satellite range. Therefore the N=2 orbit, which completes slightly more than two revolutions as the earth rotates through one revolution about its axis, is selected as baseline. Its orbital period is slightly shorter than one-half the earth's rotational period to compensate for nodal regression due to earth oblateness.

The history of range from Goddard to the relay satellite, shown in Figure 3-015 for a complete orbital revolution, illustrates the compliance of the baseline orbit with the synchronous range requirement. The range is slightly greater than 40,000 km when the relay satellite is at apogee, and it is greater than 35,000 km for almost five hours.

FIGURE 3-014 GODDARD DAILY VIEW TIME AND RANGE FOR REPEATING ORBITS

• APOGEE AT 63.4°N LAT, 91.5° W LONG

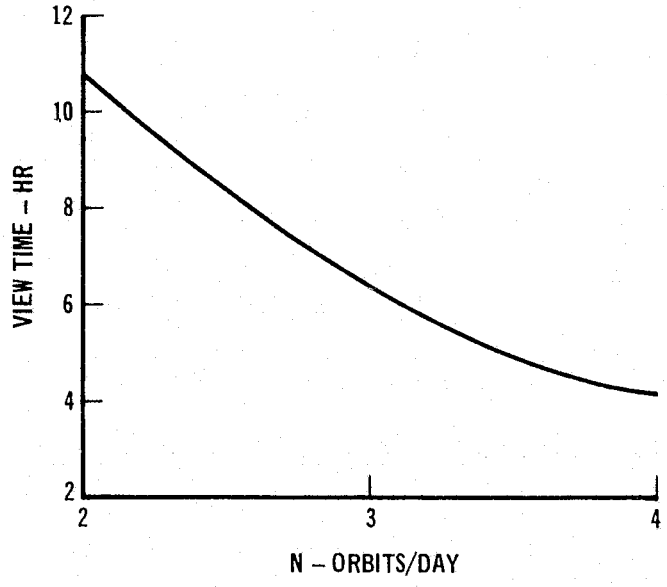

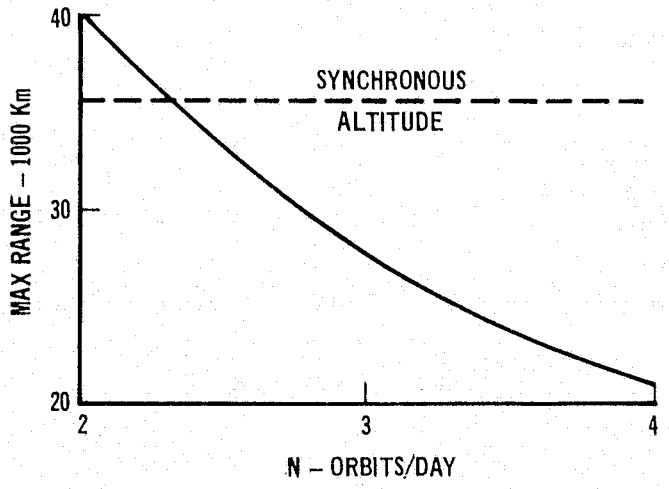

FIGURE 3-015 RELAY SATELLITE RANGE FROM GODDARD FOR BASELINE EXPERIMENT ORBIT

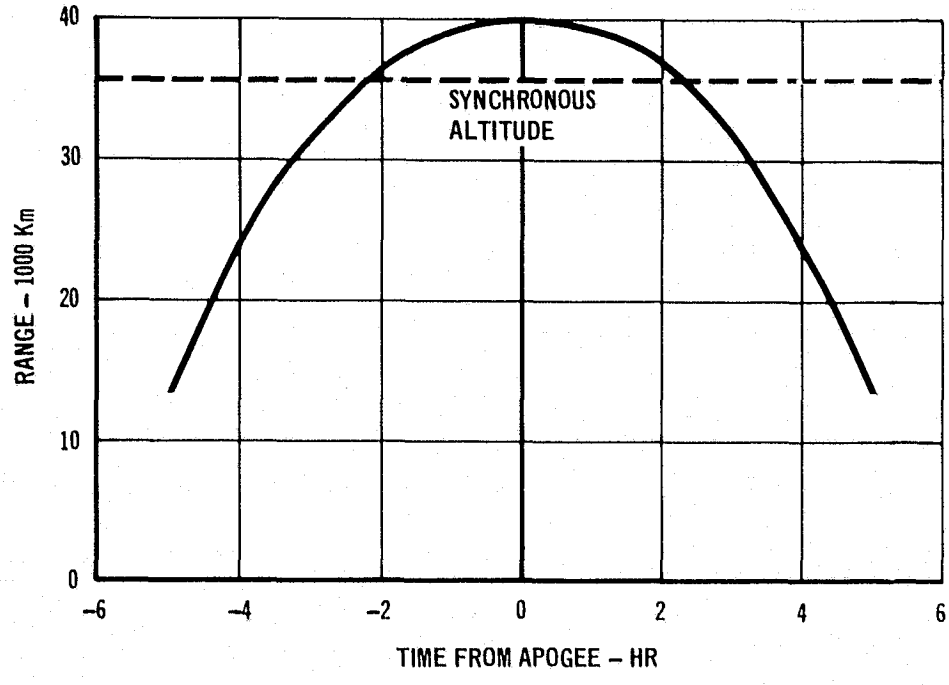

Allowable apogee location relative to Goddard is constrained by the requirement for a daily viewing opportunity at Goddard. A plot of available Goddard view time versus earth-referenced longitude of apogee relative to Goddard is shown in Figure 3-016 for the baseline orbit with apogee at 63.4 degrees North latitude. Apogee must be located within 57 degrees and 75 degrees longitude of Goddard to provide six hour viewing intervals with minimum satellite elevation angles of 40 degrees and 30 degrees, respectively.

The earth-referenced location of apogee is somewhat arbitrarily defined as 63.4 degrees North latitude and 91.5 degrees West longitude, the longitude midpoint between Goddard and Cloudcroft. This apogee location is maintained nominally throughout the mission. The resulting ground track for the baseline orbit and the corresponding satellite elevation profile at Goddard are presented in Figures 3-017 and 3-018, respectively. The daily Goddard viewing interval exceeds ten hours. It occurs approximately 4.5 minutes earlier each day since the average orbit rate is not exactly the earth's rotational rate. The resulting 27.3 hours per year shift in viewing time allows communication tests to be performed at all times of the day.

FIGURE 3-016 GODDARD VIEWING TIME VERSUS RELATIVE LONGITUDE OF APOGEE FOR BASELINE 11.96 HR ORBIT

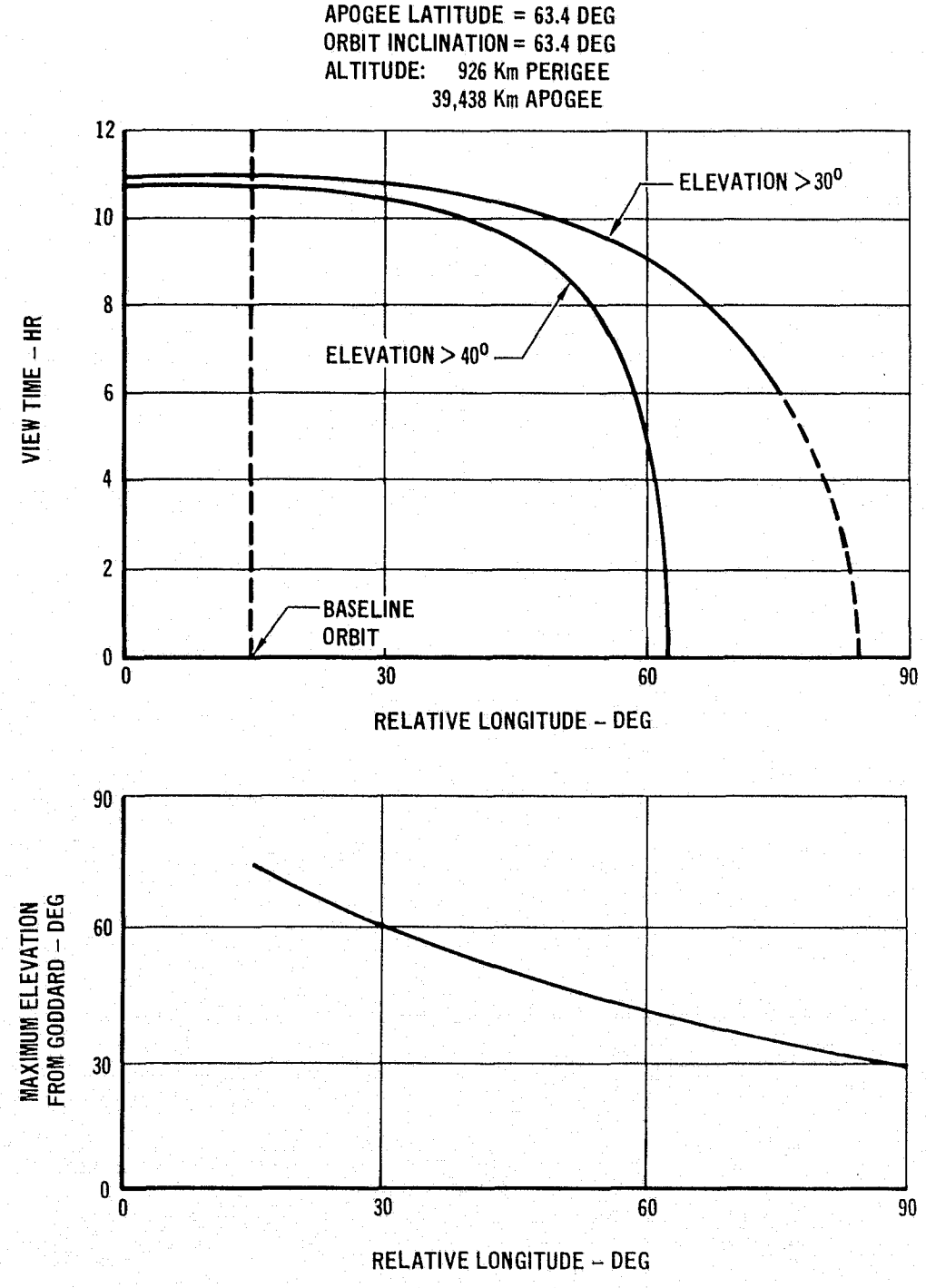

FIGURE 3-017 GROUND TRACK FOR BASELINE ORBIT

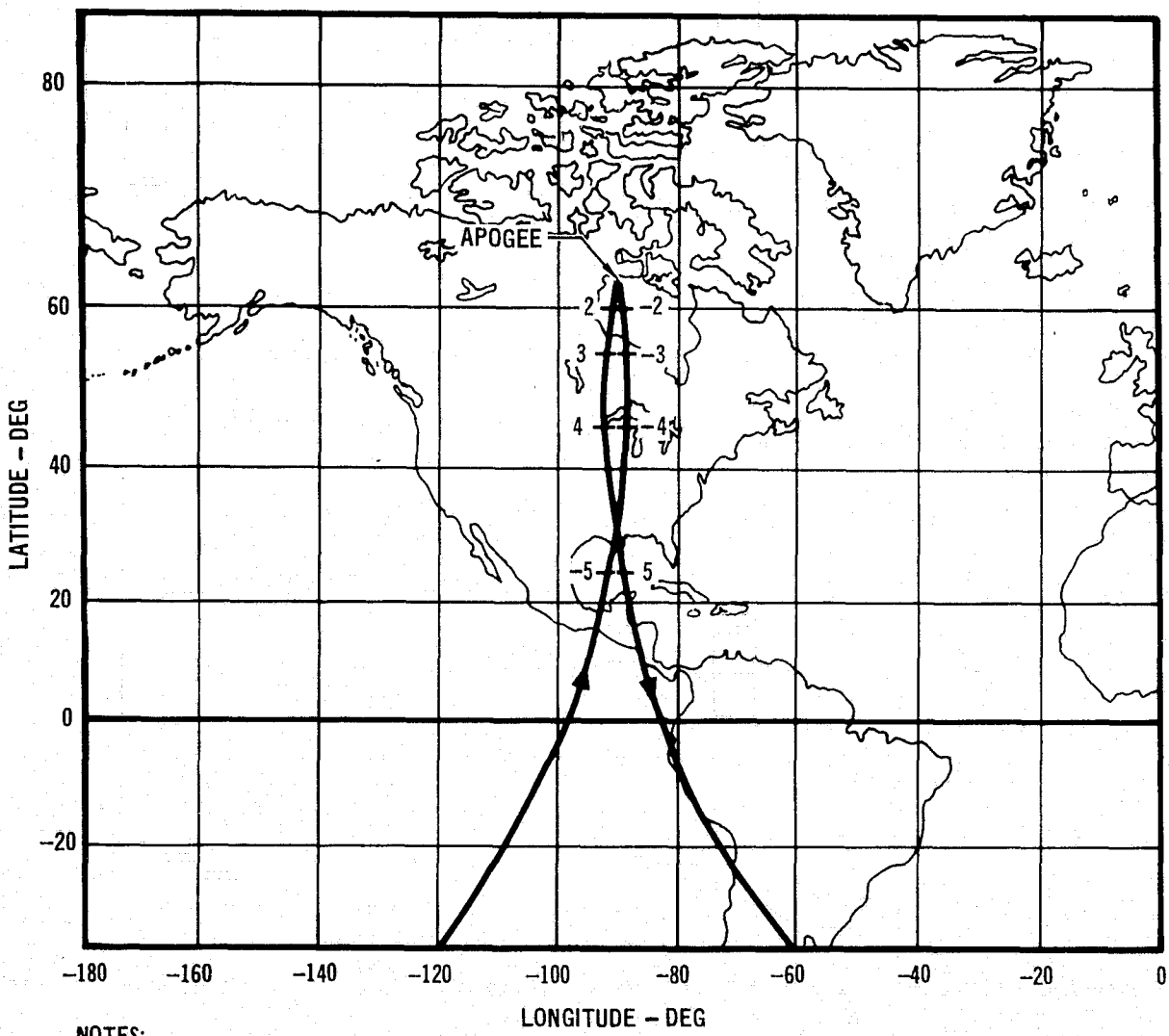

NOTES:
1) t = 0 AT APOGEE; TICK MARKS IN 1 HOUR INCREMENTS
2) APOGEE AT 63.4^0 N LAT, 91.5^0 W LONG

FIGURE 3-018 RELAY SATELLITE ELEVATION AT GODDARD

• APOGEE AT 63.4° N LAT, 91.5° W LONG

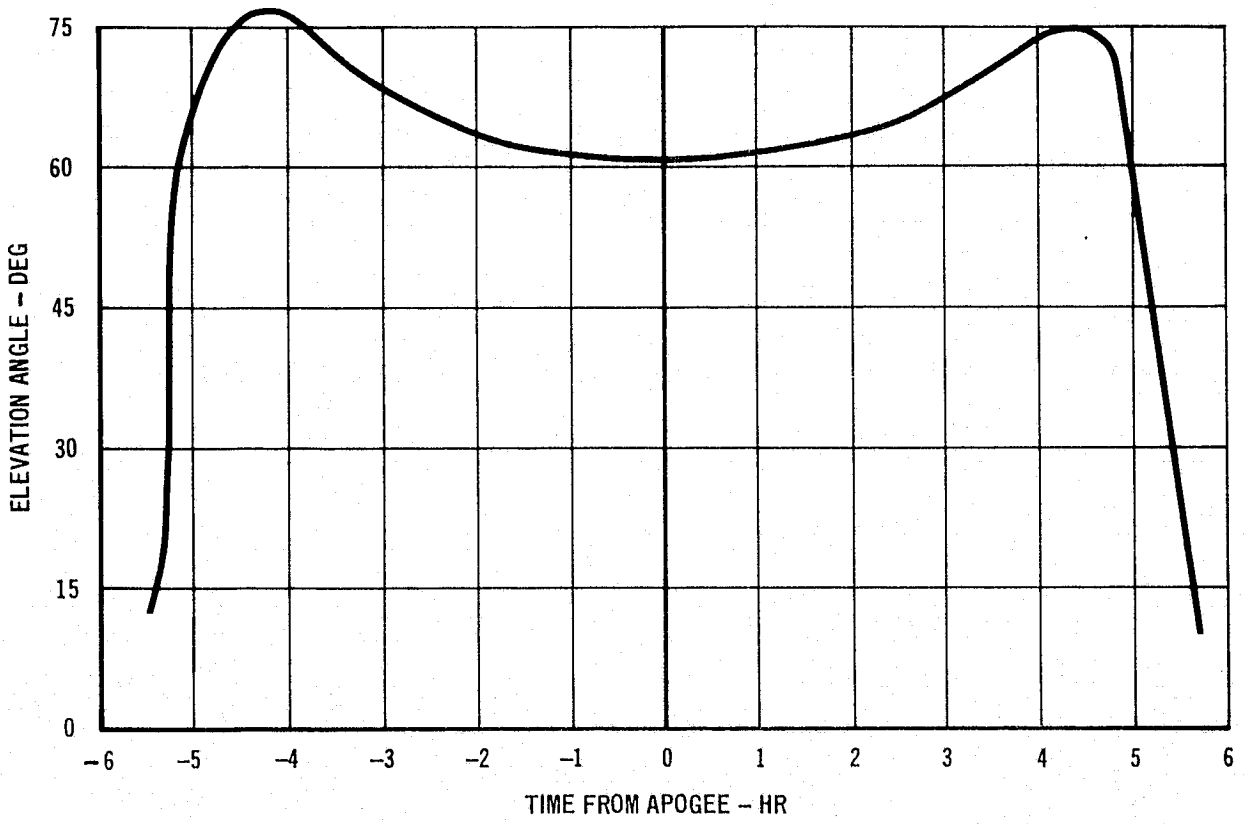

Some of the baseline orbit elements are constrained by orbital stability considerations. First order secular effects of earth oblateness on satellite earth orbits are a precession of the line of nodes (i.e. intersection of the earth's equator and orbit plane) and an advance of the line of apsides in the precessing orbit plane. These two effects, nodal precession and apsidal advance, can be "controlled" via proper selection of orbit inclination and semi-major axis to provide apogee stability relative to a selected ground site.

Orbit inclination is required to be approximately 63.4 degrees in order to maintain apogee over a fixed latitude with a non-circular orbit since the drift in the line of apsides (i.e. line between apogee and perigee) is zero for this inclination. The following equation describes the apsidal advance rate ($\dot{\omega}$) induced by the second zonal gravitational harmonic, the dominant influence.

$$\dot{\omega} = \frac{J_2 R_E^2 \sqrt{G} \, (2 - 2.5 \sin^2 i)}{a^{7/2} \, (1 - e^2)^2} \quad \text{rad/sec}$$

J_2 = Coefficient of Second Zonal Gravitational Harmonic

R_E = Earth radius

i = Inclination

a = Semimajor axis

G = Earth gravitational constant

e = Eccentricity

Nominal maintenance of apogee over a fixed ground site now is achievable for a "12-hour" orbit through proper selection of the semi-major axis of the orbit. For a spherical earth, the semi-major axis would be selected to yield an average orbit rate which is twice the earth's rotational rate. However, because of regression of the line of nodes ($\dot{\Omega}$) due to earth oblateness, the semi-major axis selected for a spherical earth representation must be modified to provide an average orbit rate that accounts for nodal regression. The nodal regression rate is defined by

$$\dot{\Omega} = \frac{J_2 R_E^2 \sqrt{G} \cos i}{a^{7/2} \, (1 - e^2)^2} \quad \text{rad/sec}$$

where a positive value for $\dot{\Omega}$ indicates westward motion. The approximate nodal regression rate for the baseline experiment orbit is 0.1356 degrees per day or 49.5 degrees per year. Therefore, the orbit period is selected to be 11.96 hours so that the satellite rises 0.08 hours (0.1356 degrees of earth rotation) earlier each day. The westward movement of the apogee caused by nodal regression is therefore negated by the eastward movement caused by the adjustment of the orbit period.

Although a payload weight penalty is incurred by raising perigee altitude, a higher perigee altitude may be required because of orbital stability considerations. Orbital decay attributable to aerodynamic drag is insignificant for the baseline orbit. However, solar radiation, the gravitational attractions of the sun and the moon, and harmonics in the earth's gravitational field do have appreciable effects on stability of the recommended experiment orbit. The precise effect of the sun and the moon is very dependent upon their relative positions, which is a function of the launch date. After a specific launch date is defined, solar and lunar effects on orbital stability must be evaluated for detailed mission planning.

3.6.1.2 CO_2 Detector Radiation Cooler Performance. A continuous view of deep space is required for the CO_2 detector radiation cooler. The cooler performance impact resulting from the moon in the view field or the sun near the view field is unknown. Therefore, orbital conditions which result in potential sun and moon interference with cooler performance were defined.

Sun Interference - The incidence angle of the sun's rays on the satellite depends upon the orbital position of the satellite (u), the position of the earth in its orbit about the sun, and the inclination of the satellite orbit plane relative to the ecliptic plane (I). The position of the earth in its solar orbit is depicted in Figure 3-019 by u_s, the position of the sun in its "apparent" orbit about the earth as viewed in an earth-centered reference frame.

The inclination of the orbit plane with respect to the ecliptic plane (I) is a function of the right ascension of ascending node of the satellite orbit plane (Ω), orbit inclination relative to the equatorial plane (i), and the inclination of the ecliptic plane relative to the equatorial plane (i_s) which is constant and approximately 23.45 degrees. For a given orbit inclination, the only variable that affects I is Ω, which is launch time dependent. For example, a launch time which results in a first operational apogee at midnight

FIGURE 3-019 GEOMETRY FOR DETERMINATION OF INCIDENCE ANGLE OF SUN'S RAYS ON SATELLITE

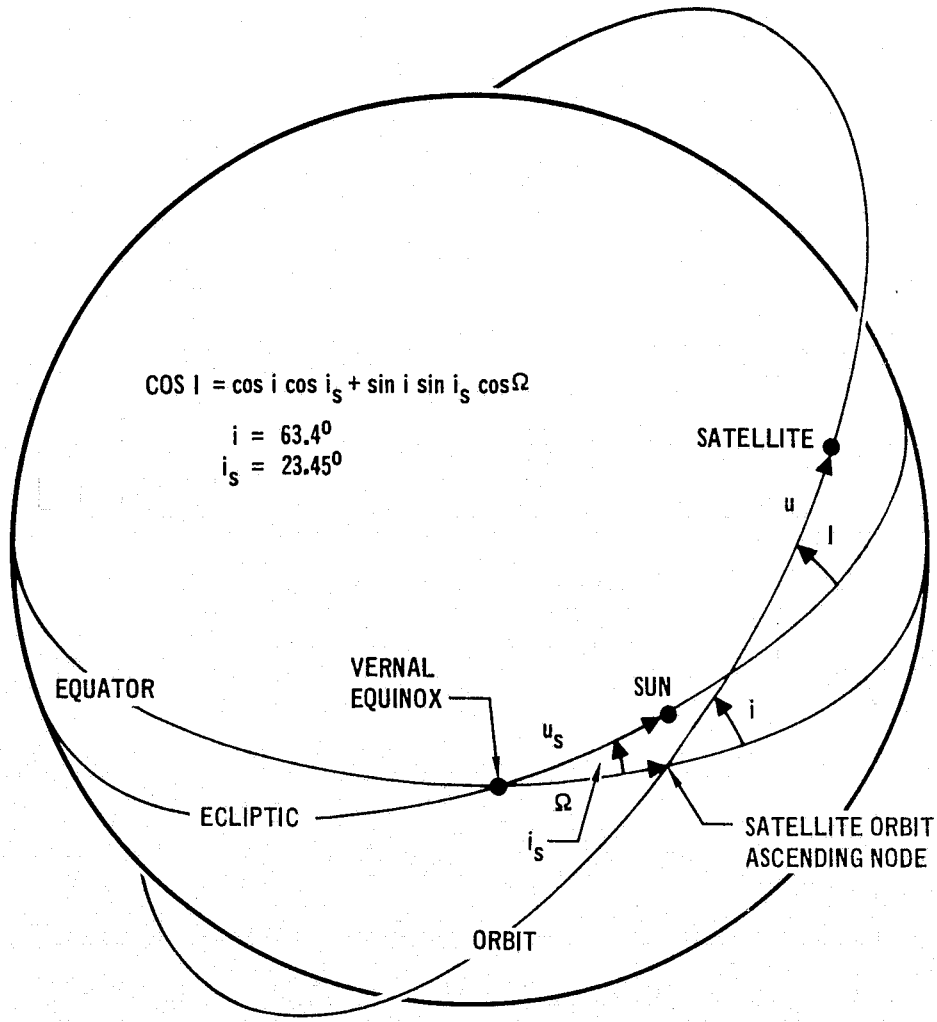

local time at apogee longitude on winter solstice corresponds to an initial Ω=0. The only subsequent variation in Ω during the mission, neglecting second order effects of earth oblateness, is a nodal regression of approximately 49.5 degrees per year due to the second zonal gravitational harmonic. Therefore, after a specific launch time has been defined, unique histories of Ω and I can be computed for the mission.

Sun azimuth and elevation angle profiles were generated for a variety of orbital conditions in order to define orbital geometry which results in the sun being in the proximity of the radiation cooler field of view. Plots of sun elevation relative to the local horizontal plane at four times of the year are shown in Figure 3-020 for Ω=0 degrees and Ω=180 degrees.

Figure 3-019 shows that for Ω=0 the ascending node of the satellite orbit plane is at vernal equinox. Therefore, when the satellite is at ascending node and the sun is at vernal equinox, the sun elevation relative to the local horizontal plane is +90 degrees since the earth, the satellite and the sun are collinear at that time. The sun zenith condition (i.e., +90 degrees elevation) also is obtained when the satellite is at descending node and the sun is at autumnal equinox, with Ω=0.

A brief parametric analysis was performed to define the worst-case combination of time of year, satellite orbit angle (u), and angle between satellite orbit ascending node and vernal equinox (Ω) which results in the sun approaching the cooler view field. The angular separation between the sun line and the radiation cooler field of view is shown in Figure 3-021 for the worst-case orbital conditions which were found. Figure 3-021 shows that the sun is within five degrees and ten degrees of the radiation cooler view field for approximately 17 minutes and 29 minutes, repectively. The tangency condition occurs approximately one hour after perigee, which allows two hours for recovery prior to the six hour communication period centered about apogee.

Moon Interference - A worst-case analysis was performed to determine the maximum length of time that the moon is in the field of view of the CO_2 detector radiation cooler. The azimuth orientation of the radiation cooler field of view "centerline" is fixed relative to the sun line. Therefore, since the right ascension of the moon relative to the sun describes a circle once each lunar orbital period ($\simeq$28 days), the moon is within the view field for some portion

FIGURE 3-020 SUN ELEVATION PROFILES FOR Ω = 0 AND 180 DEGREES

926 KM X 39432 KM, i = 63.4° ORBIT
ARGUMENT OF PERIGEE = −90°
Ω = ANGLE BETWEEN ORBIT ASCENDING NODE AND VERNAL EQUINOX

SUN POSITION
- VERNAL EQUINOX
- SUMMER SOLSTICE
- AUTUMNAL EQUINOX
- WINTER SOLSTICE

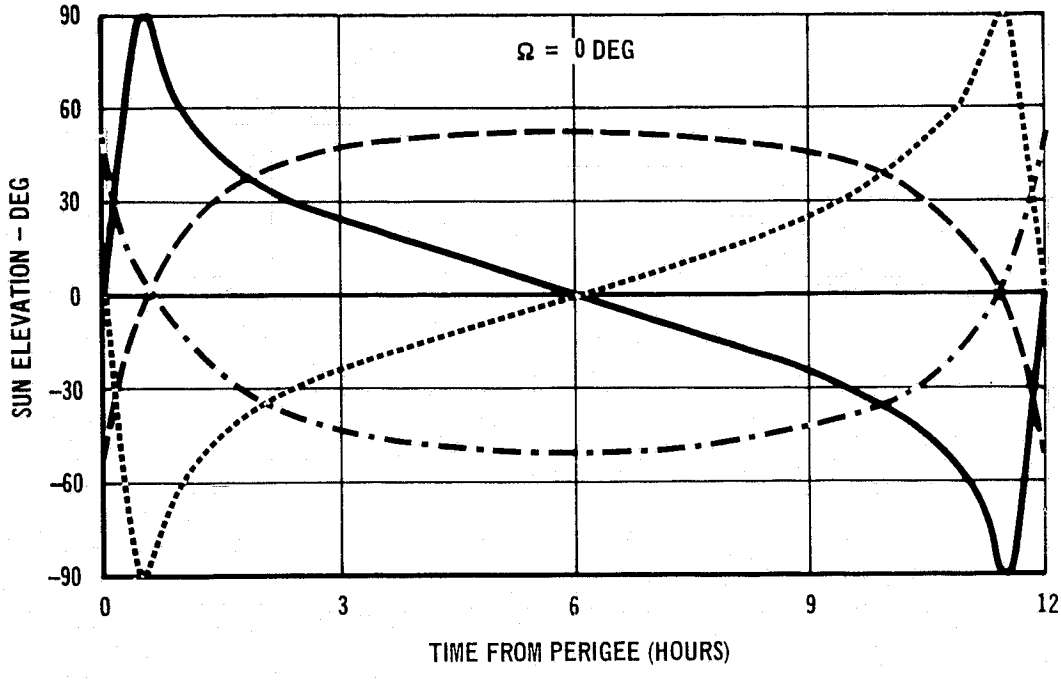

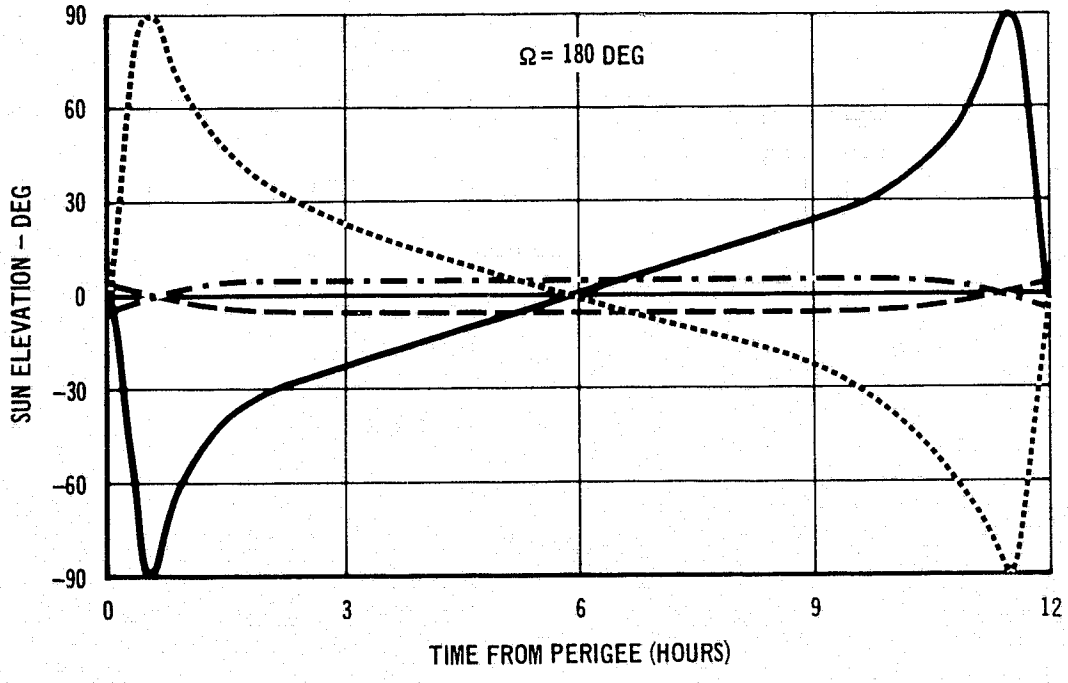

FIGURE 3-021 WORST CASE SUN LINE – CO_2 RADIATOR FOV GEOMETRY

SAME ORBIT AND TIME OF YEAR AS FIGURE Z-038

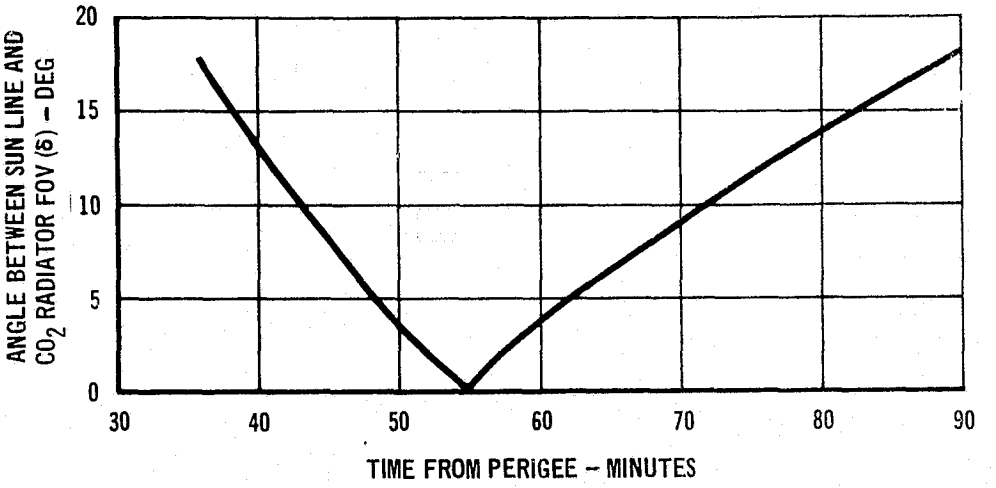

of each 28 day period. The number of days per lunar orbital period and the time per satellite orbital revolution on those days depend upon the satellite orbit plane orientation relative to the sun and the moon.

Moon interference conditions for three 30 day periods are shown in Figure 3-022 for an assumed launch time which results in a first operational apogee at 3:00 A.M. local time at 91.5 degrees West longitude on 21 December, 1978. Launch time specification uniquely defines the spatial orientation of the orbit plane relative to the sun and the moon. A simplifying assumption employed in the analysis is that the positions of the sun and moon are fixed for one day intervals. Note that the moon is inside the field of view for substantial portions of the experiment orbit for periods of a week or more.

The angle between the line of sight to the moon and the centerline of the radiation cooler field of view is plotted in Figure 3-023 for two days in which the moon is in the field of view for a complete satellite orbital revolution. The moon is only ten degrees inside the field of view for ± 4 hours about apogee in the 5 October, 1979 orbit, but it is almost in the center of the view field for several hours of the 12 April, 1979 orbit.

3.6.1.3 Relay Satellite to Shuttle Link Kinematics. Pointing angle and pointing angle rate histories were generated for the relay satellite to Shuttle link to aid in defining relay satellite and Shuttle laser terminal requirements.

FIGURE 3-022 TIME PERIOD THAT MOON-IN-THE-FOV CONDITIONS EXIST FOR SEVERAL 30 DAY PERIODS

- BASELINE RELAY SAT. ORBIT
- FIRST APOGEE AT 3 AM GODDARD LOCAL TIME, 21 DECEMBER 1978

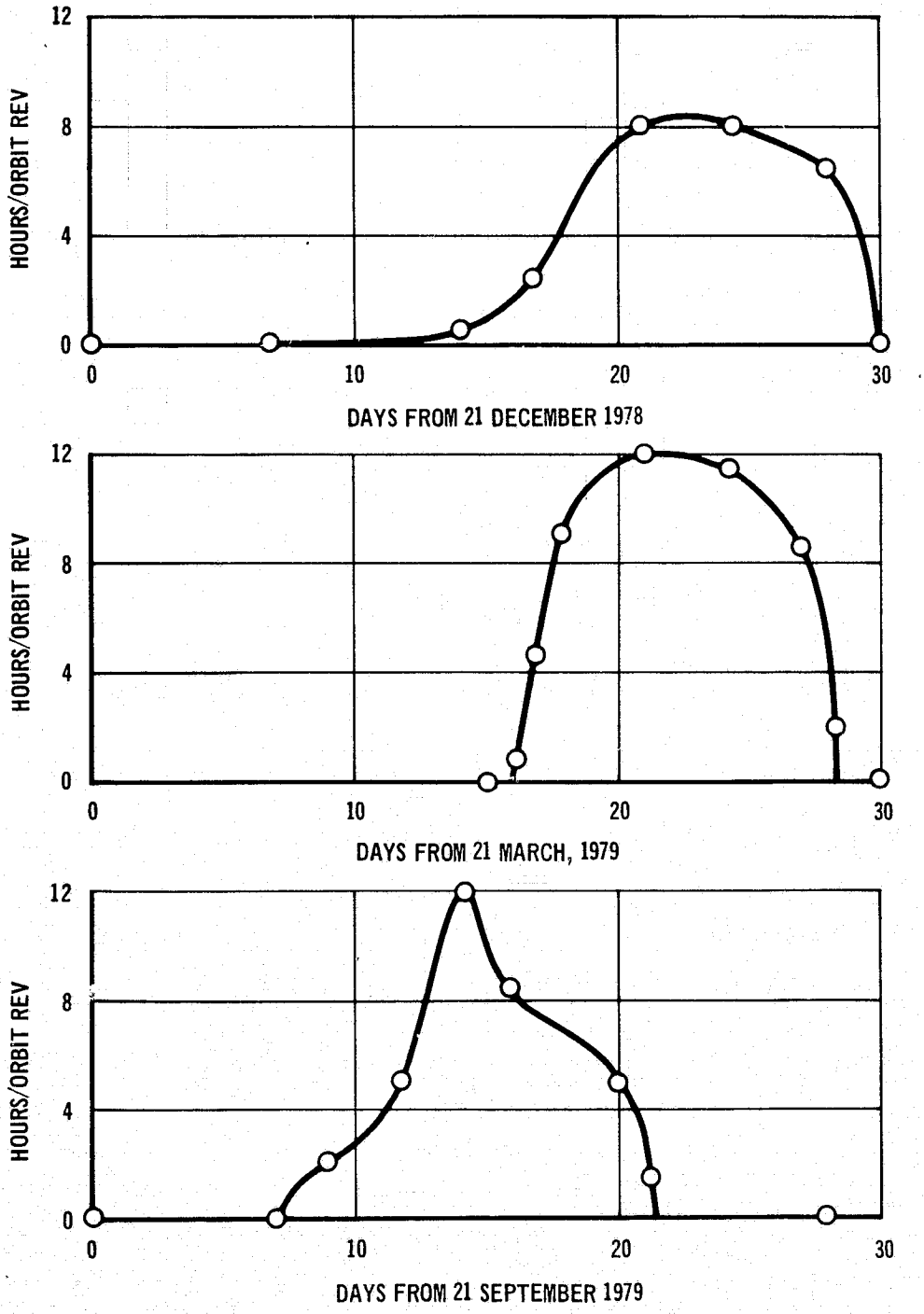

FIGURE 3-023 ANGLE BETWEEN LINE OF SIGHT TO THE MOON AND CENTER OF CO_2 RADIATION COOLER FOV

- BASELINE 926 X 39428 NM, i= 63.4° ORBIT
- FIRST APOGEE OVER GODDARD AT 3 AM LOCAL TIME ON 21 DECEMBER 1978
- RADIATOR: 120° FOV, CANTED 30° ABOVE NORMAL TO SOLAR PANELS

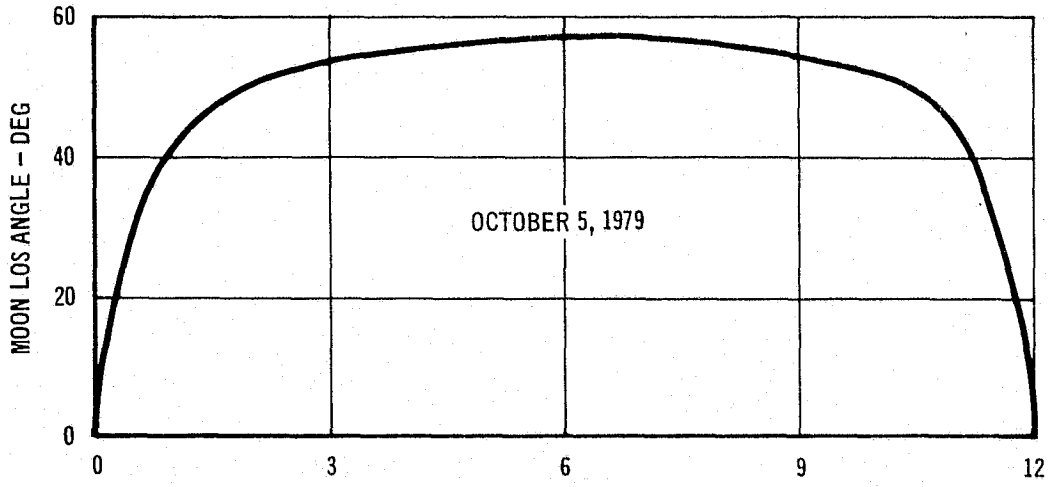

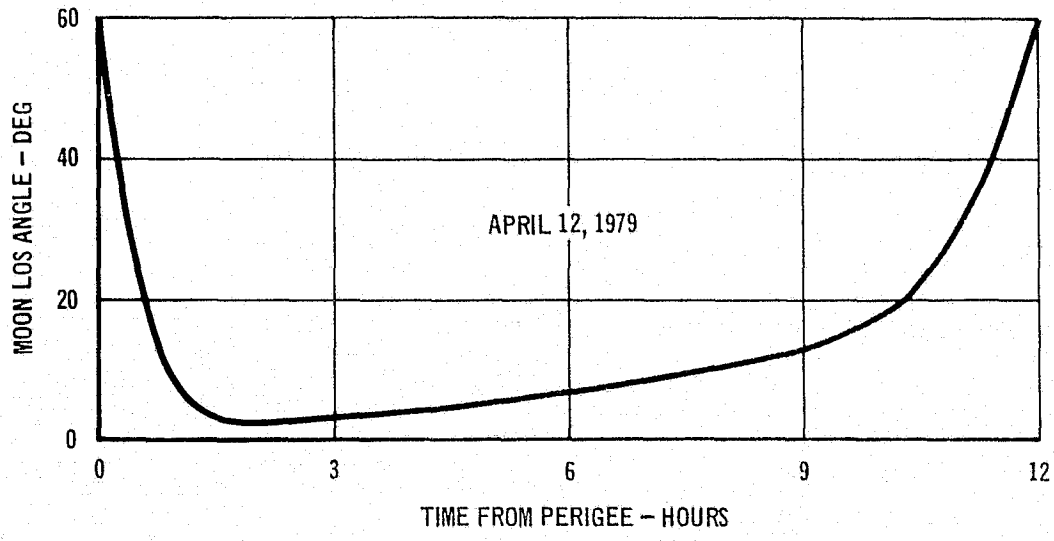

The pointing angles and pointing angle rates for both terminals were derived for a roll-pitch rotation sequence relative to local vertical/orbit plane (LV/OP) coordinates. Pointing angle geometry is illustrated in Figure 3-024. A Shuttle LV/OP, orthogonal, right-hand coordinate set (X_o, Y_o, Z_o) is defined with $+X_o$ along the local vertical and positive upward, $+Z_o$ along the velocity vector, and $+Y_o$ along the orbit normal. The Shuttle pointing angles (α, β) define the orientation of the Shuttle-to-relay satellite LOS vector relative to X_o, Y_o, Z_o coordinates, where the pointing angles are zero with the relay satellite at zenith. The first rotation in the roll-pitch sequence is through a positive roll angle ($+\alpha$) about the $+Z_o$ axis, and the second rotation is through a positive pitch angle ($+\beta$) about the new +Y axis.

The relay satellite LV/OP coordinate set (x_o, y_o, z_o) is defined with $+x_o$ along the relay satellite local vertical and positive downward, $+y_o$ along the orbit normal and positive to the right of the orbit plane, and $+z_o$ forms a right-hand, orthogonal set. The relay satellite roll and pitch pointing angles (ϕ, θ) specify the orientation of the relay satellite-to-Shuttle LOS vector relative to x_o, y_o, z_o coordinates, and the pointing angles are zero when the Shuttle is at nadir. The first rotation in the roll-pitch sequence is through a positive roll angle ($+\phi$) about $+z_o$ and the second rotation is through a positive pitch angle ($+\theta$) about the new y axis.

Note that the pointing angles are referenced to orbital coordinates, not body-fixed coordinates. Therefore, when relating the pointing angles as defined previously to payload gimbal angles, the orientation of relay satellite and/or Shuttle body axes relative to LV/OP coordinates and gimbal geometry relative to body axes must be considered. With the current baseline relay satellite concepts, the outer gimbal axis is aligned parallel to the $+Y_B$ axis as shown in Figure 3-025. The inner gimbal axis is orthogonal to the outer gimbal axis and along $-X_B$ when the outer gimbal angle is zero. Since $+X_B$ is normal to the solar panels and since the relay satellite is sun-oriented in azimuth, the only time that the outer gimbal angle is the same as the roll pointing angle defined above is when the sun line is normal to and to the right of the orbit plane.

Relay satellite to Shuttle link kinematics were evaluated for two Shuttle orbits--a 28.5 degree inclination, 370 km circular orbit and a 55 degree inclination, 370 km circular orbit. These inclinations were selected from

FIGURE 3-024 RELAY SATELLITE/SHUTTLE TERMINALS POINTING ANGLE GEOMETRY

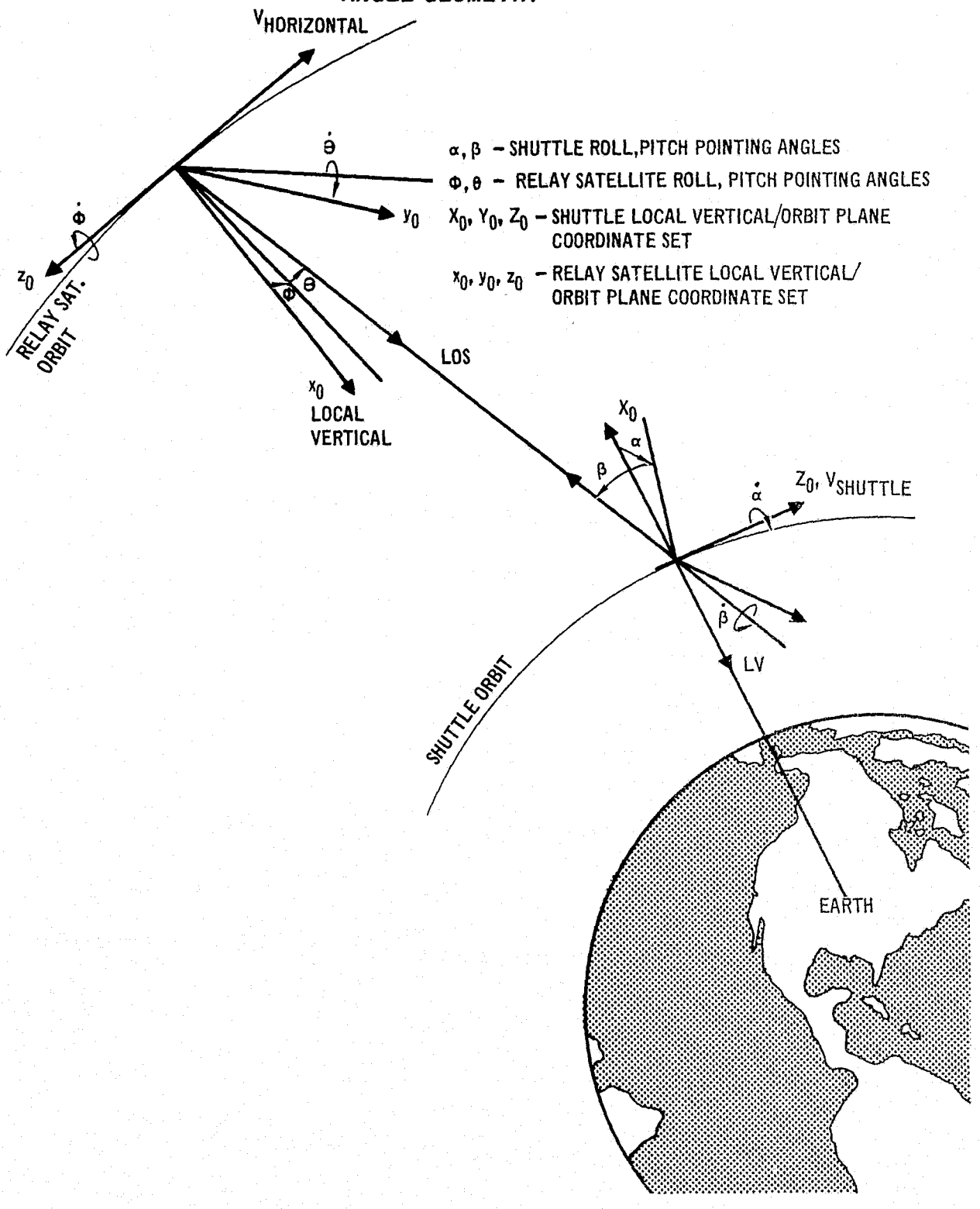

FIGURE 3-025 RELAY SATELLITE GIMBAL AXIS/BODY AXIS GEOMETRY

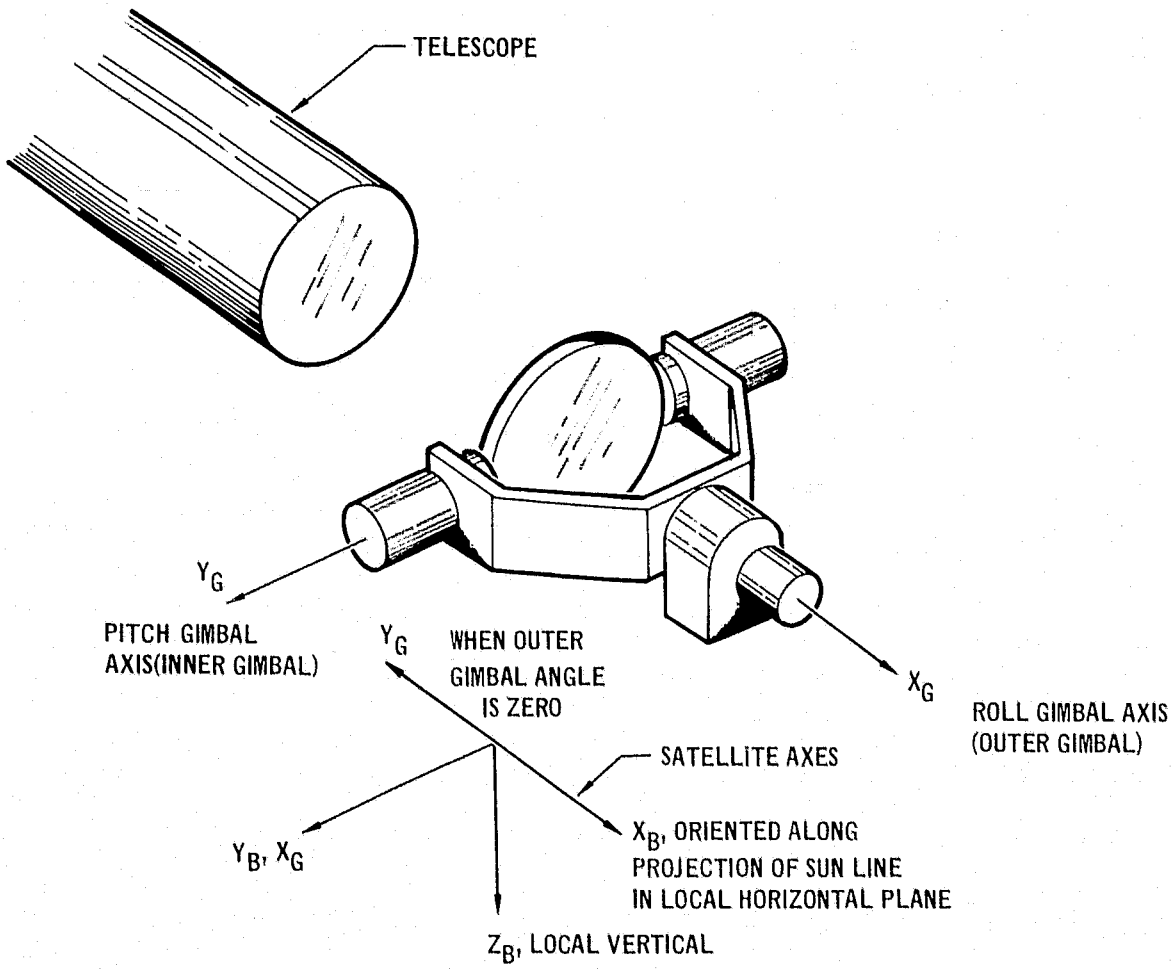

the Shuttle manifest listed in the Shuttle Interfaces section of this report. Typical pointing angles and pointing angle rate profiles at the relay satellite and Shuttle terminals are shown in Figure 3-026 and Figure 3-027, respectively for the 28.5 degree inclination Shuttle orbit with the relay satellite near apogee during a Shuttle pass. Corresponding range and range rate histories are plotted in Figure 3-028. Argument of ascending node of the Shuttle orbit is approximately 90 degrees west of apogee longitude for the Shuttle pass illustrated in Figures 3-026 through 3-028, and Shuttle argument of latitude is +90 degrees when the relay satellite is at apogee. This relative orbital phasing of the relay satellite and the Shuttle provide the peak tracking rates anticipated in this link when the relay satellite is near apogee. These pointing angles and pointing angle rates are well within the capability of the payload acquisition and tracking system.

The pointing angle and pointing angle rate capabilities required for the relay satellite depend upon the portion of the relay satellite orbit in which communication tests will be performed. Approximately 25 degrees gimbal angle range is required to provide hemispherical contact capability with the Shuttle if communication tests are performed within ± 3 hours about apogee; more than 40 degrees gimbal angle range is required if the allowable communication period is extended to ± 5 hours about apogee. A 180 degree gimbal angle range is required for the Shuttle terminal since 180 degrees gimbal angle range is needed to maintain hemispherical contact with a synchronous satellite from low altitude orbits.

Pointing angle and pointing angle rate profiles for the relay satellite and Shuttle terminals are shown in Figures 3-029 and 3-030 for a 55 degree inclination Shuttle orbit with the relay satellite near apogee. Range and range rate histories are plotted in Figure 3-031. The relative orbital phasing of the relay satellite and Shuttle for this pass provide the highest tracking rates anticipated in this link when the relay satellite is near apogee. The only significant difference between the pointing angle dynamics for the 28.5 degree and 55 degree inclination Shuttle orbits is that higher tracking rates are obtained in the 55 degree Shuttle orbit.

The link geometry presented in Figures 3-026 through 3-031 does not define the maximum tracking rates or the maximum relay satellite pointing requirements, since the relay satellite is near apogee in the cases illustrated

FIGURE 3-026 RELAY SATELLITE POINTING ANGLES AND POINTING ANGLE RATES – RELAY SAT. TO SHUTTLE LINK

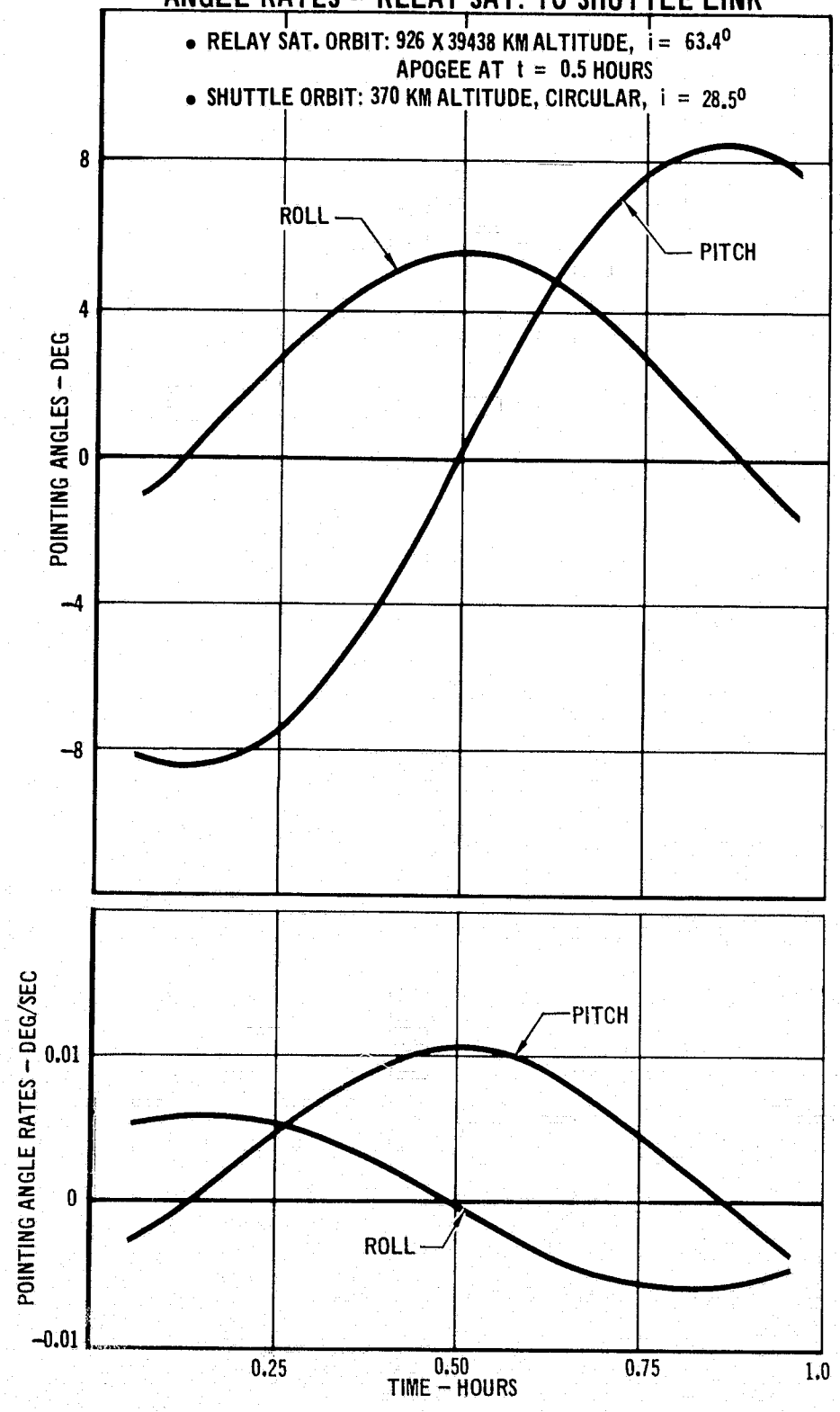

FIGURE 3-027 SHUTTLE POINTING ANGLES AND POINTING ANGLE RATES – RELAY SATELLITE TO SHUTTLE LINK

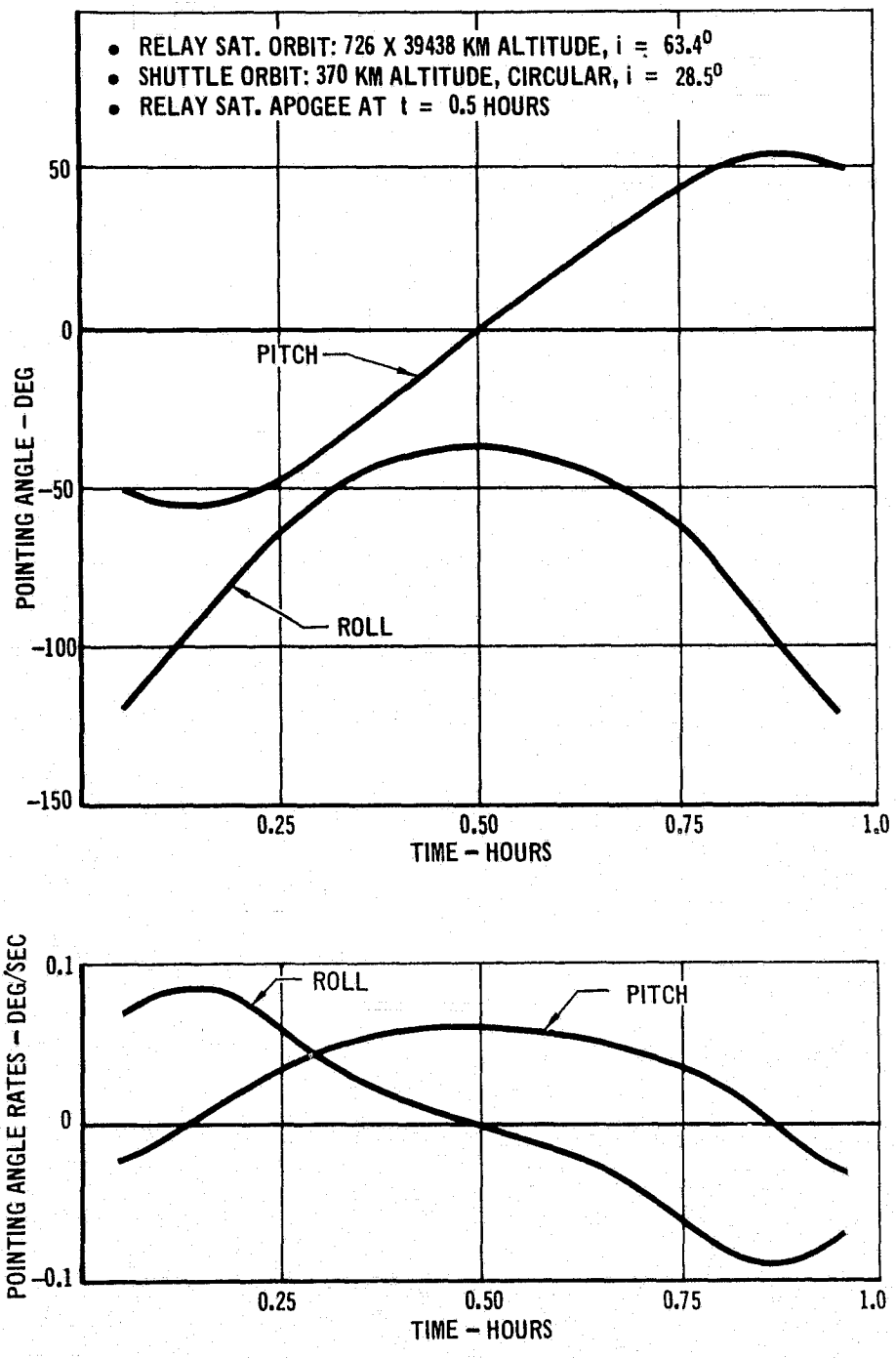

FIGURE 3-028 RANGE AND RANGE RATE HISTORIES FOR RELAY SATELLITE/SPACE SHUTTLE LINK

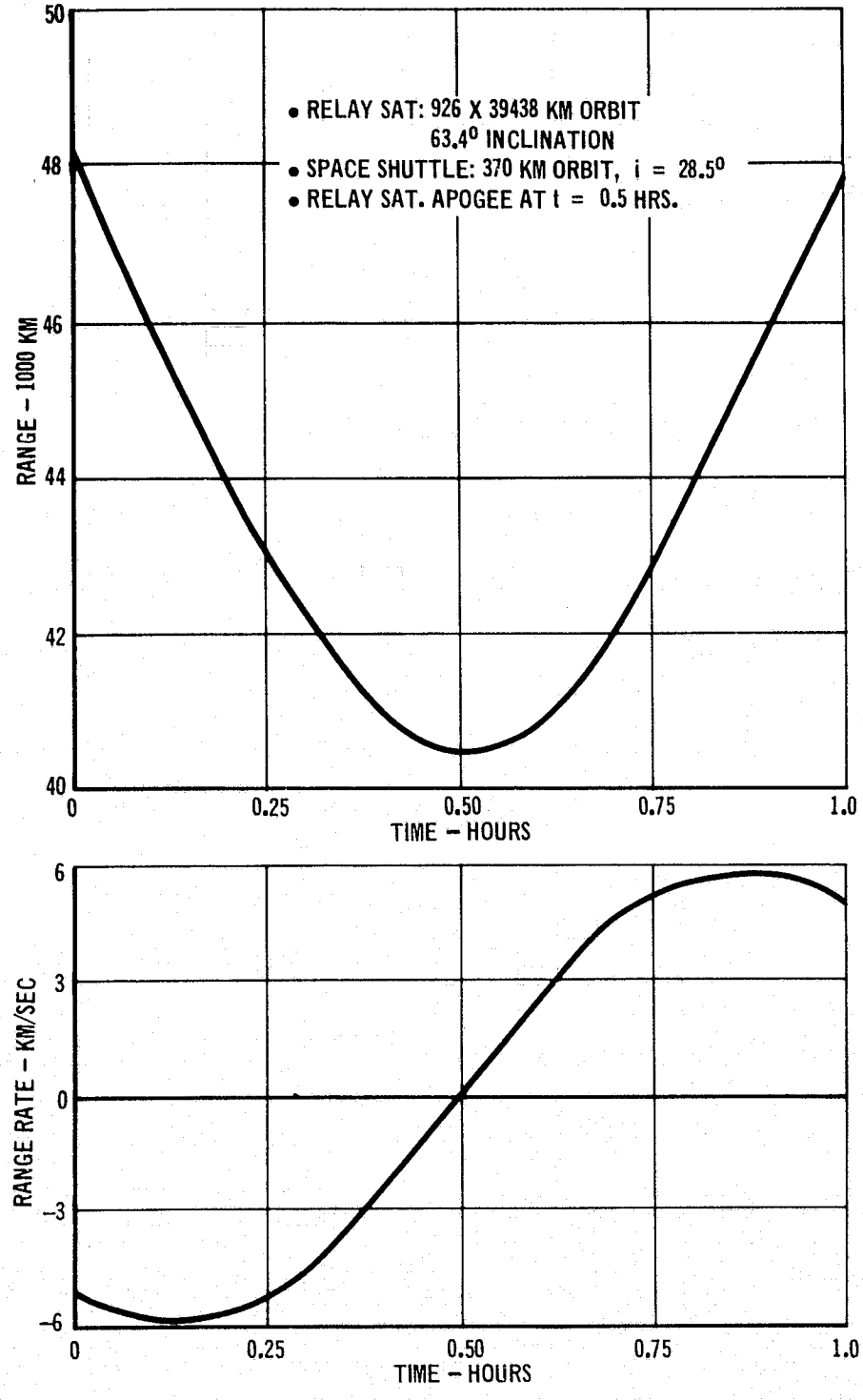

FIGURE 3-029 RELAY SATELLITE POINTING ANGLES AND POINTING ANGLE RATES – RELAY SAT./SHUTTLE LINK

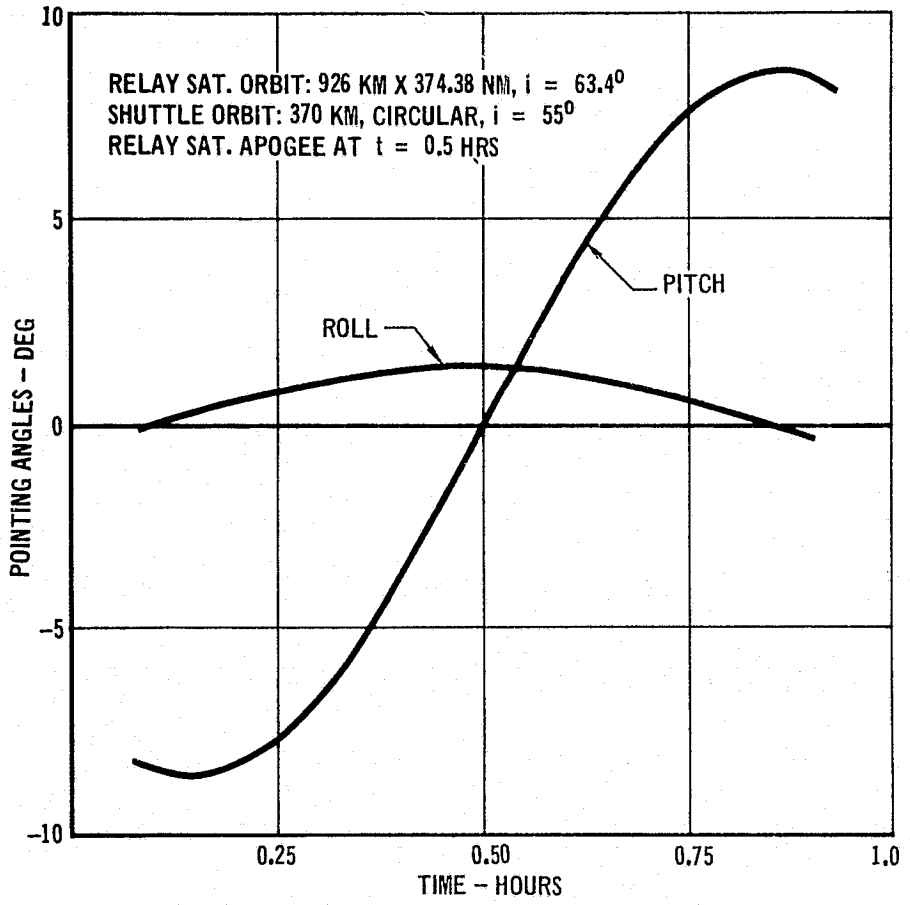

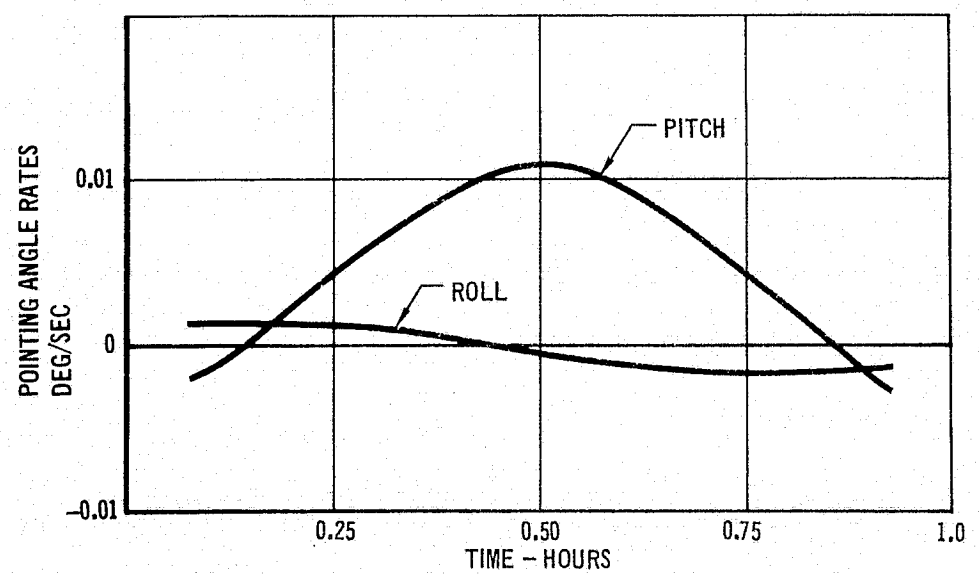

FIGURE 3-030 SHUTTLE POINTING ANGLES AND POINTING ANGLE RATES – RELAY SATELLITE/SHUTTLE LINK

RELAY SAT. ORBIT: 926 KM, 39,433 KM, i = 63.4°
SHUTTLE ORBIT: 370 KM, CIRCULAR, i = 55°
RELAY SAT. APOGEE AT t = 0.5 HRS.
EARTH-ORIENTED CONTROL

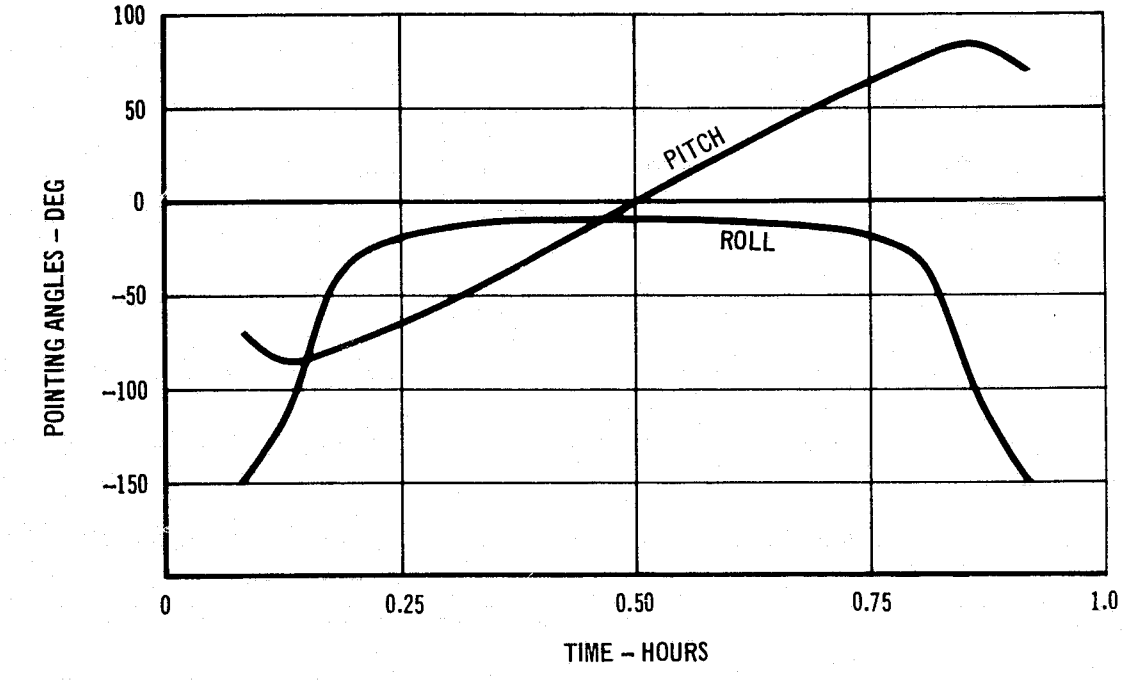

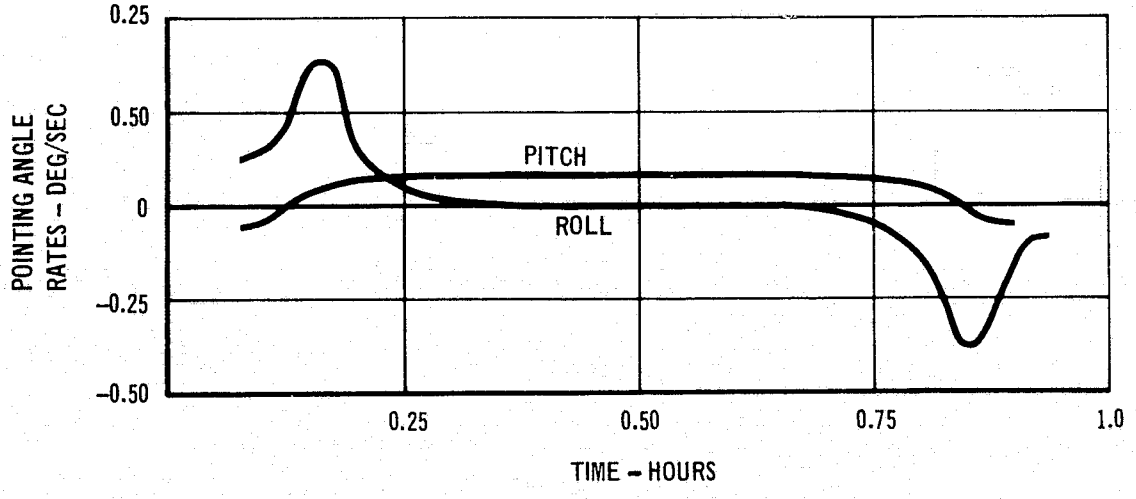

FIGURE 3-031 RANGE & RANGE RATE HISTORIES FOR RELAY SATELLITE TO SHUTTLE LINK

RELAY SAT. ORBIT: 926 x 39,438 KM, i = 63.4° ORBIT
SHUTTLE: 370 KM, CIRC, i = 55° ORBIT
RELAY SAT. APOGEE AT t = 0.5 HRS

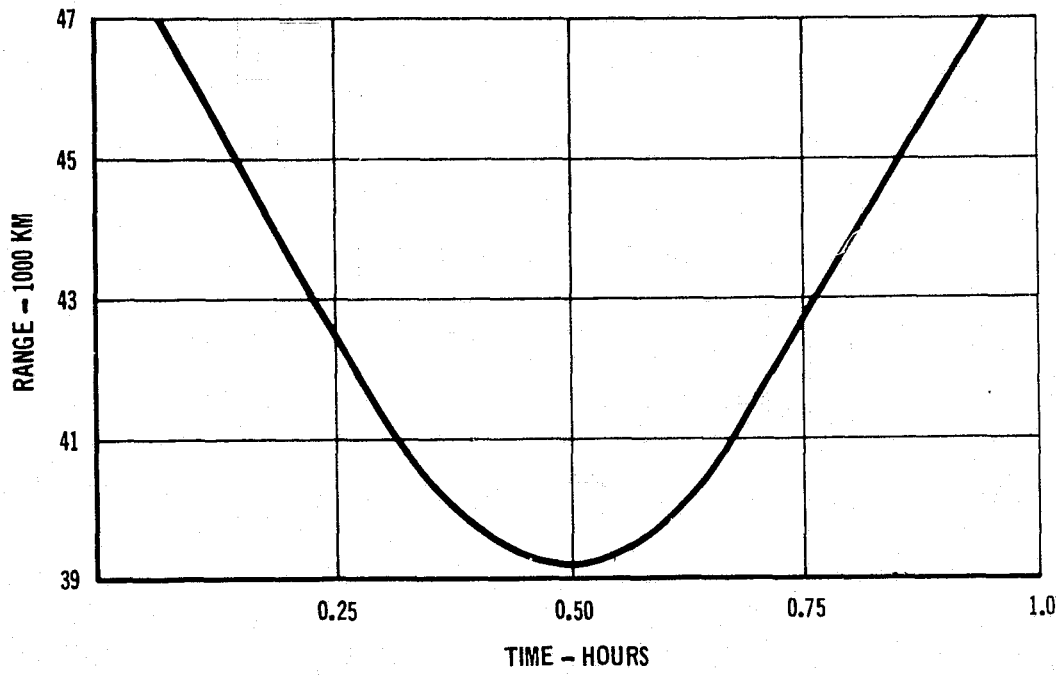

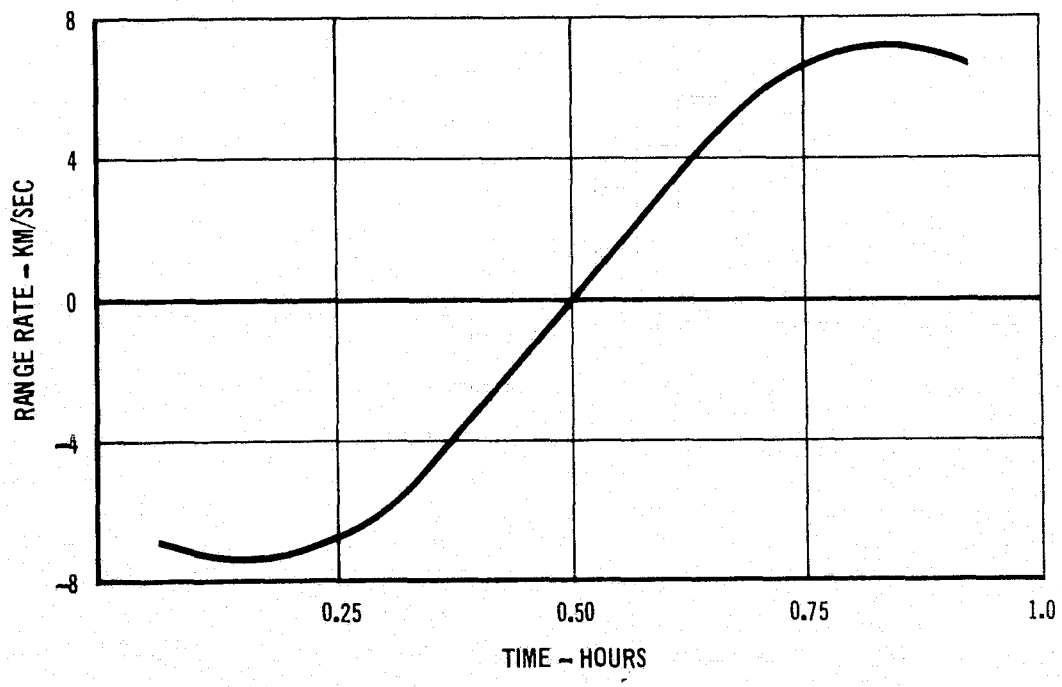

in those figures. However, they do typify the kinematics of the relay satellite to Shuttle links with the relay satellite within ±3 hours or so about apogee.

3.6.2 Alternate Experiment Orbits. Two alternate experiment orbits, a 12.5 hour orbit inclined at 63.4 degrees and a 12 hour equatorial orbit, were analyzed in order to assess their relative advantages and disadvantages compared to the baseline orbit described in Section 3.6.1.

3.6.2.1 12.5 Hour, i=63.4 Degree Orbit. The viewing interval in the baseline 12 hour orbit occurs approximately 4.5 minutes earlier on consecutive days. However, it may be desirable to have the local time of occurrence of the viewing interval change by considerably more than 4.5 minutes per day for some communication experiments. The 12.5 hour orbit provides a one hour daily variation in the local time that a viewing opportunity exists, but viewing opportunities are not available on a daily basis throughout the mission.

The available Goddard viewing time for the 12.5 hour orbit is shown in Figure 3-032 as a function of apogee longitude relative to Goddard. Six hour viewing opportunities exist whenever apogee is located within 58 degrees longitude of Goddard with a 40 degree satellite elevation requirement. Since two apogees occur every 25 hours, with the second apogee located approximately 172.5 degrees east of the first, viewing intervals exceeding six hours are obtained on an average of 64 percent of the days.

A typical scenario for a 24 day interval is shown in Figure 3-033 with apogee located at Goddard longitude on the first day. As apogee #1 moves westward at a daily rate of 15 degrees, apogee #2 is approaching Goddard at the same rate from the east. Viewing periods exceeding six hours are obtained during 15 days of the 24 day period.

3.6.2.2 Semi-synchronous, Equatorial Orbit. A brief analysis of a twelve hour, equatorial orbit with synchronous apogee altitude was performed to determine whether it offered any significant advantages relative to the baseline orbit. The daily viewing opportunity at Goddard is shown in Figure 3-034 for orbit apogee at Goddard longitude. Daily view times of approximately 8.5 hours and 5.5 hours are obtained for satellite elevation constraints of 30 degrees

FIGURE 3-032 GODDARD VIEWING TIME VERSUS RELATIVE LONGITUDE OF APOGEE FOR 12½ HR ORBIT

APOGEE LATITUDE = 63.4 DEG
ORBIT INCLINATION = 63.4 DEG
ALTITUDE: 926 KM PERIGEE
41,003 KM APOGEE

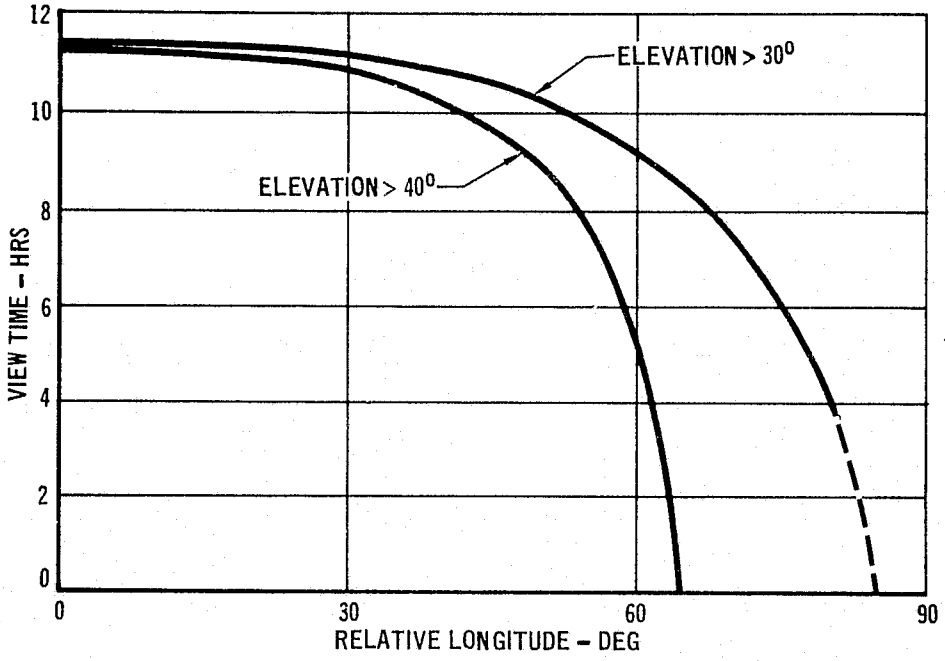

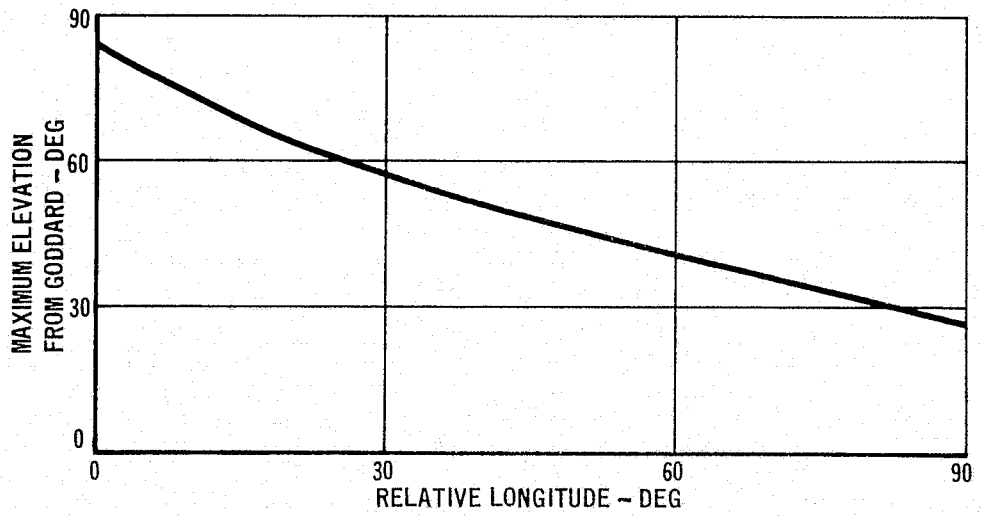

FIGURE 3-033 GODDARD VIEWING OPPORTUNITIES FOR 24 DAY PERIOD WITH A 40 DEGREE ELEVATION CONSTRAINT

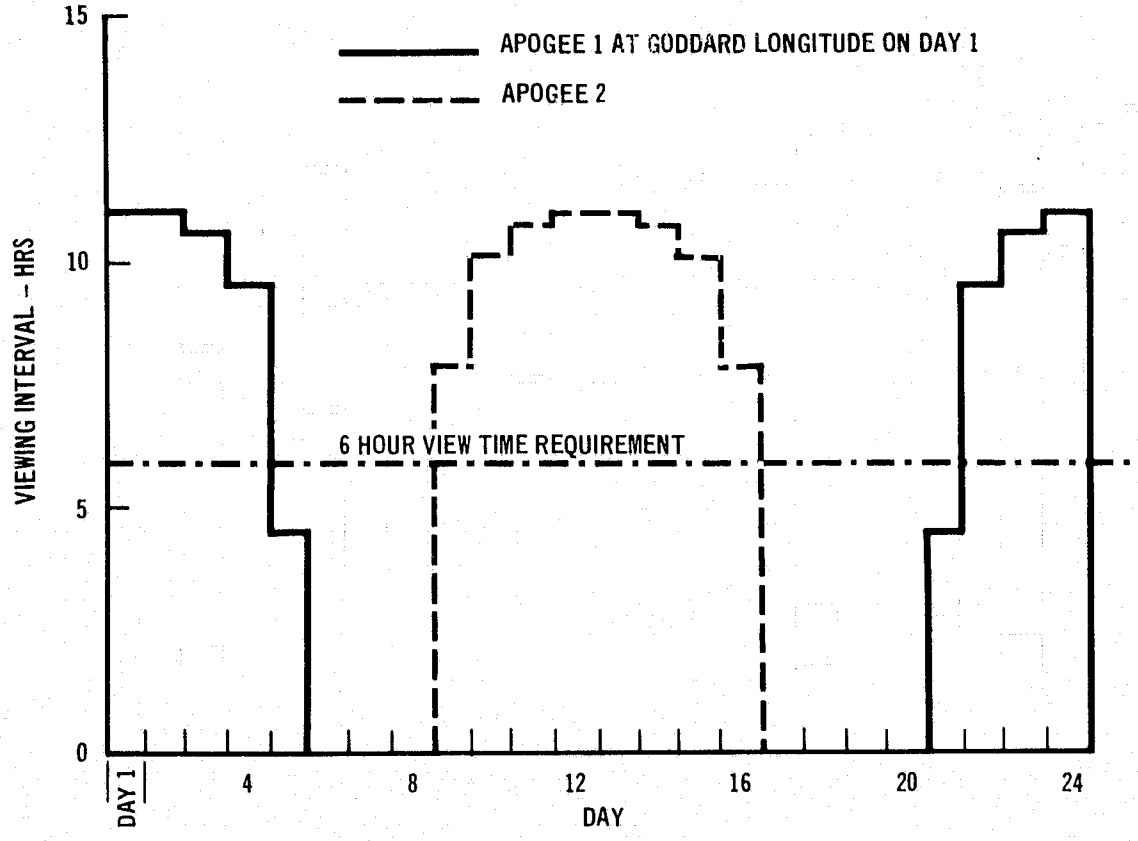

FIGURE 3-034 GODDARD VIEWING TIME FOR A SEMI-SYNCHRONOUS, EQUATORIAL ORBIT

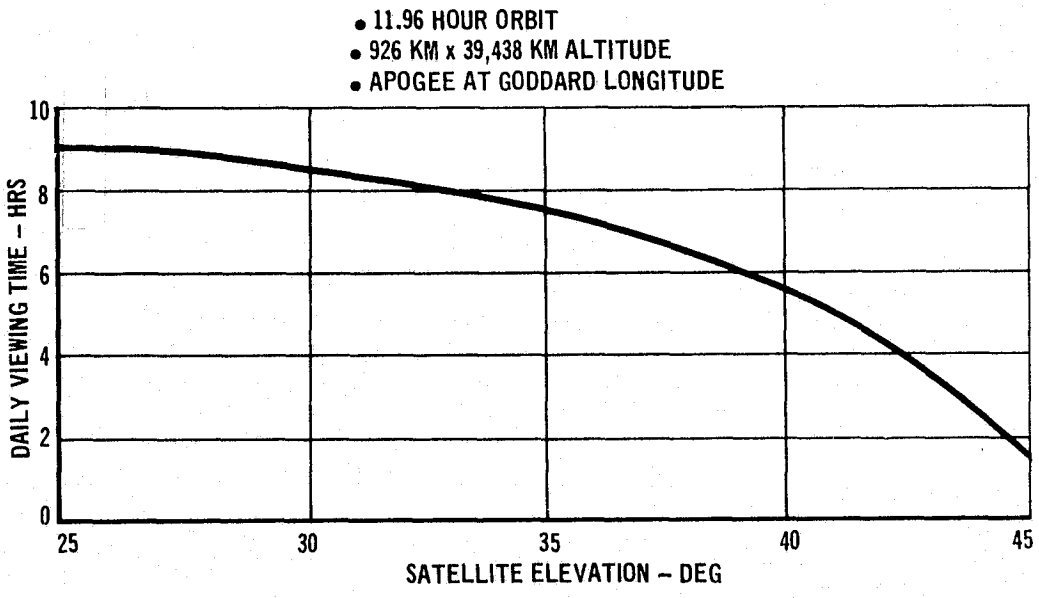

and 40 degrees respectively. Although this is less than the daily view time available with the baseline orbit, it satisfies the daily viewing requirement. Also, the semi-synchronous, equatorial orbit is more like the relay satellite orbit in the operational mission than the baseline orbit.

The most severe impact of a semi-synchronous, equatorial orbit is a reduction in payload capability. Discussions with General Dynamics, Convair indicate that the satellite on-orbit weight is reduced by nearly 50 percent due to booster and launch site constraints. This is in accordance with the study groundrule specifying an Atlas F launch out of WTR.

4. GROUND TERMINALS

4.1 GROUND STATION DEFINITION. The ground terminals are configured to be compatible with the satellite communications system and to provide experimental control and monitoring capability. The features of both the Goddard Optical Research Facility with its 48-inch diameter steerable telescope, and the 30-inch diameter mobile Ground Station have been examined, and the supporting hardware for both systems has been configured to maintain hardware commonality. In order to accomplish this commonality, it is necessary only to configure the optics of the 30-inch collector's relay lens system to produce the same effective focal length for that system as for the 48-inch collector.

Figure 4-001 is a block diagram which describes both ground terminals. The beacon laser, a 3000 PPS Q-switched 1.06 μm, Nd:YAG laser is encoded with Pulse Interval Modulation (PIM) data. An attenuator permits precise adjustment of outgoing power. The spatial filter properly shapes the beam and reduces the sensitivity of the beam direction to lateral jitter within the laser. The variable beam spoiler serves to vary the beam width over the range from 15 to 500 μrad. The device will consist of two glass plates in a solenoid actuated bracket. In the absence of any plate the optical design will produce a 15-μrad beam by illuminating a 9-centimenter diameter region on the telescope primary mirror. Depending upon what acquisition beamwidth and what tracking beamwidth are desired for a particular experiment, plates of certain thicknesses will be inserted in the bracket - one for acquisition and one for tracking. The solenoid will be actuated automatically by the mode logic during experiment operation.

The point ahead beam steerers are piezoelectric bimorphic crystals with mirrors attached. They perform high frequency beam deflection in two axes which steer the beams for tracking. We are currently evaluating the use of torque motor drivers for the steering mirrors on the Air Force 405B program. If their performance is adequate and their ruggedness can be demonstrated, they may very well replace the bimorphic benders because of lower cost and potential reliability.

The beam position monitors are silicon quadrant detectors for monitoring beam jitter. They share the angle processing electronics with the alignment detector. The mode logic switches the detector signals in accordance with the

FIGURE 4-001 GROUND STATION TERMINAL FUNCTIONAL BLOCK DIAGRAM

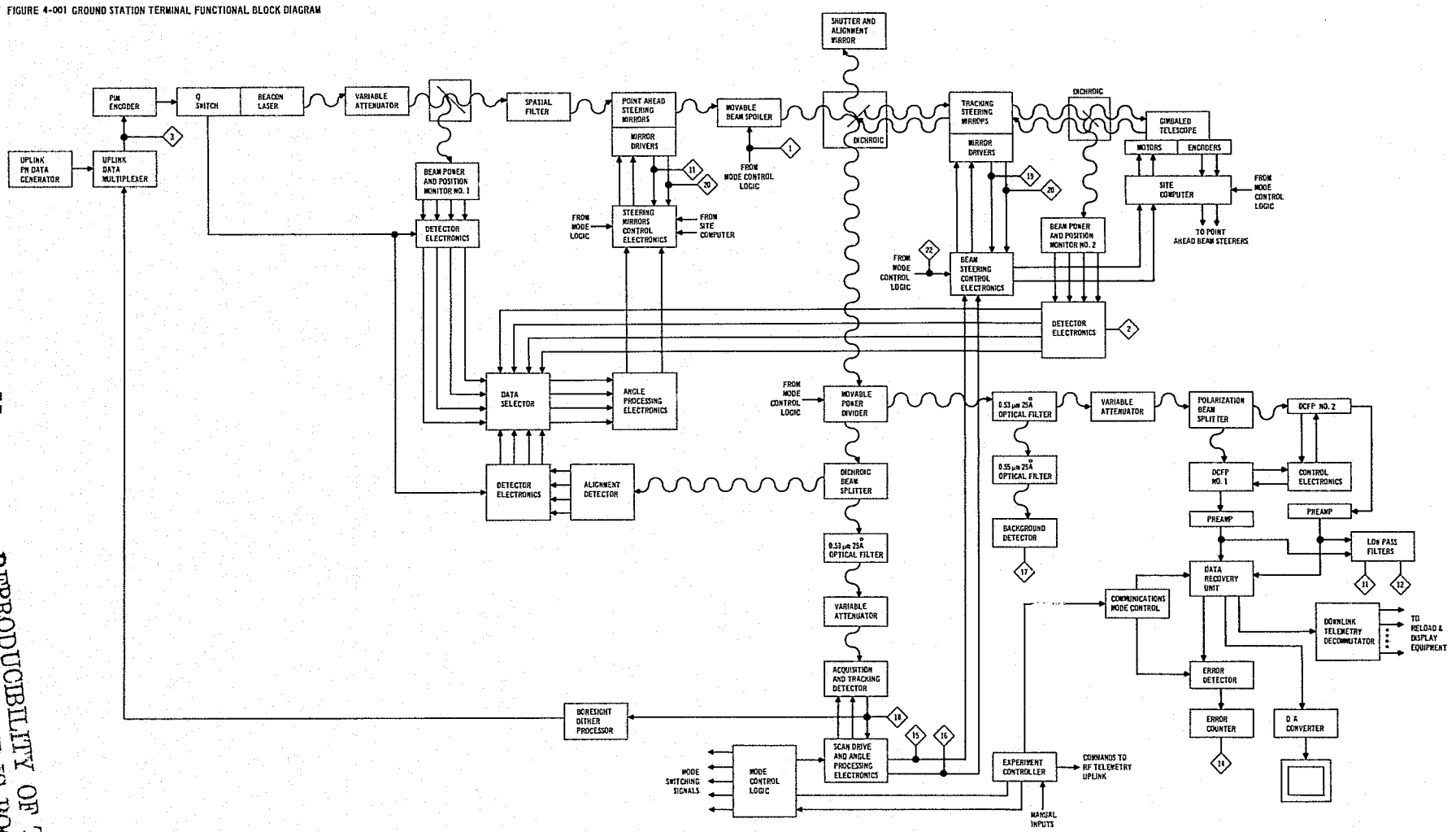

operating mode of the experiment. The x-y output of the angle processor will be monitored and recorded.

The dichroic element passes most of the 1.06 μm light from the laser on through to the telescope. However, some small amount is reflected into the alignment mirror and shutter where it is reflected into the alignment detector optics.

In addition, 0.53 μm light entering the telescope is reflected off of the dichroic into the 0.53 μm receivers. The tracking benders are included for the high pointing accuracy required when the beamwidth used is near the low end of the range of interest. Since we wish to experiment with beams as small as 15 μrad, the benders are required in the ground terminal. The telescope and controls are included in the existing ground facilities. The relative motion of satellite and ground station results in a slowly varying line-of-sight easily predicted by the computer. The deviations from the predicted motion are accommodated by a closed-loop tracking system. The commands are derived from pointing error data generated by the acquisition and tracking detector.

Looking down the receiver path, note the movable power divider. This device splits 99% of the received energy into the high data rate receiver. The receiver consists of a variable attenuator, a spectral filter, a polarization beam splitter, and two DCFP's with their associated control electronics, followed by data reconstruction and handling electronics. The power splitter is out of the optical train in the acquisition and realign modes. On the acquisition and tracking leg of the receive path, the dichroic splitter reflects the 1.06 μm leakage from the laser into the alignment detector which serves to measure the relative alignment of most of the optical elements not common both to the transmit and receive paths. The error measured by the alignment detector generates feedback signals for the point ahead beam steerers, enabling them to null out the misalignment. Because of the pulsed nature of the signal and relative abundance of power due to the proximity to the laser, the silicon quadrant detector (SQD) is excellently suited for the alignment detector role. A variable attenuator permits independent adjustment of the power into the acquisition and tracking detector. This detector must track on the received mode-locked pulse train. but need not resolve the pulses. The

image dissector tube is well suited to this task with its steerable aperture and high sensitivity. The electronics associated with the device steers its aperture and develops steering signals for the gimbals and beam steerers. The mode logic automatically switches among the acquisition, tracking, and realign modes of operation in accordance with console commands and pointing error. The received optical power is measured periodically at the output of the image dissector. This data is coded and merged with the PIM data stream for transmission to the high data rate terminal where a closed-loop boresight dither scheme removes low frequency boresight alignment errors.

An experiment controller provides the necessary sequencing of control signals to the subsystem com nents for their proper coordination during experiment operations.

4.2 OPTICAL SCHEMATICS. Figures 4-002 and 4-003 are optical schematics of the 48-inch and modified 30-inch telescopes. The 48-inch system produces a 2-inch (1.59 milliradians) field with a 1260-inch focal length. The 30-inch system should be designed to relay the image produced by the Cassegrain telescope with its 450-inch focal length to an accessible point under the gimbal mount structure where the transceiver subsystem is located. The magnification of the relay system should be 2.8 to provide an effective focal length of 1260 inches. This permits the transceiver subsystem design to be the same for both stations, thereby minimizing the design effort required to configure these ground stations and the cost of the terminals.

Figure 4-004 is an optical schematic of the common transceiver package itself, showing the arrangement of the optical element identified in the block diagram. Note the central region where the beams are collimated. This point in the optical train represents the image of the entrance pupil. Consequently the off-center introduction of the transmit beam at this point results in the off-center illumination of the primary telescope mirror which causes the transmit beam to avoid observation by the secondary mirror of the telescope. In addition, the alignment mirror can be a corner reflector whose slight motion (translational or rotational) relative to the optical axis will not affect the alignment as measured and adjusted by the auto alignment system. A system of field lenses relay the beam in a manner which avoids large linear excursions at foci while it preserves the desired field of view.

FIGURE 4-002 MOBILE GROUND STATION TERMINAL OPTICAL SCHEMATIC

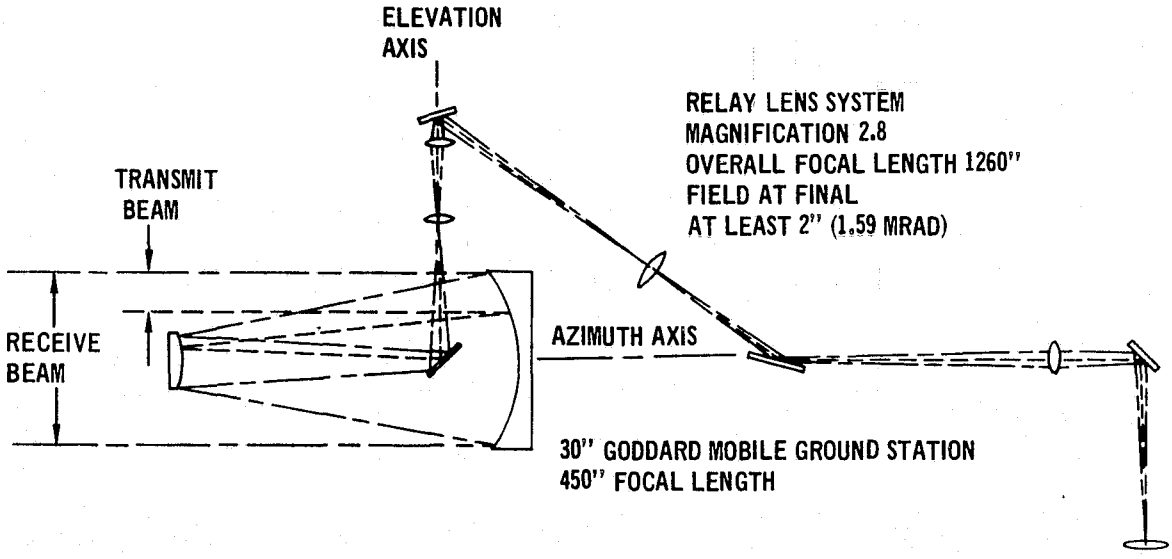

FIGURE 4-003 STATIONARY GROUND STATION TERMINAL OPTICAL SCHEMATIC

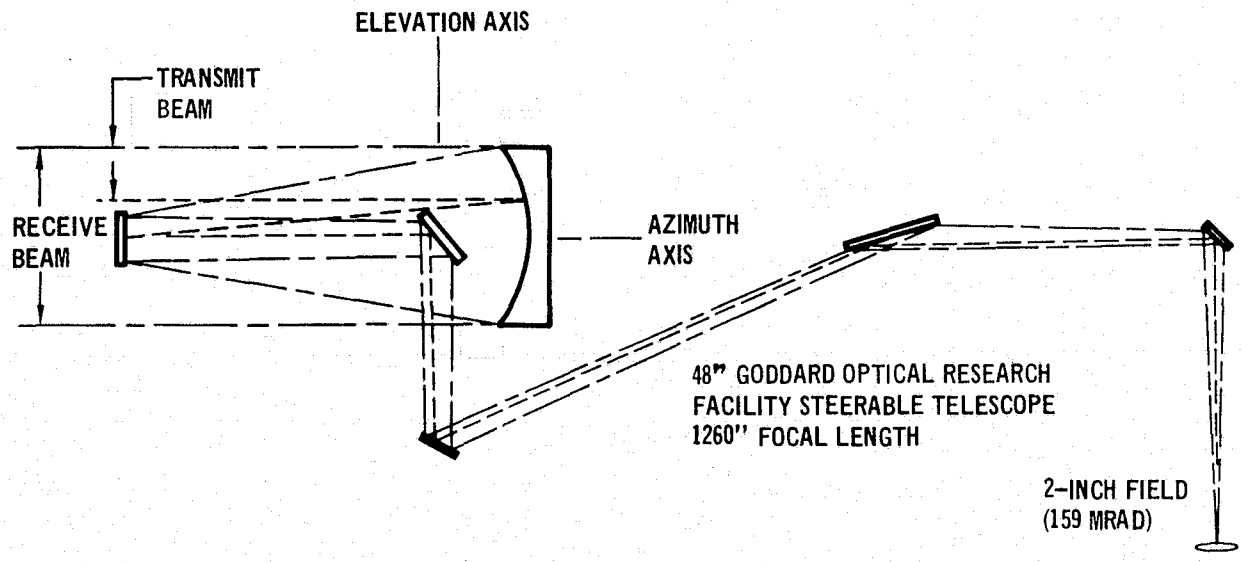

FIGURE 4-004 LASER TERMINAL OPTICAL SCHEMATIC

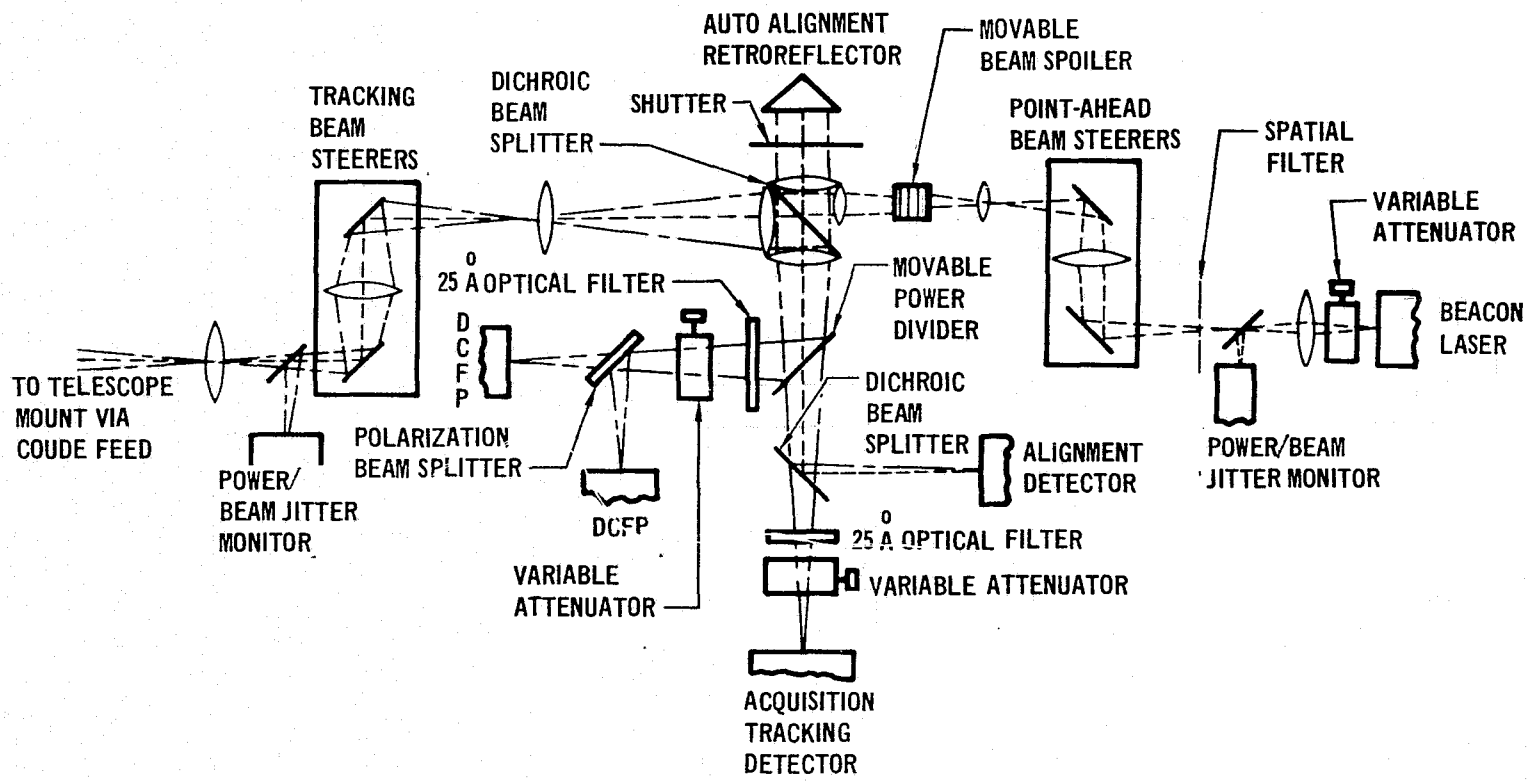

4.3 GROUND STATION INSTRUMENTATION. Figure 4-001 identifies the ground station monitor points which will be recorded both for immediate consideration and for post-flight data analysis. Figure 4-005 illustrates the general scheme for organizing, recording, displaying, and time tagging this data and the data received by telemetry from the satellite. The ground station monitor points are conditioned where necessary, and fed to a patch panel. The decommutated telemetry data also enter this same patch panel. The panel permits cross connection to constant bandwidth (CBW) voltage-controlled oscillator (VCO). These produce a series of subcarrier signals frequency modulated in accordance with the various monitored signals and produce frequency-multiplexed composite signals suitable for magnetic recording in bandwidths which permit efficient utilization of the tape data packing speed and density. The "A" channels are spaced 8 kHz apart from center frequencies of 16 kHz to 112 kHz and have maximum frequency deviation limits of ± 2 kHz for a full ± 5 volts input. Their nominal bandwidth is 400 Hz but can be stretched to near 2 kHz. The "B" channels are spaced 16 kHz apart, deviate by ± 4 kHz, and have nominal bandwidth of 800 Hz with maximum theoretical bandwidths of 4 kHz. In addition to the VCO's, a digital multiplexer permits combining of the digital signals for high data rate recording, and a pulse amplitude modulation (PAM) analog multiplexer combines samples of a number of low frequency analog channels. Pulse delay modulation (PDM) or pulse code modulation (PCM) may be used if existing units using these formats are handy.

One channel on the tape will be used to record IRIG A time signals generated from WWV time signals. An absolute time accuracy of 10 milliseconds can be established with this signal, and relative time will be recorded to microsecond accuracy.

The telemetry data received from the laser downlink is recorded directly and decommutated for realtime display on strip chart recorders. Also, certain key data is sent over from the Goddard telemetry receiving station via ground link for immediate display in the event that the optical downlink degrades or fails.

The monitor points will be buffered to preclude instrumentation failures from affecting the system performance. The buffer amplifiers will provide gain adjustment capability for scaling the signal dynamic range to suit the

FIGURE 4-005 GROUND STATION INSTRUMENTATION BLOCK DIAGRAM

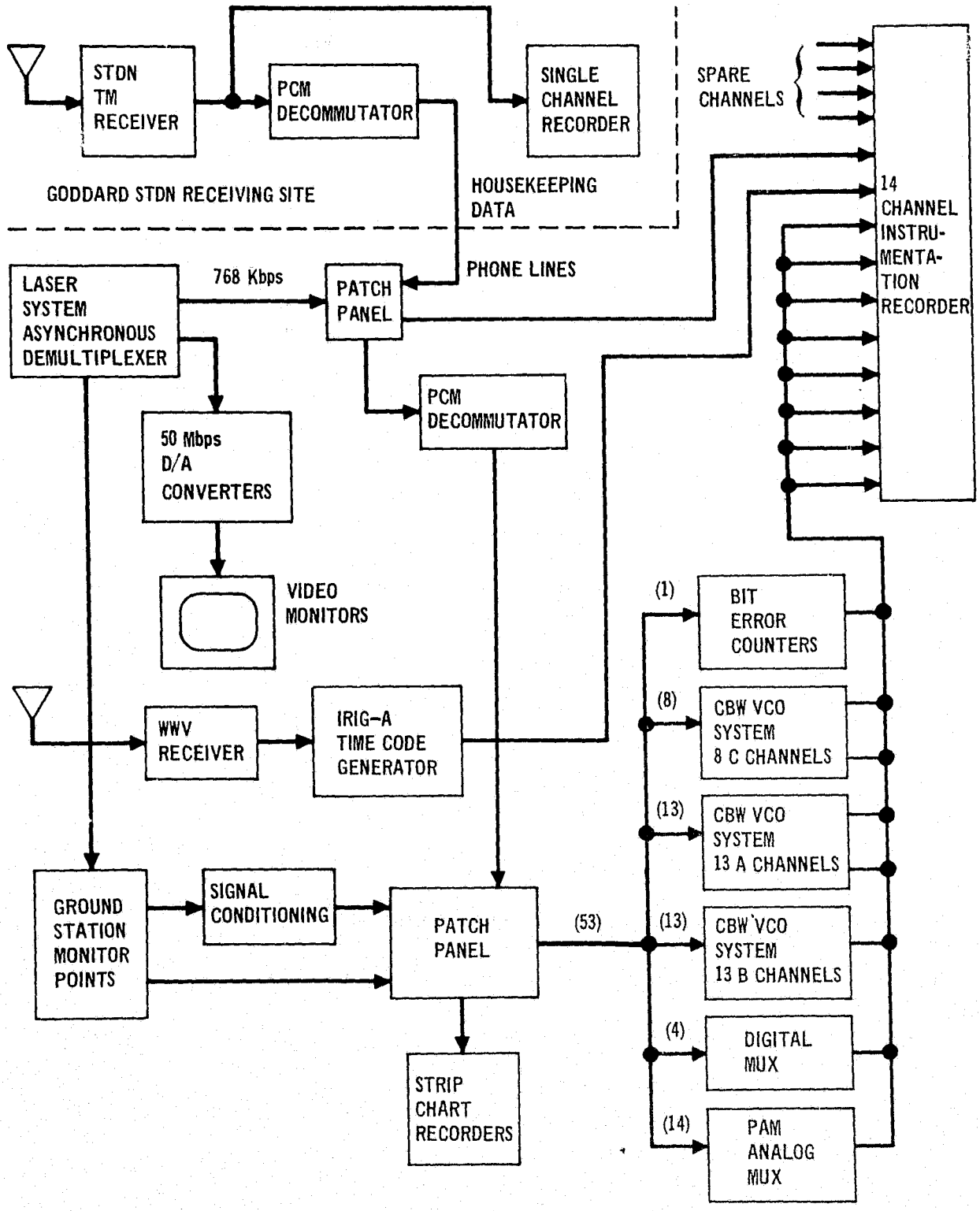

VCO input, where used. Also the bit error counting and recording, shown in Figure 4-005 will be performed as illustrated in Figure 4-006. The two counters observe errors in alternate 1 millisecond periods under control of a digital controller. The buffer device constructs a smooth 17 kilobit (one word identifier bit) data stream for direct recording on one channel of the magnetic tape. This permits recording of bit error probabilities as high as 0.065 while observing 1 millisecond bursts of errors during short term fades.

The 14-track tape recorder is run at 30 inches per second (ips). At this speed, recorders with the so-called Wideband I characteristics (such as Ampex FR1800) can record signals with 375 kHz bandwidth. This is adequate for recording the down link telemetry data, which has the highest data rate of any single channel. Wideband II characteristics (such as those exhibited by the Ampex FR2000) permit 500 MHz bandwidth recording at 30 ips, but only allow 250 MHz at 15 ips, so a 30 ips speed is required.

FIGURE 4-006 BIT ERROR MEASUREMENT INSTRUMENTATION

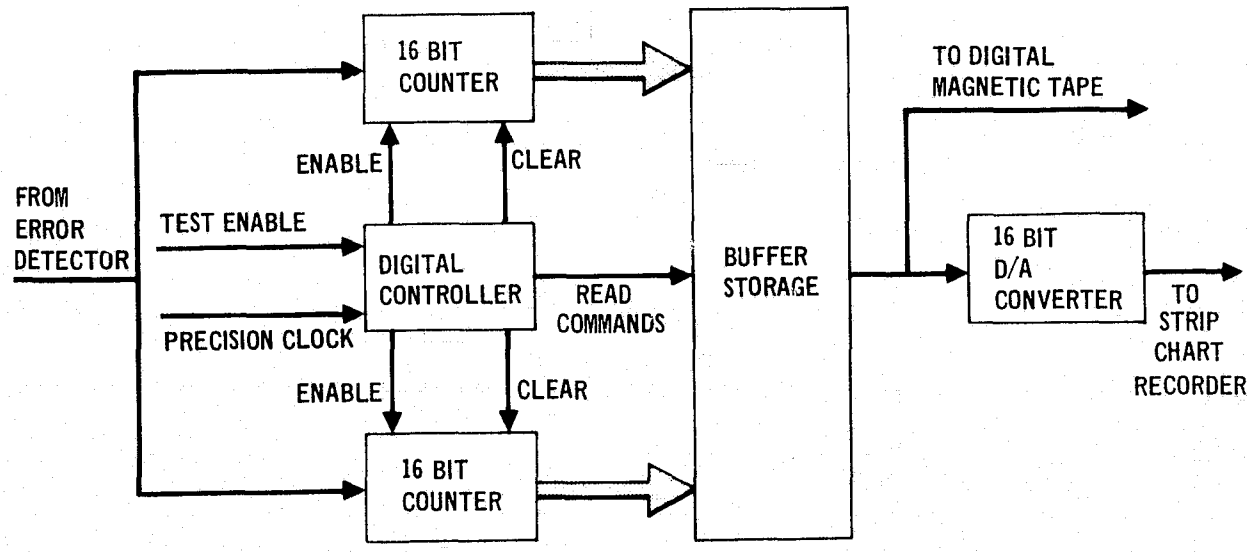

5. EXPERIMENT MEASUREMENTS PLAN

5.1 EXPERIMENT PLAN SUMMARY. The following sections define the parameters which should be measured both in the spacecraft and on the ground, the methods of combining these parameters to measure link quality and the sequence of performing the experiments.

The sequence of experiments is defined such that those experiments with the highest data value are performed first. The sequence begins with the necessary initial checkout after the final orbit adjust maneuver. A set of benchmark tests is then defined which is a set of reference measurements performed periodically to determine long term performance changes in the equipment. Several levels of tests are defined to be performed after the benchmark tests with the highest priority tests being performed first.

None of the tests has a different risk associated with it than any other test so that technical risk does not play a part in the experiment plan. All of the communication links defined are links which could exist in a low earth orbit to synchronous system or a synchronous to synchronous system. Therefore all the tests performed are equally realistic to the operational user community. Lamp pumped Nd:YAG tests which are applicable to a low earth orbit sensor satellite are defined as well as sun pumped Nd:YAG tests which are applicable to the synchronous orbit relay satellite.

Specific tests where the CO_2 payload is cross-strapped to the Nd:YAG payload have been considered. These are not identified as separate tests since the evolving Nd:YAG payload will have provision for accepting asynchronous data from a source with the data rate capability of the CO_2 uplink. Therefore, the CO_2 uplink data can be input to the Nd:YAG subsystem directly where the data will be multiplexed with other downlink data prior to modulation of the Nd:YAG downlink beam.

5.2 PARAMETER MEASUREMENTS. Table 5.2-1 lists the hardware and link parameters which are required to perform the system quality measurements described in Section 5.3. The characteristics of the parameters and the type of system quality measurement in which the parameter is used are listed for each parameter. Since instrumentation subsystems are not yet designed, both analog and digital characteristics are listed. The bandwidth and resolution listed are the desired characteristics of the measuring equipment and telemetry channels.

TABLE 5.2-1 MEASURED PARAMETERS CHARACTERISTICS

	CHARACTERISTICS					PURPOSE									
	BANDWIDTH (Hz)	RESOLUTION (%)	SAMPLES PER SECOND	BITS PER SAMPLE	DATA RATE (Kbps)	UPLINK BER	UPLINK TRACKING	UPLINK POINTING	UPLINK BEAM PATTERN	DOWNLINK BER	DOWNLINK BURST RATE	DOWNLINK TRACKING	DOWNLINK BEAM & POINTING	ACQUISITION TIME
SATELLITE RECEIVER AND POINTING SUBSYSTEM														
PCM OUTPUT					10.0	X								
FTD AGC	12.0	2.0	24	6	0.144	X	X	X	X			X		
ANGLE PROCESSOR SUM CHANNEL			3000	12	36.0	X	X	X	X			X		
FTD THRESHOLD	0.5	2.0	1	6	0.006	X	X							
CAD THRESHOLD	0.5	2.0	1	6	0.006	X	X							
ACCELEROMETERS (12 CHANNELS)	300.0	5.0	600	60	36.0		X							
SERVO BANDWIDTH			1	2	0.002		X							
ANGLE PROCESSOR AZIMUTH OUTPUT			3000	12	36.0		X			X		X		
ANGLE PROCESSOR ELEVATION OUTPUT			3000	12	36.0		X			X		X		
SATELLITE TRANSMITTER														
COMMUNICATIONS LASER OUTPUT	1000.0	2.0	2000	6	12.0					X		X		
TRANSMITTER LOSS		10.0	1	4	0.004					X		X		
EXTINCTION RATIO	1000.0	10.0	2000	4	8.0					X		X		
SATELLITE EXPERIMENT EQUIPMENT														
CALIBRATION DETECTOR	1.0	2.0	2	6	0.012	X	X							
GROUND STATION RECEIVER & POINTING SYSTEM														
DCFP 1 AVERAGE OUTPUT	1000.0	0.1	2000	10	20.0					X		X		
DCFP 2 AVERAGE OUTPUT	1000.0	0.1	2000	10	20.0					X		X		
BIT SYNC LOCK DETECTOR	1000.0	BINARY	2000	1	2.0									X
ERRORS PER MILLISECOND			1000	16	16.0					X				
ANGLE PROCESSOR x OUTPUT	200.0	0.05	400	11	4.4							X		
ANGLE PROCESSOR y OUTPUT	200.0	0.05	400	11	4.4							X		
DOWNLINK BACKGROUND DETECTOR	<1.0	2.0	1	6	0.006					X		X		
TRACKING DETECTOR OUTPUT	500.0	1.0	1000	7	7.0	X	X	X			X			
x AXIS BENDER POSITION	300.0	0.1	600	10	6.0			X	X					
y AXIS BENDER POSITION	300.0	0.1	600	10	6.0			X	X					
APERTURE SIZE			1	2	0.002					X		X		
SERVO BANDWIDTH			1	2	0.002							X		
GROUND STATION TRANSMITTER														
UPLINK BEAMWIDTH			1	2	0.002	X	X							
BEACON LASER OUTPUT		2.0	1600	6	9.6	X	X							
UPLINK TRANSMITTED DATA					10.0	X								
START SCAN TIME	20.0	1.0	40	7	0.28									X
GROUND STATION EXPERIMENT EQUIPMENT														
SPATIAL CORRELATION FUNCTION DETECTOR	500.0	2.0	1000	6	6.0	X	X	X						
STELLAR MOTION MONITER						X	X	X					X	
TURBULENCE PROFILE DETECTORS (4 CHANNELS)	500.0	2.0	1000	24	24.0	X	X	X					X	
VISIBILITY		2.0	1	6	0.006	X	X			X		X		
SEISMIC SENSORS (3 CHANNELS)	1000.0	2.0	2000	6	12.0							X		
1 Gbps PN DATA GENERATOR					10^6					X				
CALCULATED PARAMETERS														
DELAY TIME	CALCULATED FROM EPHEMERIDES					X		X	X					
RANGE LOSS						X	X			X		X		
LOS DYNAMICS (ANGULAR RATES)							X					X		
GROUND STATION BORESIGHT ERROR								X						
SATELLITE BORESIGHT ERROR	CALCULATED FROM PREVIOUS CALIBRATION DATA												X	
DOWNLINK BIT PERIOD										X		X		
GROUND STATION OPTICS LOSS						X	X			X		X		

5.2.1 Satellite Parameters. The following is a review of each satellite parameter listed in Table 5.2-1.

PCM Output - This is the output of the PIM to PCM conversion electronics. The data are generated in a digital form and therefore never exist in an analog form.

FTD AGC - This parameter is used in determining the uplink received signal strength. The 12 Hz bandwidth reflects the latest concepts of design engineers.

Angle Processor Sum Channel - The signal from the four quadrants of the illuminated detector are summed to provide a normalization signal for the difference signals and to provide the largest signal possible to the PIM to PCM conversion electronics. The uplink signal strength is measured by a combination of this summing process and the FTD AGC. This sum signal is updated each time a PIM pulse is received.

FTD Threshold - This threshold for the Fine Tracking Detector is set to establish a constant false alarm (false pulse received) rate. The FTD is a thermal noise limited detector and this threshold setting is an indication of that thermal noise.

CAD Threshold - The Coarse Acquisition Detector is a background noise limited detector. The threshold setting is an indication of the uplink background.

Accelerometer Outputs - These accelerometers will probably be included for two purposes. The first purpose is to measure launch and ascent vibration levels to assure that the laser subsystem does not experience vibration levels higher than qualification levels. These levels could cause highly degrading or catastrophic failures to occur. The second purpose is to measure the low level vibrations during experiment performance such as vibration from thrusters firing or momentum wheels turning. Monitoring these levels will allow correlation between experiment subsystem performance and vibration input to the subsystem.

Servo Bandwidth - If possible, several bandwidths should be designed into the experiment pointing subsystem. These bandwidths would be changed periodically by a switch to verify system models which correlate servo bandwidth and subsystem performance.

Angle Processor Azimuth Output - The signal from two quadrants of the active detector is subtracted from the signal from the other two quadrants after digitizing. This difference is normalized by the sum channel signal and then is output to the pointing subsystem as the azimuth beam bender pointing error.

Angle Processor Elevation Output - This signal is processed the same as the Angle Processor Azimuth Output.

Communication Laser Output - Laser output is not variable but the output amplitude and amplitude jitter is monitored to assure proper laser operation and correlate any laser degradation with communication link degradation.

Transmitter Loss - The degradation in transmittance of the telescope should be measured periodically during a calibration period. One concept for this measurement is to turn the scanning flat normal to the telescope thereby reflecting the transmitted beam back to the uplink detectors. These detectors and associated optics are optimized for 1.06 μm and the capability to accurately measure the amplitude of a 0.53 μm signal is questionable. No accurate method of measuring the optics performance at 0.53 μm is currently known.

Extinction Ratio - The extinction ratio is a measure of the modulator capability to insert the laser energy into the proper polarization and time state and exclude the energy from the other 3 states. The method of measuring extinction ratio is unknown at this time.

Calibration Detector - A method of measuring the receiver optics efficiency is needed. One method of performing this measurement is to provide a separate uplink detector whose output can be compared with the output of the beacon detector. This calibration detector would be a satellite body mounted, wide field-of-view detector whose output is integrated over a long time period compared to the beacon detector.

5.2.2 Ground Station Parameters

DCFP Average Output - The output of these communication detectors is a measure of the received signal as corrupted by all noise sources. Noise sources include laser instabilities, downlink pointing errors, background and atmospheric effect.

Bit Synchronizer Lock Detector - The lock-up of the bit synchronizer is the last event to occur in the acquisition sequence. The time of lock-up is noted to define acquisition time.

Errors Per Millisecond - This is a parameter derived from an error detector operating on the downlink data. The errors per millisecond data are stored and then manipulated to determine error statistics.

Angle Processor x Output - These data define the ground station x axis pointing error.

Angle Processor y Output - These data define the ground station y axis pointing error.

Downlink Background Detector - This detector should be implemented with either an off axis view field (spatial separation from downlink beam) or an optical filter (frequency separation from downlink beam) to measure the downlink background level.

Tracking Detector Output - The output level from this DPMT is processed along with the output of additional dispersed detectors to define pointing error and beam pattern.

Bender Position - These data define the precise pointing angl s of the uplink beam.

Aperture Size - The aperture size should be changeable with a manual input to the data processing capabilities.

Servo Bandwidth - The servo bandwidth should be changeable with a manual input to the data processing capabilities.

Uplink Beamwidth - The beamwidth of the beacon laser will be changed and entered into the data processing manually.

Beacon Laser Output - The uplink transmitted power will be varied with an attenuator and the data manually input to the data processing capability.

Uplink Transmitted Data - The PCM data will be stored until the data from the satellite PIM to PCM converter is returned. Comparison of these 2 data streams is the primary measure of uplink communications quality.

Start Scan Time - The time of implementation of the acquisition sequence will be recorded. The time of occurrence of other events will be compared to this time for a measurement of acquisition time.

Lateral Coherence Length - This detector measures the lateral coherence length of the atmosphere, which is the primary atmospheric parameter required to predict uplink beam wander.

Turbulence Profile Detectors - A set of balloon-borne turbulence detectors should be used to correlate the effects of the atmosphere on the laser beam with the measured turbulence profile. Either free-flying or tethered balloons can be used.

Visibility - Horizontal visibility at both 1.06 μm and 0.53 μm should be measured to correlate this parameter with communication losses.

Seismic Sensors - Both natural and man-made ground station vibrations will impact the uplink pointing capability. These vibrations should be measured in order to extract any effect from the communications measurements.

1 Gbps PN Data Generator - A data generator must be included in the ground station which provides a code identical to the spaceborne data generator. Comparison of the generator output and the downlink detected data results in the downlink bit error rate.

Calculated Parameters - A number of calculated parameters must be input to the comparison models in Section 5.3. Delay Time, Range Loss and Line-of-Sight Dynamics are all calculated from orbital data. Ground Station Boresight Error, Satellite Boresight Error, Downlink Bit Period and Ground Station Optics Loss should be stored for each calibration period. The change between calibration periods should be determined and the expected value of the parameter calculated whenever required.

5.3 LINK QUALITY MEASUREMENTS. The previously described parameters which are measured in the spacecraft and in the ground station are used to determine the quality of the acquisition, tracking, and communications. The methods of determining the quality of these characteristics are described in the following sections.

5.3.1 Uplink Bit Error Rate. The bit error rate (BER) is the most complete test of a communication link since all other quality parameters will impact this parameter. The BER is a function of all of the other parameters to be measured as discussed in paragraphs which follow (i.e.; Tracking Error, Pointing Error, and Beam Pattern).

Uplink communications is implemented with a Q-switched laser with a pulse interval modulation (PIM) format. This format allows communication of a number of bits in each Q-switched pulse. Assuming n bits per pulse, the pulse is inserted in any one of 2^n time slots or with any one of 2^n intervals between pulses. The exact method of implementing the uplink communications for this spaceflight experiment has not been decided; however previous studies have determined that a PIM format with six bits per pulse (n=6) and a pulse rate of 1.6 Kpps is an effective method of implementation.

Three types of errors can occur in a PIM communications system. The first occurs when a pulse is transmitted but is missed by the receiver. The second type of error occurs when the receiver detects a pulse where a pulse was not transmitted. The third type of error occurs when a transmitted pulse is detected but is interpreted to be in the wrong time slot or interval. The types of errors which predominate will provide data in determining the cause of low performance, and therefore the experiment should be designed to determine the type of error.

Pulse errors rather than bit errors should be counted when performing the uplink BER for the following reasons:

a. Errors in the optical pulse detection and timing will be more frequent than those occuring in the PIM to PCM conversion.

b. PCM errors are expected to occur in bursts of six errors in a row.

c. The usual technique of counting PCM "1" errors and "0" errors is meaningless since the largest error contributors have no correlation with the PCM one and zero states.

In order to count errors the received data in the satellite must be compared with the transmitted data on the ground or on shuttle. The received time slot or pulse interval must be identified and telemetered to the ground or Shuttle where the comparison is made. The easiest method of identifying the time slot or interval is to utilize the PCM data after PIM to PCM conversion. The transmitted PCM data is compared to the received PCM data to detect errors. When a bit error is detected, all six of the bits in that PIM word must be assumed to be in error and one PIM error is counted. Examination of the erroneous word will identify the time slot or interval in which a pulse was received. These slots will then allow definition of the type of error which occurred in the detection process.

As with any low data rate channel, the measurement of a low bit error rate is very time consuming. For example, if we desire to count 10 errors to assure a moderate confidence level in the error rate, the length of the test will be approximately 1.6 hours to measure a 10^{-6} error rate. This lengthy time is unacceptable in the spaceflight experiment because the range, atmospheric turbulence, atmospheric transmission, atmospheric path length, gimbal rates, and point ahead can all be changing during this time period. These dynamics will make the resultant data meaningless in relating the measured error rate to

a specific set of link conditions. The error rate measurements must therefore be made at signal levels which result in a high error rate, probably no less than 10^{-4}. The required length of a test to accumulate 10 errors will then be one minute. The communications link should first be established with a strong signal. The laser power should then be reduced until the SNR indicates that the appropriate signal strength has been established to perform the measurement.

Figure 5-001 shows the method of performing the analysis of BER data. The analysis method is to use a link model to predict the performance of the link, measure the actual link performance, and compare the predicted with the actual to verify the accuracy of the model. Assuming that the model is determined to be accurate, the methodology then exists on which to build an operational system with adequate but not overly conservative margins.

The Word Error Detector compares the transmitted and received words to detect errors. The ground to satellite to ground delay time is provided to this error detector which establishes the amount of time which the transmitted data must be delayed for the error detector to quickly establish a lock between the transmitted data sequence and the received data sequence. When an error is detected an error indication is output to a counter for BER measurement. At the same time, the error indication, the transmitted word, and the received word is output to a computer for error type determination. The program calculates the transmitted and received time slots or intervals and then determines the most likely type of error which occurred.

Even though the measurement is intended to determine the error rate of the optical PIM detector the PIM to PCM electronics in the satellite are used to identify the time slot of the PIM detector output pulses. Therefore the PIM to PCM electronics are considered to be part of the measuring equipment which must have negligible errors compared to the devices being measured. The analysis method provides a test for this negligible error assumption. The Expected Error Rate Calculation block, implemented in the ground station computer, utilizes the signal statistics at the output of the PIM detector to calculate the expected error rate. This error rate is compared to the measured error rate with the variation between the two being displayed on a strip chart. Wide variations between these quantities will indicate degradation in the PIM to PCM electronics or a defective model of these electronics.

FIGURE 5-001 UPLINK BIT ERROR RATE ANALYSIS

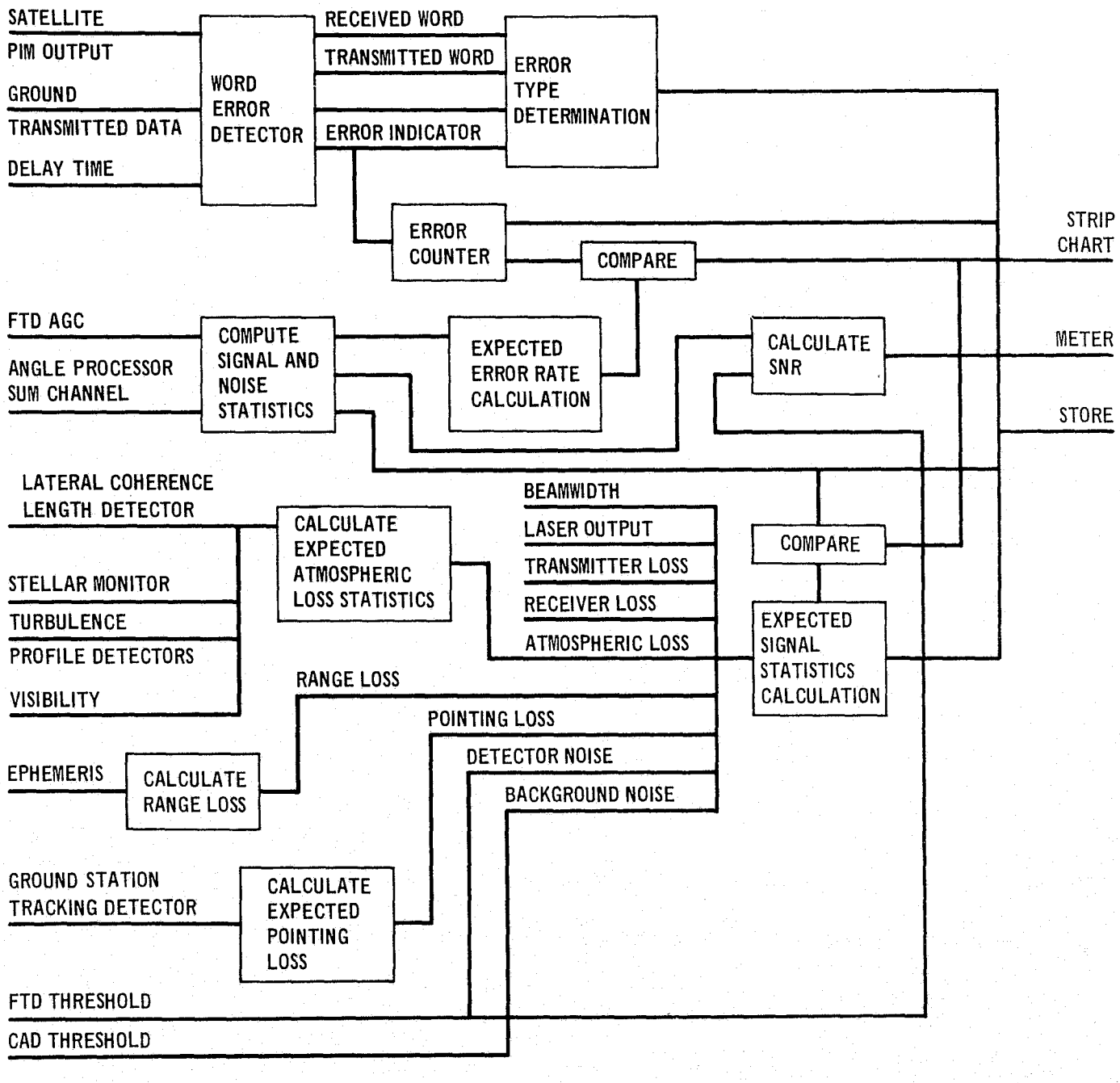

The most significant comparison in this BER analysis is the comparison of actual signal output from the optical PIM detector with the expected signal output. The calculation of the expected signal output distribution utilizes the outputs of all sensors which detect either losses or variations in the communications path. The variation of the measured signal statistics is output to a strip chart recorder to monitor the adequacy of the prediction model or to flag the existence of undetected degradation sources in the communication channel.

5.3.2 Uplink Tracking Error. The uplink tracking error is a measure of the capability of the satellite communications terminal to maintain the optics axis pointed at the uplink signal. The receiver has a relatively wide angular field of view and therefore a small tracking error will have a negligible impact on uplink bit error rate. However, the downlink beamwidth is only 5 microradians, and a small displacement or jitter of the optics can cause a significant degradation in downlink bit error rate.

Figure 5-002 shows the method of data analysis for uplink tracking error. Calculation and measurement of received signal statistics at the satellite is identical to the Uplink Bit Error Rate analysis discussed previously. This calculation requires inputs from all sensors which detect degradation or variations in the communications channel. The calculated signal statistics are compared to the signal statistics at the angle processor sum channel output. This comparison is displayed on a strip chart recorder to provide a monitor which will provide an indication of any unexpected channel disturbances. The measured signal statistics are used along with satellite rigid body (LOS Dynamics) and nonrigid body (Accelerometers) measurements and the designed control bandwidth to calculate tracking error. This tracking error is then compared with the measured tracking error at the output of the azimuth and elevation channels of the satellite angle processor. This comparison is also displayed on a strip chart recorder to warn of any unexpected tracking error disturbances. Intermediate results are stored for later recall if necessary.

5.3.3 Uplink Pointing Error. The uplink pointing error is a measure of the capability of the ground station to maintain its uplink beam axis pointed at the satellite detector. Noise from the downlink tracking detector, downlink to uplink optical boresight misalignments and nonreciprocal atmospheric disturbances will all impact the ground station pointing capability.

FIGURE 5-002 UPLINK TRACKING ERROR ANALYSIS

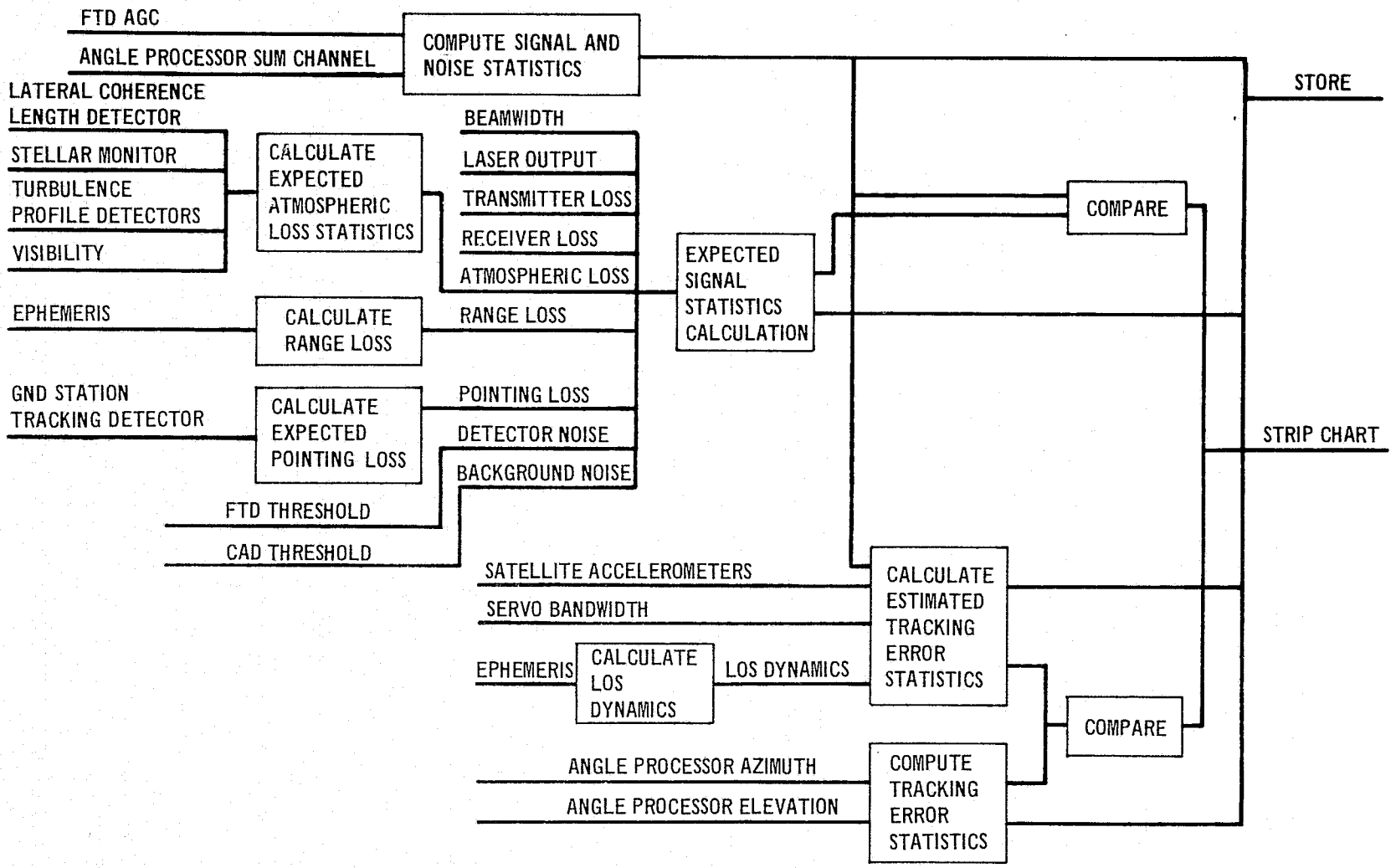

Figure 5-003 shows the method of analyzing the pointing error. The uplink beam is conically scanned about the computed pointing position. Conical scanning is implemented by imposing a sine signal on one bender and a cosine signal on the orthogonal bender. This will cause the uplink beam to describe a circle about the satellite detector. Since the beam has equal gain in all directions from the axis no variation of signal strength will occur at the satellite if the following conditions are satisfied:

a. Pointing error of the computed beam pointing position is near zero.

b. Atmospheric variations are negligible.

c. Beam pattern is well shaped.

During the period of experimentation the beam pattern will be mapped and the errors caused by this factor should be negligible or known so that they can be removed. Atmospheric variations are expected to have a maximum frequency of about 100 Hz. By selecting an experiment period when the atmosphere is quiet and by using a 200 Hz scan frequency the atmospheric effects can be made negligible. Therefore only the error in the computed beam pointing position will affect the measurement. This error will cause the beam axis to be closer to the satellite detector on one side of the detector than it will be 180° later on the other side of the detector. In other words the detector is offset from the center of the scan circle. The signal from the detector will therefore be a 200 Hz sine signal. The amplitude of the signal will indicate the magnitude of the offset or pointing error. The phase of the signal, when compared to the sine signal imposed on the ground station benders, will indicate the direction of the pointing error.

Figure 5-003 shows the satellite sum channel output being compared with the appropriately delayed ground station bender signals in a synchronous detector. This detector determines the amount and direction of the pointing error. This error is then compared with the estimated error which requires estimations of atmospheric variations, boresight errors, and signal to noise output from the ground tracking detector.

FIGURE 5-003 UPLINK POINTING ERROR ANALYSIS

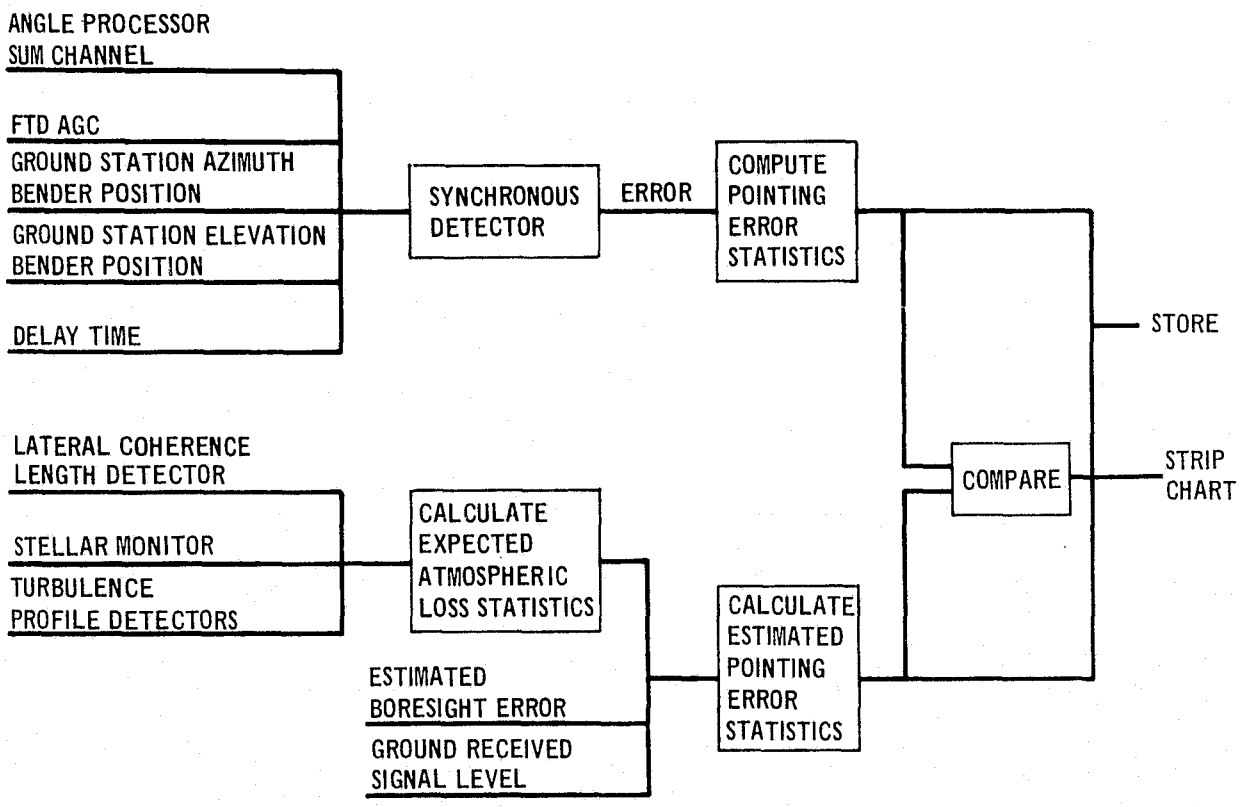

5.3.4 Uplink Beam Pattern Measurement. Measurement of the uplink far field antenna pattern has two objectives:

1. Demonstrate that the type of telescope used is acceptable for an operational ground to space link, if such a link is established.
2. Determine that pattern irregularities are sufficiently small to have negligible impact on other link characteristics such as bit error rate and tracking error.

Figure 5-004 shows the method of measuring the beam amplitude at a single point, storing the data and plotting the data. The received signal amplitude at each point in the pattern must be normalized by dividing by the on axis signal strength. In order for this normalization to be accurate the time between measurement of on axis signal strength and the signal strength at the other point must be no greater than 10 milliseconds. This speed is required to assure that atmospheric degradation remains nearly constant throughout the measurement. The measurement involves the Fine Tracking Detector in the satellite

FIGURE 5-004 UPLINK BEAM PATTERN MEASUREMENT

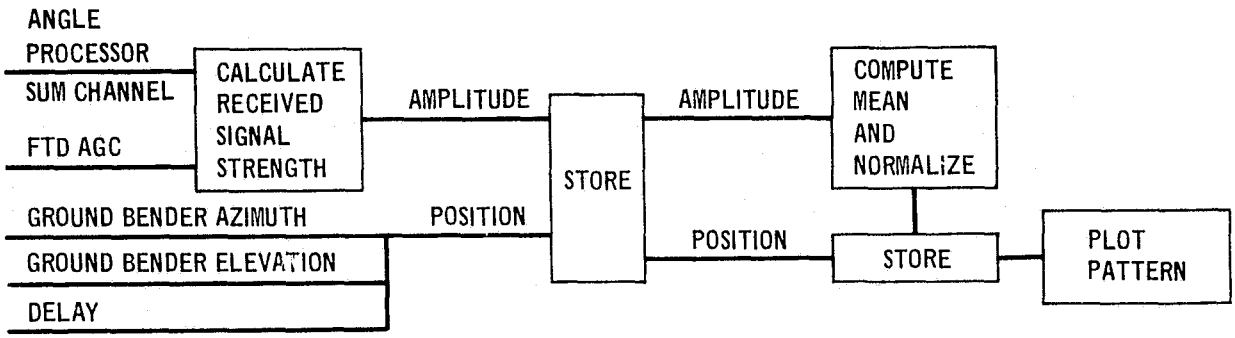

which is thermal noise limited. The measurements should include a number pulses at strong signal levels to minimize the effect of detector noise on the measurement.

Several methods for performing this have been evaluated. The first method is to measure the beam pattern during the conical scan used for pointing error analysis. The amplitude of the conical scan would be changed periodically to scan in concentric circles around the beam axis. Even though this method offers test efficiency, it was discarded for 2 reasons. The first reason is that the on axis signal strength cannot be obtained within the required 10 μsec. The second reason is that only 2 pulses are measured at any particular pattern point in a 10 μsec interval. The measurement of the amplitude of one point (or one circle about the beam axis) on a Gaussian distribution is insufficient to define the shape of the curve and therefore the on axis gain. Measurement of at least 2 points is required to define beamwidth and on axis gain. Two levels of conscan cannot be implemented within 10 μsec. Each cycle of conscan requires 5 μsec which means that the amplitude at any pattern point is measured with 2 pulses within the 10 μsec time constraint.

The second method considered was a modification of the first method. The beamwidth of the uplink beam will have been measured during calibration of the ground station. This measurement could be used along with the measurement at one point in the beam during conscan to define the beam shape. These two data points would provide sufficient data to calculate on axis gain. However, this method can be impacted by the corruption of the beam width by atmospheric degradation and therefore was discarded.

A third test method is to offset the beam slightly during conscan providing a different off axis measurement point on each side of the beam. This technique results in defining the beam shape from measurements at closely spaced points on the Gaussian distribution. Large errors can result from small measurement errors with this technique. The amplitude at each point is measured with only 2 pulses within a 10 μsec period which can result in measurement errors. The resultant error probabilities causes this technique to be inadequate.

A fourth test technique is to point the beam directly at the satellite, swing it off axis and return. This technique depends on the pointing error being zero when pointing directly at the satellite. A method which approaches this zero pointing error is to perform a pointing error analysis and if the pointing error is determined to be sufficiently low immediately point the beam directly at the satellite. After 5 μsec (8 pulses) the beam would be driven to a preselected off axis point for 5 μsec providing all of the data required within the 10 μsec period. The amplitudes at each point would be averaged and the off axis amplitude normalized with the on axis amplitude. The process would be continued alternating between pointing error analysis and beam pattern measurement until the beam pattern has been plotted (50 to 100 points) or until an increased pointing error indicates that the process should be terminated.

Figure 5-004 shows the signals telemetered from the satellite which are processed to determine received signal strength (amplitude) at the satellite. The azimuth and elevation beam pointing positions are entered along with the round trip delay time so that amplitude and beam position are keyed together in storage. The amplitude at each point either on or off axis is averaged, the off axis data is normalized and the resulting normalized average is stored with beam position data. After all measurements are processed the beam profile can be plotted or curves fit to the data to determine pattern errors.

5.3.5 Downlink Bit Error Rate. Data for the downlink communications channel is derived from several sources:

1. Satellite data generators
2. Satellite sensors (instrumentation or scientific)
3. Data derived from uplink CO_2 communications channel

Since a separate downlink high data rate channel does not exist only that data which has a known sequence can be used in BER measurement. The satellite data generators can be duplicated on the ground and the data on the uplink CO_2 is generated on the ground so these two data sequences can be used for BER measurement. The sensor data is not predictable and therefore cannot be used for this purpose.

Figure 5-005 shows the method of performing BER analysis. The data derived from the downlink laser is compared with identical data sequences generated on the ground. When an error is detected an error indication is output to a counter. Each millisecond the contents of the counter are output to storage. The stored data is then used to compute the measured BER. This BER is compared with the expected BER to assure that analytical models are sufficiently accurate and the communications equipment is functioning correctly. The expected BER prediction is based on the measured signal and noise characteristics at the output of the receiver. These measured characteristics are compared to expected signal and noise characteristics which are based on the measured values of detailed hardware and link parameters. The comparisons are output to a strip chart recorder to monitor link performance and analytic model accuracy.

Two pseudorandom data sequences should be used for a complete functional check of this high data rate link. The primary sequence would be a 1024 bit sequence to measure BER as discussed above. Where an anamoly is noted which appears to be caused by hardware degradation a 31 bit sequence should be used for a more detailed diagnosis of the problem. While using the 31 bit sequence the error rate per bit position is measured. Identifying the bit positions with the highest error rates will provide additional insight into hardware degradation. For example, errors where bits are alternately ones and zeroes will indicate high frequency rolloff problems whereas errors where the data is a series of ones will indicate lack of low frequency response. The 31 bit sequence is a diagnostic tool whereas the 1024 bit sequence more adequately simulates random operational data and therefore is a better test overall link quality.

FIGURE 5-005 DOWNLINK BIT ERROR RATE ANALYSIS

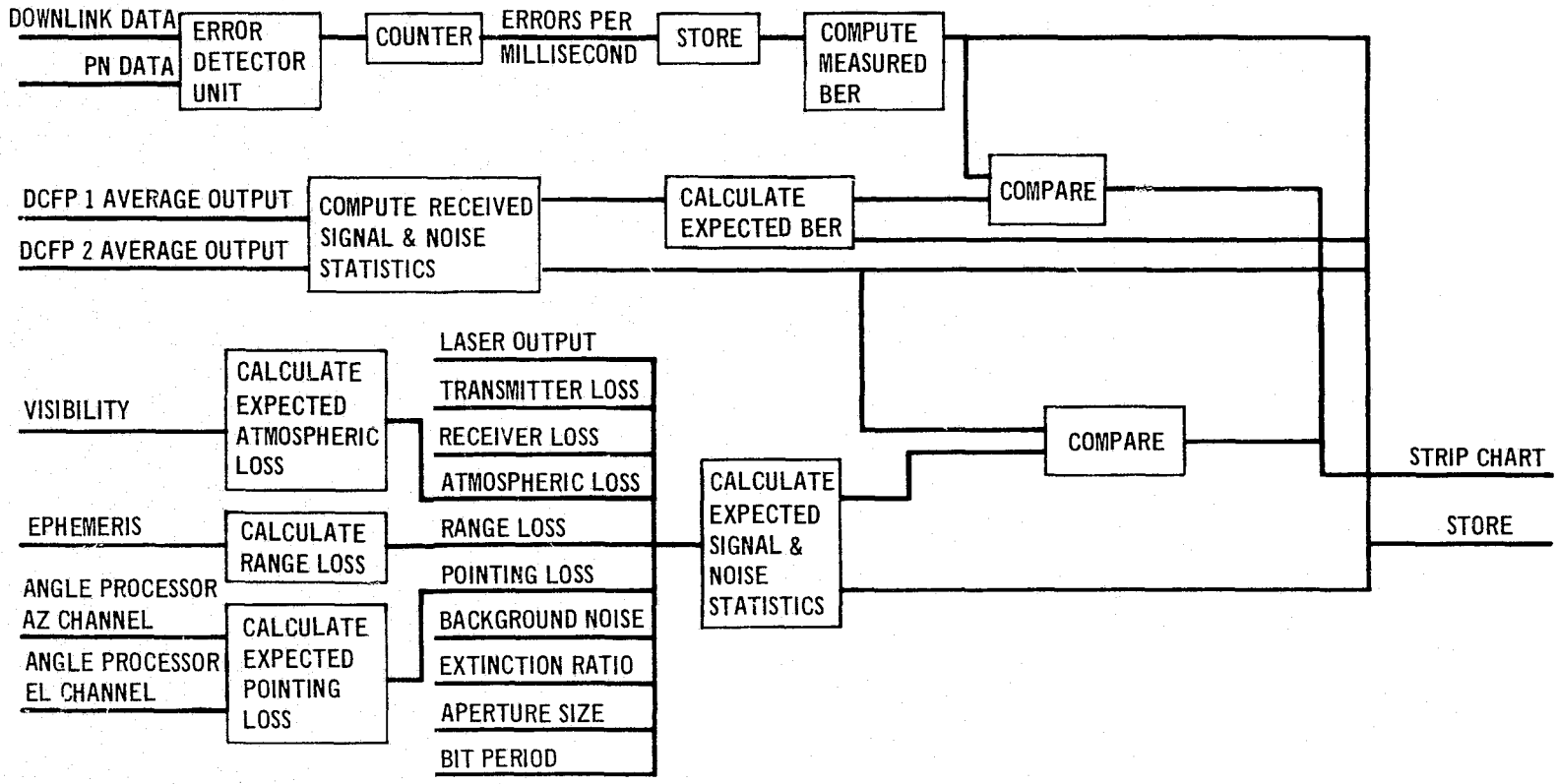

5.3.6 Downlink Burst Rate. Period of communications when the BER is degraded are most likely to be dominated by low frequency degradation mechanisms which will cause the errors to occur in bursts. Figure 5-006 illustrates the analysis method to determine the extent of burst error degradation. The errors per millisecond as derived in the BER analysis is compared to a burst threshold. This threshold is set to a specific number, n, so that any millisecond period containing more than n errors is considered to be a part of a burst of errors. The threshold is set from the BER being measured such that the probability of n or greater errors in a millisecond period (10^6 bits) is quite low. This probability should be variable to provide a flexible measurement technique. When the errors in a millisecond exceed the threshold an indication is output to a counter. The counter counts the consecutive intervals which exceed the threshold which is a measure of the burst length. The burst length and time between bursts statistics can be accumulated from the counter output. These statistics are compared with predictions to determine analytic model adequacy or hardware degradations.

FIGURE 5-006 DOWNLINK BURST RATE ANALYSIS

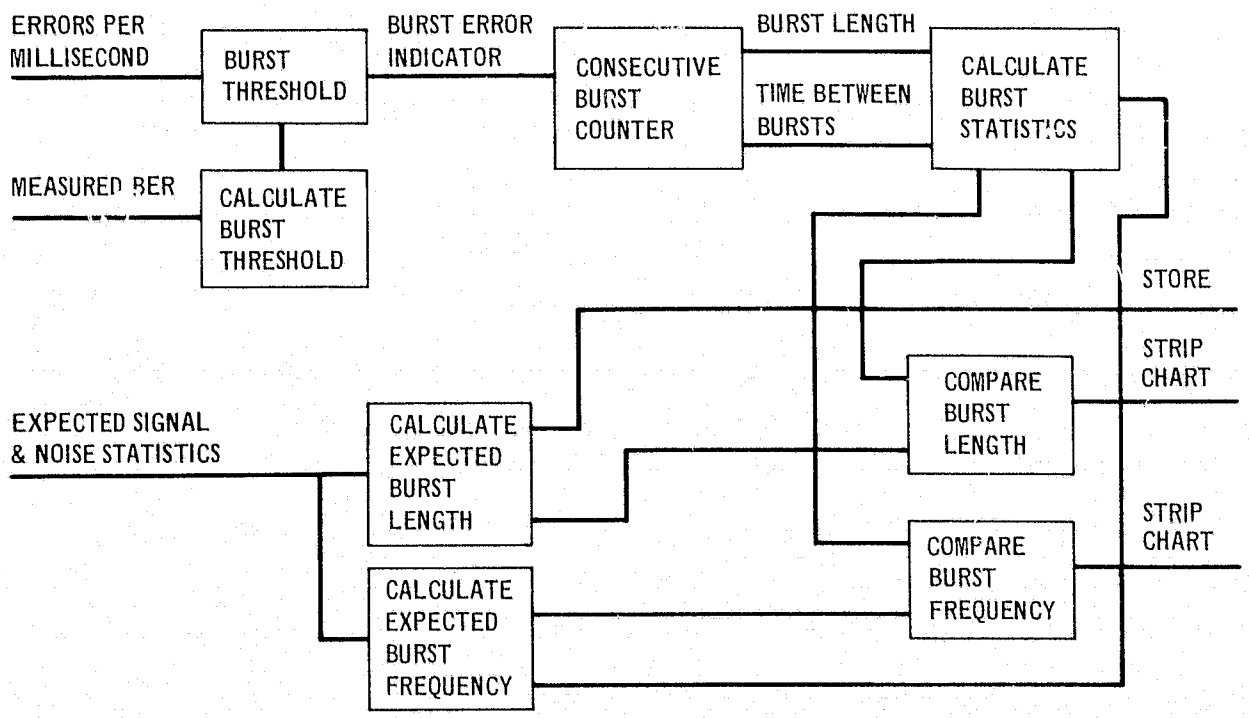

5.3.7 Downlink Tracking Error. Figure 5-007 illustrates the method of analyzing the downlink tracking error. The tracking error is measured from the output of the azimuth and elevation channels of the ground station angle processor. This measured tracking error is then compared with the predicted tracking error which is based on the measurement of link parameters which tend to degrade the tracking error. The comparison is output to a strip chart recorder which indicates the adequacy of the analytic prediction model or provides an indication of hardware degradation.

5.3.8 Downlink Beam Pattern and Pointing Error. Two detector arrays should be included as part of the ground station. The first array, a tracking array, should consist of 4 detectors located on the corners of a square which is 600 feet on each side. The second array, an acquisition array should include 4 detectors located on the corners of a square whose sides are as long as practical with the preferred length being 2.5 miles. The tracking array offers the capability to analyze pointing error and plot the downlink beam pattern.

Figure 5-008 illustrates the methods of measurement and analysis. The beam center position is computed by using the signal strength from the detector array and the communication subsystem tracking detector. The error between the beam center position and the intended beam center position (the location of the communications optics) is the pointing error. The statistics of this pointing error are compared with the predicted pointing error which is based on measured values of link parameters. This comparison is then output to a strip chart recorder to monitor adequacy of the prediction model and link performance.

The distance between the beam center position and the location of detector is computed to determine the off axis position of each of the detectors. The off axis position is stored along with the normalized signal amplitude at each detector. Intentional or unintentional movement of the beam will then allow mapping the amplitude of a large number of points in the beam pattern. The amplitude and position of these points are stored until the entire beam pattern can be plotted.

5.3.9 Acquisition Time. A number of definitions of acquisition time can be postulated. The time always begins with an instruction to the ground station beacon to begin a search. The time could end with the insertion of the tracking mirror in the ground station optics at which time the tracking channel

FIGURE 5-007 DOWNLINK TRACKING ERROR ANALYSIS

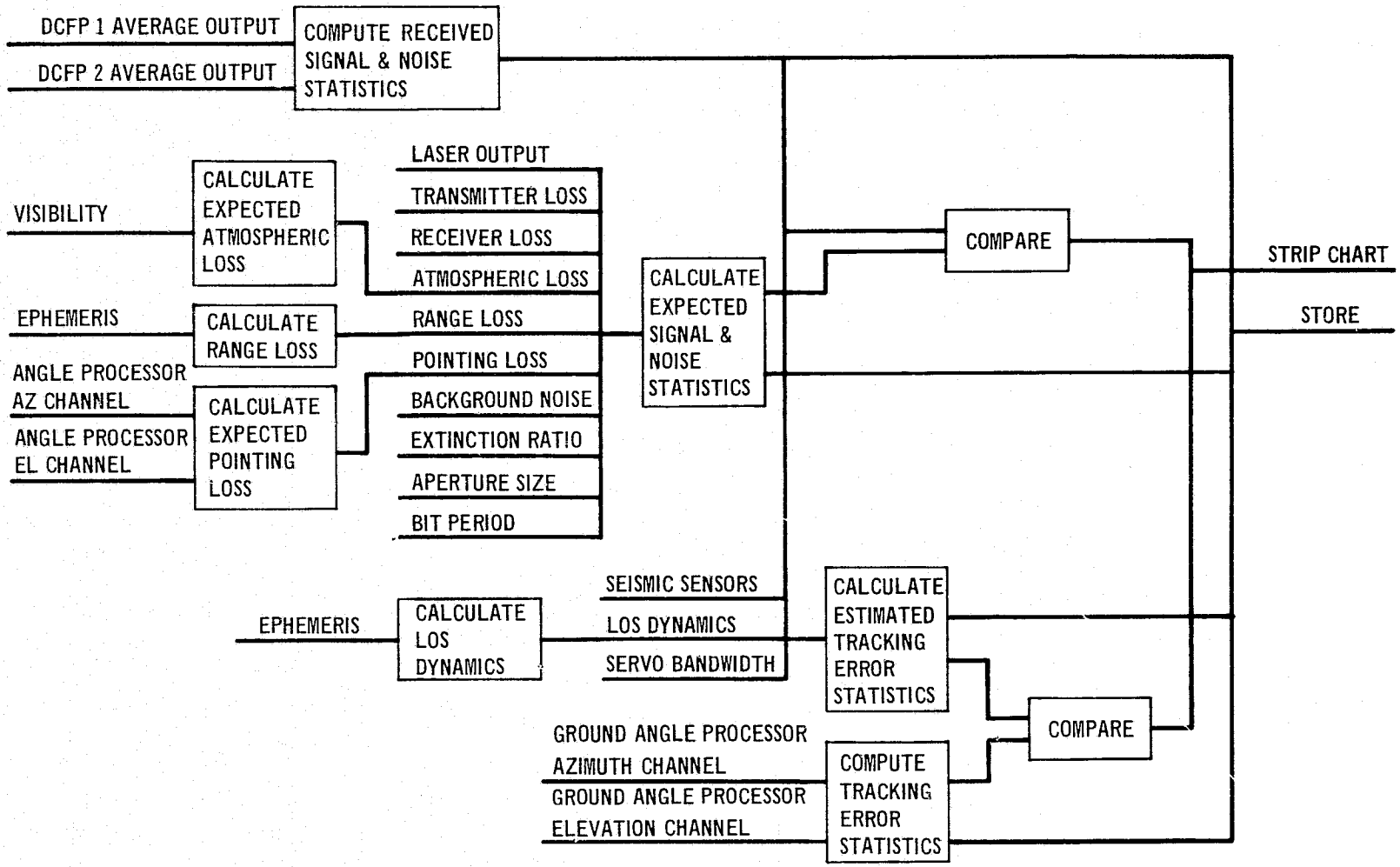

FIGURE 5-008 DOWNLINK BEAM PATTERN AND POINTING ERROR MEASUREMENT

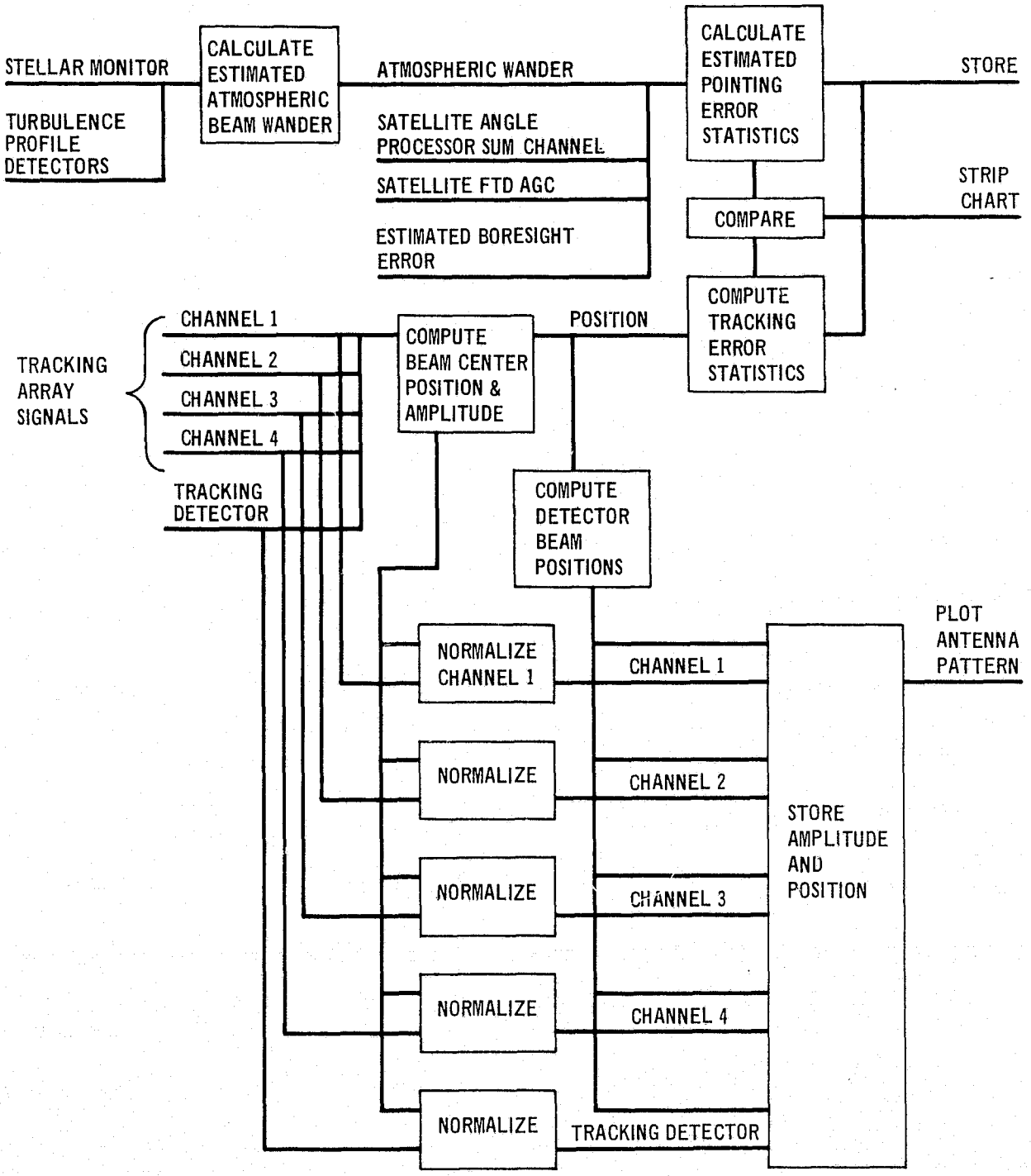

is in lock. The time could also end when the ground bit synchronizer is in lock at which time the communications channel is in lock. The third alternative is to consider the time to end when the first useful data is communicated. For the purposes of this experiment the bit synchronizer lock detector should be used to note the completion of acquisition.

The acquisition time measurement as shown in Figure 5-009 is simply noting the time from beginning a search to the bit synchronizer lock. However, for diagnostic purposes other event times should be calculated. These other events include satellite CAD signal reception, FAD signal reception, and acquisition mode change and ground station tracking detector signal reception, tracking mirror insertion, and DCFP signal reception. The events in the satellite occur prior to communications channel lock and therefore a problem exists in determining these event times. If a downlink rf telemetry capability does not exist to monitor these events in real time then the time of these events must be stored on board the satellite and dumped after communications channel lock. By reading the time of day from the satellite clock and comparing it to the ground station clock, event timing should be correctable within an acceptable level of precision. The event times would then be output to a printer at the ground station.

FIGURE 5-009 ACQUISITION TIME MEASUREMENT

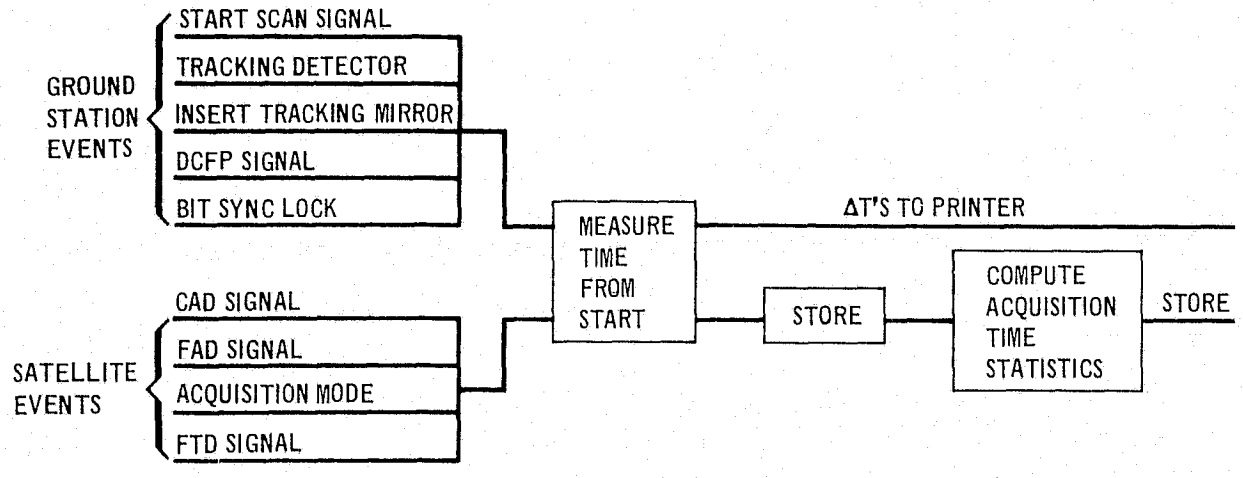

5.4 EXPERIMENT SCHEDULES. A complete experiment timeline and detailed schedules must await the final design of the payload; however some conceptual guidance has been developed and is included in this section as the foundation for further efforts.

5.4.1 Experiment Schedule Orbit Considerations. The experiment schedule must be designed to make the best use of the experiment orbit. A complete orbit definition is included in Section 3. The satellite comes over the horizon slightly west of south of the ground station approximately 5.6 hours before apogee and moves up and north. At 5 hours before apogee the satellite is southwest of the station at an elevation of greater than 60°. During the next ten hours the elevation angle to the satellite remains above 60° as the satellite moves north of the ground station and returns along a similar trajectory as it descends in the south approximately 5.5 hours after apogee. During the primary experiment period, apogee $\pm$3 hours, the satellite remains in a small angular region of about 16° in elevation and about 10° in azimuth. The merits of performing special experiments during time periods other than around apogee must be evaluated to capitalize on the changing viewing geometry and range to the satellite. Around apogee the range is approximately 40,000 km and the link closely simulates the link from a low altitude satellite to a geosynchronous relay satellite. Range reduces to only 15,000 km at a time of 5 hours from apogee. This reduced range may offer advantages for some limited special experiments although the majority of communication tests will be performed when the satellite is near apogee.

One attractive feature of the experiment orbit is that sun interference is minimum. When the sun position is near the ground-site-to-satellite viewing vector, the suns radiation can obviously interfere with the optical link. The vector to the satellite can never be closer than approximately 45° to the sunline during the period of apogee $\pm$3 hours; depending on the season of the year, the sun can be directly behind the satellite during evening hours as both the sun sets and the satellite rises in the southwest. The local time of day of apogee (at the ground station) will change at the rate of 27.2 hours/year due to the combined earth motion around the sun and orbit plane precession. Since the sun position at the time of satellite apogee has an important influence on the background viewed by the satellite detectors, the preferred sun location at the beginning of the test flight mission should be identified as part of the mission timeline.

5.4.2 Ground Station Design. The design of the ground station will influence the efficiency of the test performance. Typical functional requirements for ground station monitor and control are discussed in the following paragraphs.

Experiment Monitor - A central console will be required to provide top-level visibility into all spacecraft payload and ground station subsystems status and configuration. This station will enable the experiment conductor to control the experiment by giving direction to subsystem monitor and control personnel to handle any occurrence. Control of the general conduct of the experiment should be implemented at the experiment monitor.

Payload Monitor - This monitor must have two main components; the first should monitor and control the configuration of the high data rate communication hardware and the second component is for monitor and control of the acquisition and tracking plus the sun pump hardware. The high data rate communication monitor and control operations should provide for control of all optical communication equipment including the Nd:YAG downlink modulation format (PQM, PPBM, PDBM, and PGBM), the 10 Kbps PIM optical uplink, and signal source selection (PRN code or data source). Communication performance and telemetry monitor data should be displayed at this monitor. The configuration of the ground station optical communication equipment and data processing/storing equipment (related to optical communication) should also be monitored. The acquisition and tracking monitor should provide control of the acquisition subsystem configuration (mode, bandwidths, beamwidths) and monitor of the payload status and performance. In addition, monitor and mode control of the ground station acquisition and tracking subsystems should be implemented at this monitor to provide a single point control of the cooperative acquisition and tracking process.

Ground Station Monitor - This monitor will provide for the detailed monitoring and control of the ground station equipment. Subdivisions of this function are the communication equipment and diagnostic components, ground station acquisition and tracking equipment, and data processing, control, and recording hardware and software.

Payload Telemetry Monitor - The telemetry monitor will illustrate the configuration and data flow via RF or optical telemetry between the satellite and ground station. The primary role of this monitor should be one of support of the commands from the various other monitors to assure an orderly and correct flow of commands to the payload and downlink parameters from the payload.

5.4.3 Initial Functional Checkout. The first test sequence begins after the final orbit adjust maneuver by the satellite to establish the operational orbit conditions. The functional operation tests are expected to require three weeks to complete. Objectives of the tests are to exercise every mode of the payload and Ground Site systems to establish the complete status of all components. The tests also provide the first measurements of downlink and uplink communications as well as acquisition and tracking. The test sequence begins with a series of ten tests of the SFTS in a sun pumped laser mode.

Operation of the sun pumped laser is the first step in the sequence. The solar collector gimbal control is activated in an open loop pointing mode to point toward the sun based on ground commanded angles; the sun detector in the solar collector is monitored to observe presence of the sun on the detector. Automatic sun tracking is intitated and the electronic boresight of the tracker adjusted to optimize the solar pumped laser operation. The laser output power reserve and stability are monitored and any adjustments to the beam power, stability and position which are possible are made. After nominal laser operation is achieved, modulator tests are initiated. Modulator transmission and extinction ratio are measured for the different modulator configurations. Modulator output beam position is monitored and adjusted in the autoalignment mode. Optical transmission for the 0.53 μm and 1.06 μm optical wavelengths are then measured using in orbit calibration sources and sensors. Telescope gimbal operation in the Realign mode is tested by commanding various pointing angle conditions and monitoring the shaft angle encoders. After these tests, the FAD, CAD, and FTD are tested without signals present to observe false alarms as a function of threshold settings for various background conditions (earth pointing, space pointing). Optical transmission at the 1.06 μm wavelength is then tested by pointing the telescope gimbal to reflect any calibration source available into the optics system. The gimbals are pointed to direct the source to each of the quadrant in each detector to provide measurements for adjusting the electronic boresights of the detectors and observe the FAD and CAD fields of view.

Following verification of operation of the sun pumped laser, modulators, optics, gimbal control, and the acquisition and tracking detectors, acquisition and tracking operation will be verified. Similar operations will be conducted at the Ground Site to assure that the ground based equipment is operational and in readiness for testing the link. Preacquisition tests consist of pointing

the spaceborne gimbal to the Ground Site with the Ground Site in the acquisition mode (beacon scan), and observing detections by the FAD and CAD. This operation should be performed with various scan patterns from the ground to observe the open loop pointing conditions at the satellite and the Ground Site. The payload should then be commanded to the acquisition mode and coarse pointing performance monitored. The next step is to select the auto mode in both systems and enter into tracking with a spoiled beam from the spacecraft. The boresights of both the SFTS and Ground Site will be monitored and beam patterns measured. The final step in the sequence is to enter the auto mode with the narrow beam from the spacecraft and enter tracking with the nominal 1 Gbps link established.

This series of tests will require about one week to complete. Following these tests, the first detailed tests of the downlink and uplink will be conducted. The payload and Ground Site should then be configured in the nominal optical and acquisition and tracking configurations and tracking established. Downlink communication tests should be conducted for appropriate combinations of modulation format, synchronous/asynchronous operation, data channels and sources, burst error thresholds, and received photoelectrons per bit at the Ground Site. Uplink communication tests will exercise appropriate combinations of beacon laser power, threshold level, and burst error threshold levels. Functional verification of the many possible optical link communication configurations is estimated to require one week to complete for the the sun pumped laser system.

The third week of the verification tests addresses the functional operation of the lamp pumped laser system. The lamp pumped laser output power, beam position and stability are monitored and controlled if possible. Modulator performance is then evaluated using similar procedures as for the sun pumped laser. Spaceborne optical transmission is then evaluated using in orbit calibration sources and detectors. Acquisition and tracking tests are then initiated followed by tests of the various configurations of the lamp pumped laser downlink. These tests conclude the functional verification tests and are followed by benchmark tests which will serve as the baseline for the evaluation of long-term trends in system performance.

5.4.4 Long Term Schedules. The benchmark tests are used to define nominal link performance and should be designed to monitor long-term changes in system performance. These tests should be repeated on a regular basis at approximately six week intervals. Following the benchmark tests, Level 1 tests are conducted for a four week period plus a two week contingency period. Level 1 tests are the highest priority tests, designed such that system performance is described in detail upon completion. All possible payload and Ground Station configurations are not evaluated in the Level 1 tests, however those combinations considered to be most important are tested. For example, all levels of the photoelectrons per bit configurations of the HDR receiver might not be tested but the entire range would be evaluated with say four levels. A similar philosophy would be utilized for acquisition and tracking tests in the Level 1 tests. The benchmark tests should be repeated after the Level 1 tests and followed by a two-week test period consisting of tests which will be planned on the basis of prior results from the test flight. Level 2 tests are then conducted; these tests are defined here to include detailed communication and acquisition/tracking tests encompassing lower priority test levels than the Level 1 tests. Benchmark tests are repeated following the Level 2 tests.

5.4.5 Typical Experiment Sequence. Operations for conducting experiments on a particular contact period should begin immediately after the previous experiment period when results of that experiment interval are reviewed, documented, and accounted for in the overall experiment plan. Experiment requirements for the next contact period should then be derived and test plans formulated. Various support computer programs should be exercised to quantify the satellite orbit effects including sun and moon interferences, and meteorological factors. Specific experiment schedule and procedures should then be generated for the ground station monitor and control activities. The ground station computer should be utilized to generate tabulated printouts of procedures, console switch positions, and TM command parameters for the experiment sequence.

Prior to overflight by the satellite the ground station should be activated, and checked out for configuration and function. Payload configuration commands are uplinked via RF command to prepare the satellite for the experiment sequence. The ground station telescope should be activated to perform open loop pointing so as to track the satellite trajectory based on computer commands generated as

continuous functions of time from SCF orbit emphemeris data. The payload then responds to a command for the sun pump to enter the ACQUISITION telescope pointing control mode. In this mode the sun pump telescope is pointed to the expected sun line at the satellite based on orbit emphemeris. When the sun is indicated on the sun pump tracking detector, the payload enters the AUTO mode as the tracking mode is automatically activated and the sun is tracked. The sun pumped laser is activated and the gimbals pointed along the predicted line-of-sight to the ground station. The ground station acquisition and tracking subsystem is set to the ACQUISITION mode and the beacon laser is scanned to illuminate the satellite with the acquisition beacon signal. When the system is in a TRACK condition, the acquisition and tracking operator selects the automatic boresight alignment mode at the satellite to eliminate boresight shifts in the optical system. Operation in the TRACK mode is then monitored briefly to assure that the link is operating nominally prior to beginning the planned communication experiments.

Communication experiments are then initiated; a typical sequence involves the evaluation of BER as a function of time for each modulation format for particular HDR and beacon laser power levels and signal sources. In this sequence the experiment operator will select the modulation format and direct the ground station monitor operator to configure the data processing and recording equipment for the required scoring and record keeping of tests. The high data rate communication monitor operator will monitor the communication performance and advise the experiment controller as necessary. Throughout the communication experiment the ground station monitor and spacecraft acquisition and tracking monitor operators continually observe system operation and support the experiment operator as required.

After completing the communication performance tests as a function of modulation format for the one laser power level, the next experiment phase could typically be repeated for other HDR power levels, signal sources, and receiver thresholds in the communication link without breaking tracking lock. Variation of this HDR power would be implemented by attenuating the received power at the ground site. Operations to implement the signal strength attenuation would be directed by the experiment controller and performed from the ground station monitor console. This test would be conducted with the same procedures and

monitoring as the previous communication test. Communication tests of this type could typically occupy an entire experiment plan for a specific satellite pass without breaking tracking lock.

The test sequence for acquisition and tracking tests involve modifying the payload configuration commands, changing the ground station configuration, and introducing rigid body and flexible body rotational excitations in the satellite via the RF TT&C. A typical test is the generation of acquisition time statistics for various beacon laser power levels. In this sequence the initial payload pointing angles would be adjusted such that the initial off-boresight condition is known. The ground station beacon power level is then attenuated to the appropriate level. The acquisition process is then monitored by the experiment operator and acquisition time determined and recorded by on-line data processing of controller commands and payload Mode Logic outputs. After completing acquisition, the payload is returned to the REALIGN mode and acquisition repeated for the same beacon laser power level and initial pointing conditions. This sequence is repeated to generate the sample base for the particular beacon power. In generating the acquisition time data, the initial pointing conditions would be changed to include effects of the initial boresight error in the statistics.